

Si-Al Pitzer dataset

Consistent set of Pitzer activity model interaction parameters of Al and Si species, for modelling cements in saline systems with THEREDA. 80 p.

29.07.2024

George Dan Miron¹

¹ Laboratory for Waste Management, Paul Scherrer Institute, Villigen, Switzerland

Keywords

Si, Al, thermodynamic database, oceanic salts, Pitzer model, THEREDA, cementitious systems

THEREDA Si–Al Pitzer dataset

Abstract

The Si and Al thermodynamic data and Pitzer interaction parameters (IPs) from THEREDA were re-evaluated in order to extend the applicability of THEREDA database for modelling cementitious systems from low to highly saline systems. This work consisted of reassessing the standard reference thermodynamic data for Si and Al aqueous species and some relevant anchor solids (quartz, gibbsite, boehmite) and of producing a new consistent set of polythermal Pitzer interaction parameters for the Si and Al aqueous species within the oceanic salt system Al–Si–Ca–Mg–Na–K–Cl–SO₄–CO₃–H₂O. In some cases the polythermal parameters were derived from measured data, in others from estimates, and in some cases no data were available and no IPs were selected (Table 4-1). To reduce the number of all possible interactions, aqueous species interactions were selected based on the predominance of these species against the speciation of ions in the oceanic salt system. Experimental data were collected from available published research, if available, with measurements at different temperatures, and were used in an optimization procedure to fit the interaction parameters and their temperature coefficients. When no data were available, estimation methods in analogy with other species or correlations with the SIT (Specific ion Interaction Theory) aqueous activity model parameters were used to fill the gaps in order to avoid gross errors.

For Si in the acidic to neutral regions, polythermal interaction parameters for Si(OH)₄(aq) were determined based on a rich dataset of binary and ternary experimental data (section 2.2). Measured data in binary and ternary electrolyte systems at different temperatures and concentrations can be well reproduced by the derived dataset of binary interaction parameters.

The formation constant for the first silicic acid hydrolysis and its temperature dependence were assessed together with interaction parameters in NaCl (section 2.4). For the second hydrolysis species only limited temperature data were available requiring the use of estimation methods (isoelectric reaction). Interaction parameters with K⁺ were estimated by analogy to the IPs between K⁺ and HCO₃⁻ and the ones with Na⁺. In the presence of Ca and Mg at high pH, the precipitation of silicate hydrates is expected. The effect of these ions was accounted for in the present dataset by using complexes between Si and alkaline earth metals. To be consistent, no IPs between Ca²⁺ and Mg²⁺ cations and the Si hydrolysed species were selected in the dataset. Additional experimental data is necessary to better constrain interactions of silica species with K⁺ and to evaluate the temperature dependence of the alkaline earth metals silicate complexes.

At high Si concentrations (> 0.01 m), polymeric species play a role in the aqueous speciation of Si. Due to limited experimental data and the many different possible polymeric species it is difficult to derive a unique dataset. Selecting only the silica tetramer (Si₄O₈(OH)₄₄⁻) and its binary IPs was sufficient to reproduce the measured amorphous Si solubility data at high pH in NaCl solutions and should be sufficient for most calculations, due to the precipitation of silicate phases and the reduction of dissolved silica.

Low and high pH data for Al in solution have been evaluated. Standard thermodynamic properties of aluminium ions, hydrolysed species and hydroxide phases were derived using gibbsite as the anchor phase and a large number of solubility measurements at various electrolyte concentrations and temperatures (section 3.1). Based on existing experimental data, no temperature coefficients were required for interactions in the Al–Cl–H₂O system. This led to similar results in the subsequent ternary and quaternary systems, where IPs at 25 °C were sufficient to describe the measurements in the 0–100 °C temperature interval. Complexes between aluminium and sulphate are known to form in the acidic range, but their effect was accounted for by the $\beta^{(2)}$ interaction parameter and its temperature dependence. Data on Al–Si in the acidic region are limited. The selected AlSiO(OH)₃²⁺ species may play a role and is valid for low concentrations (section 3.2).

At intermediate pH conditions, there are few measurements to derive IPs for the hydrolysed aluminium species. IPs have only been derived with Cl^- . No data were available to obtain IPs between the positively charged Al hydrolysed species, SO_4^{2-} and HCO_3^- . The IPs of $\text{Al(OH)}_3(\text{aq})$ were assumed to be the same as those of $\text{Si(OH)}_4(\text{aq})$ (section 3.4.1).

At high pH conditions, the extensive gibbsite solubility data sets for a wide range of electrolyte concentrations and temperatures (0–150 °C) allowed a consistent set of IPs to be derived for the Na–K–Cl–OH– Al(OH)_4 system (section 3.4.2). Potential IPs with Ca^{2+} and Mg^{2+} were not selected because at these high pH values in cementitious systems Ca and Mg bearing phases will precipitate, keeping their concentrations at low values where IPs don't play a significant role. This can be different when interacting with $\text{CaCl}_2/\text{MgCl}_2$ solutions and needs to be tested in future investigations. Ternary IPs with SO_4^{2-} and CO_3^{2-} were estimated using OH^- as an analogue species for Al(OH)_4^- . This approximation was based on observations from the Na–K–Cl–OH– Al(OH)_4 system and gave satisfactory predictions from independent measurements of gibbsite solubilities in Na_2CO_3 and Na_2SO_4 solutions. No significant interactions between Si and Al were expected at high pH conditions, and their negatively charged species could well describe the measured data in cementitious systems. In addition, the precipitation of cement phases such as C–S–H or M–S–H will keep the Si concentration low.

Finally, the updated Pitzer model data set for aqueous speciation of Si and Al was compared with independent data on solutions in equilibrium with cement hydrate phases (e.g. C–S–H) and invariant points in electrolyte solutions of moderate concentrations up to 85 °C (section 3.5). The model performed well, although additional testing against salt-rich systems is required and further investigations that can close the gaps are recommended (chapter 4).

Fitted parameter values are marked in **bold**, estimates that were sensitive to measured data but kept fixed during the fit are given in normal typeface, estimated values not backed up by data (were estimated) are reported in *italic* typeface.

The updated dataset of parameters was implemented in THEREDA (<https://www.thereda.de/>). It is now available for the use in calculations. The present report provides detailed documentation on the work rationale for selecting data, model development, and optimization procedure.

Zusammenfassung

Die thermodynamischen Daten für Silizium (Si) und Aluminium (Al) und die Pitzer-Wechselwirkungsparameter (IPs für „interaction parameters“) in THEREDA wurden neu bewertet, um die Anwendbarkeit der THEREDA-Datenbasis für die Modellierung zementhaltiger Systeme sowohl bei niedrigen als auch hohen Salzgehalten zu erweitern. Diese Arbeit bestand aus einer Neubewertung der thermodynamischen Standardreferenzdaten für wässrige Si- und Al-Spezies und für einige relevante Ankerfeststoffe (Quarz, Gibbsit, Böhmit) sowie der Erstellung eines neuen konsistenten Satzes von polythermalen Pitzer-Wechselwirkungsparametern für die wässrigen Si- und Al-Spezies innerhalb des ozeanischen Salzsystems Al-Si-Ca-Mg-Na-K-Cl-SO₄-CO₃-H₂O. In einigen Fällen wurden die polythermalen Parameter aus gemessenen Daten abgeleitet, in anderen aus Schätzungen, und in einigen Fällen waren keine Daten verfügbar und es wurden keine IPs ausgewählt (Table 4-1). Um die Anzahl aller möglichen Wechselwirkungen zu reduzieren, wurden nur solche Wechselwirkungen berücksichtigt bei denen die beteiligten Spezies unter den relevanten Bedingungen im ozeanischen Salzsystem gemeinsam in bedeutenden Konzentrationen auftreten. Experimentelle Daten wurden aus verfügbaren veröffentlichten Forschungsarbeiten und, soweit vorhanden, aus Messungen bei verschiedenen Temperaturen gesammelt und in einem Optimierungsverfahren zur Anpassung der Wechselwirkungsparameter und ihrer Temperaturkoeffizienten verwendet. Wenn keine Daten verfügbar waren, wurden Schätzmethoden in Analogie zu anderen Spezies oder Korrelationen mit den Parametern des SIT (Specific ion Interaction Theory) wässriges Aktivitätsmodells verwendet, um die Datenlücken zu füllen und so grobe Fehler zu vermeiden.

Für Si im sauren bis neutralen pH-Bereich wurden polythermale Wechselwirkungsparameter für Si(OH)₄(aq) auf Grundlage eines umfangreichen Datensatzes von binären und ternären experimentellen Daten bestimmt (Abschnitt 2.2). Gemessene Daten in binären und ternären Elektrolyt systemen bei unterschiedlichen Temperaturen und Konzentrationen konnten durch den abgeleiteten Datensatz binärer Wechselwirkungsparameter gut reproduziert werden.

Die Bildungskonstante für die erste Kieselsäurehydrolyse und ihre Temperaturabhängigkeit wurden zusammen mit den Wechselwirkungsparametern in NaCl bewertet (Abschnitt 2.4). Für die zweite Hydrolyse-Spezies sind nur begrenzte Temperaturdaten verfügbar, so dass Schätzmethoden (isoelektrische Reaktion) verwendet werden mussten. Die IPs mit K⁺ wurden in Analogie zu den IPs zwischen K⁺ und HCO₃⁻ und denjenigen mit Na⁺ geschätzt. In Anwesenheit von Ca und Mg bei hohem pH-Wert wird die Ausfällung von Silikathydraten erwartet. Die Wirkung dieser Ionen wird im vorliegenden Datensatz durch die Verwendung von Komplexen zwischen Si und Erdalkalimetallen berücksichtigt. Aus Gründen der Konsistenz wurden im Datensatz keine IPs zwischen Ca²⁺- und Mg²⁺-Kationen und den hydrolysierten Si-Spezies ausgewählt. Zusätzliche experimentelle Daten sind erforderlich, um die Wechselwirkungen von Siliziumdioxid-Spezies mit K⁺ besser einzugrenzen und auch die Temperaturabhängigkeit der Erdalkalimetallsilikatkomplexe zu bewerten.

Bei hohen Si-Konzentrationen (> 0,01 m) spielen polymere Spezies bei der wässrigen Speziation von Si eine bedeutende Rolle. Aufgrund der begrenzten experimentellen Daten und der vielen verschiedenen möglichen polymeren Spezies ist es schwierig, einen eindeutigen Datensatz abzuleiten. Die Einbeziehung von Siliziumdioxid-Tetramer (Si₄O₈(OH)₄<4->) und seine binären IPs ist geeignet, die gemessenen Daten zur Löslichkeit von amorphem Si bei hohem pH-Wert in NaCl-Lösungen zu reproduzieren, und stellt aufgrund der Ausfällung von Silikatphasen und der Reduzierung von gelöstem Siliziumdioxid auch für die meisten Berechnungen eine gute Basis dar.

Die Daten für Al in Lösung bei niedrigem und hohem pH-Wert wurden ausgewertet. Thermodynamische Standarddaten von Aluminiumionen, hydrolysierten Spezies und

Hydroxidphasen wurden unter Verwendung von Gibbsit als Ankerphase und einer großen Anzahl von Löslichkeitsmessungen bei verschiedenen Elektrolytkonzentrationen und Temperaturen abgeleitet (Abschnitt 3.1). Auf der Grundlage vorhandener experimenteller Daten wurden für die Wechselwirkungen im System Al-Cl-H₂O keine Temperaturkoeffizienten ermittelt. Auch bei der nachfolgenden Betrachtung von ternären und quaternären Systemen reichen IPs bei 25 °C zur Beschreibung der Messungen bei 0-100 °C aus. Es ist bekannt, dass sich im sauren pH-Bereich Komplexe zwischen Aluminium und Sulfat bilden, ihre Wirkung wurde durch den Wechselwirkungsparameter $\beta^{(2)}$ und seine Temperaturabhängigkeit berücksichtigt. Die Daten über Al-Si-Wechselwirkungen im sauren pH-Bereich sind begrenzt. Die ausgewählte AlSiO(OH)₃²⁺-Spezies könnte eine Rolle spielen und ist bei niedrigen Al-Konzentrationen präsent (Abschnitt 3.2).

Bei neutralen pH-Werten gibt es nur wenige Messungen zur Ableitung von IPs für die hydrolysierten Aluminiumarten. IPs wurden nur mit Cl⁻ abgeleitet. Es liegen keine Daten vor, um IPs zwischen den positiv geladenen Al-hydrolysierten Spezies SO₄²⁻ und HCO₃⁻ anzupassen. Aufgrund von Analogiebetrachtungen wurde angenommen, dass die IPs von Al(OH)₃(aq) dieselben sind wie die von Si(OH)₄(aq) (Abschnitt 3.4.1).

Bei hohen pH-Werten ermöglichen die umfangreichen Gibbsit-Löslichkeitsdatensätze für einen breiten Bereich von Elektrolytkonzentrationen und Temperaturen (0-150 °C) die Ableitung eines konsistenten Satzes von IPs für das Na-K-Cl-OH-Al(OH)₄-System (Abschnitt 3.4.2). Potenzielle IPs mit Ca²⁺ und Mg²⁺ wurden nicht angepasst, da bei den relevanten hohen pH-Werten in zementhaltigen Systemen Ca- und Mg-haltige Phasen ausfallen und deren Konzentrationen auf Werte begrenzt, bei denen Wechselwirkungen keine bedeutende Rolle spielen. Dies kann bei der Interaktion mit CaCl₂/MgCl₂-Lösungen anders sein und muss in zukünftigen Untersuchungen getestet werden. Ternäre IPs mit SO₄²⁻ und CO₃²⁻ wurden unter Verwendung von OH⁻ als analoge Spezies für Al(OH)₄⁻ geschätzt. Diese Näherung basiert auf Beobachtungen aus dem Na-K-Cl-OH-Al(OH)₄-System und liefert zufriedenstellende Vorhersagen aus unabhängigen Messungen der Gibbsit-Löslichkeiten in Na₂CO₃- und Na₂SO₄-Lösungen. Bei hohen pH-Werten werden keine signifikanten Wechselwirkungen zwischen Si und Al erwartet, und ihre negativ geladenen Spezies können die gemessenen Daten in zementartigen Systemen gut beschreiben. Darüber hinaus wird die Ausfällung von Zementphasen wie C-S-H oder M-S-H die Si-Konzentration begrenzen.

Schließlich wurde der aktualisierte Datensatz des Pitzer-Modells für die wässrige Speziation von Si und Al mit unabhängigen Daten zu Lösungen im Gleichgewicht mit Zementhydratphasen (z. B. C-S-H) und invarianten Punkten in Elektrolytlösungen mäßiger Konzentrationen bis zu einer Temperatur von 85 °C verglichen (Abschnitt 3.5). Diese Systeme konnten mit den ermittelten Pitzer-Parametern gut reproduziert werden. Zusätzliche Tests in salinaren Systemen sind erforderlich und weitere experimentelle Untersuchungen werden empfohlen, um die bestehenden Datenlücken schließen zu können (Kapitel 4).

Anangepasste Parameterwerte sind **fett** gedruckt, Schätzungen, die auf Messdaten beruhen und während der Anpassung fixiert wurden, sind in normaler Schrift angegeben, geschätzte Werte, die nicht durch Daten gestützt werden, sind *kursiv* gedruckt.

Der aktualisierte Datensatz von Parametern wurde in THEREDA eingegeben und steht nun für die Verwendung in Berechnungen zur Verfügung. Der vorliegende Bericht enthält eine detaillierte Dokumentation der Arbeitsgrundlagen für die Datenauswahl, die Modellentwicklung und das Optimierungsverfahren.

Table of Contents

Abstract	III
Zusammenfassung.....	V
Table of Contents	VII
List of Tables	VIII
List of Figures	IX
List of Acronyms	XII
List of Symbols	XIII
1 Introduction	1
1.1 Parameterization strategy.....	5
2 Si.....	8
2.1 Standard thermodynamic data for the system Si–O–H.....	8
2.2 Polythermal IPs for Si(OH) ₄ (aq).....	9
2.3 Hydrolysis of silicic acid	18
2.4 IPs for SiO(OH) ₃ ⁻ and SiO ₂ (OH) ₂ ²⁻	19
2.5 Metal silicate complexes.....	25
2.6 Si polymeric species	26
3 Al	29
3.1 Standard thermodynamic data for the system Al–O–H	29
3.2 Al polymeric species and interactions with Si at low pH	32
3.3 IPs in the Al–Ca–Mg–Cl–OH ⁻ SO ₄ ⁻ CO ₂ system at low pH	32
3.3.1 Al–Cl–H ₂ O	33
3.3.2 Al–Na–K–Ca–Mg–Cl–H ₂ O	34
3.3.3 Al–SO ₄ –H ₂ O and Al–Na–K–Mg–SO ₄ –H ₂ O systems	38
3.3.4 Al–CO ₂ –H ₂ O	43
3.4 IPs in the Al–Ca–Mg–Cl–OH ⁻ SO ₄ ⁻ CO ₂ system at intermediate to high pH	44
3.4.1 IPs for aluminium hydrolysed species	44
3.4.2 IPs for Al(OH) ₄ ⁻	45
3.4.2.1 System Na–K–Cl–OH–Al(OH) ₄	45
3.4.2.2 System System Ca–Mg–CO ₃ –SO ₄ –Al(OH) ₄	48
3.4.3 Al – Si and polymeric species	49
3.5 Benchmark against experimental data on the solubility of cement hydrates	50
4 Status of data, implications and data gaps	56
5 List of References.....	58

List of Tables

Table 1-1	Relation between SIT and Pitzer parameters for different ion combinations at 25 °C (Plyasunov et al., 1998).....	6
Table 2-1	Reference standard thermodynamic properties for Si element and quartz.....	9
Table 2-2	Experimental data on SiO ₂ (am) solubility in electrolyte solutions. * only data up to 300 °C were used in the fit.....	10
Table 2-3	Coefficients for the temperature function (Eq. 1–1) of ion IPs with Si(OH) ₄ (aq).....	13
Table 2-4.	Coefficients for the temperature function (Eq. 1–1) of ion IPs with SiO(OH) ₃ ⁻ . Values in bold were fitted against experimental data. In round brackets are initial values from (HCO ₃ ⁻) before the fit.....	20
Table 2-5.	Coefficients for the temperature function (Eq. 1–1) of ion IPs with SiO ₂ (OH) ₂ ²⁻	24
Table 3-1	Reference standard thermodynamic properties for Al element and gibbsite. * from solubility as a function of temperature.....	29
Table 3-2	Pitzer IP coefficients (Eq. 1–1) in the system Al–Cl–H ₂ O. Bold values were evaluated in this study.....	33
Table 3-3	Experimental data used to asses the IPs in the system Al–Na–K–Ca–Mg–Cl–H ₂ O.....	34
Table 3-4	Pitzer IP coefficients (Eq. 1–1) in the system Al–Na–K–Ca–Mg–Cl–H ₂ O. Bold values were evaluated in this study.....	37
Table 3-5	Experimental data used to asses the IPs in the system Al–Na–K–Ca–Mg–SO ₄ –H ₂ O.....	39
Table 3-6	Pitzer IP coefficients (Eq. 1–1) in the system Al–Na–K–Ca–Mg–SO ₄ –H ₂ O. Bold values were evaluated in this study.....	41
Table 3-7	Experimental data used to asses the IPs in the system Al–Na–K–Cl–H ₂ O.....	44
Table 3-8	Pitzer IP coefficients (Eq. 1–1) for first and second Al hydrolysis species.....	45
Table 3-9	Pitzer IP coefficients (Eq. 1–1) in the system Al–Na–K–Cl–H ₂ O at elevated pH. Bold values were evaluated in this study. Values in regular font were derived from equivalent IPs of OH ⁻ and corresponding cations and anions (see text for details). Al concentrations in solution up to 1.5 mol·kg ⁻¹ H ₂ O.....	48
Table 3-10	Pitzer IP coefficients (Eq. 1–1) in the system Al–SO ₄ –CO ₃ at elevated pH. Values in regular font were derived from equivalent IPs of OH ⁻ and corresponding anions (see text for details).....	49
Table 3-11	Mineral phases in equilibrium for invariant points calculations. NaOH and KOH solution concentration in mol kg ⁻¹ H ₂ O	54
Table 3-12	Measured and calculated elemental concentrations of solutions in equilibrium at invariant points of different cement hydrate phases (Table 3-12) in mmol kg ⁻¹	55
Table 4-1	Status of polythermal parameters in the system Al–Si–Ca–Mg–Na–K–Cl–SO ₂ –CO ₂ –H ₂ O. Interactions between ions of the same charge are expected to only be relevant for highly concentrated multicomponent solutions.....	57

List of Figures

Fig.1–1	Carbon and sulphur aqueous speciation as a function of pH at 25 °C (a,b) and 100 °C (c,d) in 0.1 m NaCl background electrolyte using THEREDA 2021 database.	3
Fig. 1–2	Comparison between calculations using THEREDA database (release 2020) with GEM–Selektor (curves) and Phreeqc (symbols x)	4
Fig. 1–3	Workflow for extending the Pitzer model with interaction parameters for Al and Si species consistent with the THEREDA database, form modelling of cementitious materials in highly saline systems.	7
Fig. 2–1	Si aqueous speciation as a function as a function of pH at 25 °C (a) and 100 °C (b) in 0.1 NaCl background electrolyte.	8
Fig. 2–2	Comparison between measured (symbols) and calculated (lines) amorphous silica solubility in different binary electrolyte solutions at different temperatures. Empty symbols in a, and b are experiments done in HNO ₃ and NaNO ₃ solutions but modelled assuming HCl and NaCl solutions of equivalent concentrations.	14
Fig. 2–3	Comparison between measured (full circles) and calculated (empty circles) amorphous silica solubility in ternary electrolyte solutions at 25 C.	15
Fig. 2–4	Solubility of amorphous silica in Na ₂ SO ₄ –K ₂ SO ₄ solutions at 25 C from Meyer (2006) (a), measured (full circles) compared with model calculated (empty circles) (b). (c) calculated using ζ –zeta(Si(OH) ₄ (aq)–K ⁺ –SO ₄ ^{2–}) 0.25 16	
Fig. 2–5	Comparison between measured (full circles) and calculated (empty circles) amorphous silica solubility in ternary electrolyte solutions at elevate temperatures. (a, b) Datasets of Meyer & Willms (2008) before correction (see text). (b, c, d) Datasets of Meyer & Willms (2008) after correction (see text).	17
Fig. 2–6.	Comparison between measured (full circles) and calculated (empty circles) amorphous silica solubility in ternary electrolyte solutions at elevate temperatures. Datasets of Meyer & Willms (2008) after correction (see text).	18
Fig. 2–7	Comparison between measured (full red circles) and calculated (empty blue circles) and ionization constant data, at different temperatures, with initial IPs values from HCO ₃ [–] (a), and adjusted IPs from Table 2-4 (b).	20
Fig. 2–8.	Comparison between measured (full red circles) and calculated (empty blue circles) osmotic coefficient (a, b, m represents the Na ₂ SiO ₃ mol kg ^{–1}) and ionization constant data (C, D), at 25 C, with initial IPs values from CO ₃ ^{2–} (A, C), and adjusted IPs from Table 2-5 (B, D).	22
Fig. 2–9.	Comparison between measured (circles) (Busey and Mesmer, 1977) and calculated (lines) second hydrolysis constants at 1 m NaCl as a function of temperature.	23
Fig. 2–10	Solubility of SiO ₂ (am) in NaCl media at 25 C. Measured data points from (Zarubin and Nemkina, 1990), calculated line using the data for species revised in this study. (a) only monomeric species; (b) with the Si ₄ O ₈ (OH) ₄₄ [–]	

	added (slope of 4) and derived $\log_{10}K(298.15) = -36.812$, $\beta^{(0)} 1.35$, and $\beta(1)$ 11.0 as given in Felmy et al. (2001).	27
Fig. 3–1	(a) Comparison between calculated (3–1, 3–2) and selected model extrapolated solubility data (symbols) by (Brown and Ekberg, 2016); (b) Comparison between calculated (3–1, 3–3) and measured data for boehmite selected in this study from (Bénézeth et al., 2001; Palmer et al., 2001) and from (Verdes et al., 1992).....	30
Fig. 3–2	Measured (symbols) data for $\text{Al}^{3+} + 4\text{H}_2\text{O} = \text{Al}(\text{OH})_4^- + 4\text{H}^+$ in the range 0 – 200°C range selected by (Brown and Ekberg, 2016) and calculated model (3–7).....	31
Fig. 3–3	(a) Data from (Robinson and Stokes, 1965) at 25 and at elevated temperatures from (Richter et al., 2000) (b) circle (Cheng et al., 2023), square (Wang et al., 2016), left arrow (Zeng et al., 2019), diamond (Brown et al., 1979), and triangle (Farelo et al., 2005), dashed line calculated with the model from (Christov et al., 2007).	34
Fig. 3–4	Comparison between calculated (empty circles) and measured experimental data (full circles) for (a) gibbsite and boehmite solubility $\log_{10}Q_s(T) = [\text{Al}^{3+}]/[\text{H}^+]^3$ (Palmer et al., 2001; Palmer and Wesolowski, 1992); (b) NaCl(cr) in AlCl ₃ (Farelo et al., 2005; Zeng et al., 2019); KCl(cr) solubility in AlCl ₃ (c) (Farelo et al., 2005) (d) (Christov et al., 2007; Linke, 1965; Patel K. and Seshardi S., 1966); (e) AlCl ₃ ·6H ₂ O solubility in KCl (Cheng et al., 2023); (f) AlCl ₃ ·6H ₂ O solubility in CaCl ₂ (Cheng et al., 2023).	36
Fig. 3–5	Comparison between calculated (lines) and measured experimental data (full circles) for the binary salt system MgCl ₂ ·6HO (Bischofite, red line in equilibrium) – AlCl ₃ ·6H ₂ O (green line in equilibrium). Measured data from (Patel K. and Seshardi S., 1966) (orange), and (Liu et al., 2022) (purple).	38
Fig. 3–6	Measured stoichiometric osmotic coefficient in Al ₂ (SO ₄) ₃ solution at 25 C (Robinson, 1937) (squares) and (Burge, 1963) (circles)	40
Fig. 3–7	Calculated (lines) and measured (symbols) gypsum solubility Al ₂ (SO ₄) ₃ (a) solution at 25 C (Mosgovykh et al., 1984) and in AlCl ₃ solutions at various temperatures (b) (Li and Demopoulos, 2006).....	40
Fig. 3–8	Calculated (lines) and measured (symbols) solubilities in ternary salt systems: (a) Na ₂ SO ₄ –Al ₂ (SO ₄) ₃ circles (Dobbins and Addleston, 1931), diamonds (DRUZHININ et al., 1961); (b) MgSO ₄ –Al ₂ (SO ₄) ₃ (Bassett and Watt, 1950); (c) K ₂ SO ₄ –Al ₂ (SO ₄) ₃ squares (Britton, 1922), circles (Reardon and Stevens, 1991).....	42
Fig. 3–9	Calculated (lines) and measured (symbols) (Yasunishi and Yoshida, 1979) solubility of CO ₂ (mol·kg ⁻¹ H ₂ O) in (a) AlCl ₃ and (b) Al ₂ (SO ₄) ₃ solutions.	43
Fig. 3–10	Measured (Palmer and Wesolowski, 1993), full, and calculated, empty, symbols of first aluminium hydrolysis formation constant as a function of IS at different temperatures.....	45
Fig. 3–11	Measured, full, and calculated, empty, symbols: (a) gibbsite solubility at different T in KOH solutions (Wesolowski, 1992) and (Luo et al., 2020); (b) gibbsite solubility at different T in NaOH solutions (Wesolowski, 1992) and (Russell et al., 1955); (c) osmotic coefficient of NaAl(OH) solutions at different T (Sipos et al., 1998); (d) osmotic coefficient of NaOH–AlCl ₃ solutions at 25 °C (Park and Englezos, 1999b); (e).gibbsite solubility in	

	NaCl–KCl solutions (Wesolowski, 1992); (f) gibbsite solubility in NaCl–NaOH solutions at different temperatures (Wesolowski, 1992).....	47
Fig. 3–12	Comparison between measured (symbols) and model calculated gibbsite solubility in (a) Na ₂ CO ₃ solutions at 60 °C (Königsberger et al., 2006), (b) synthetic Bayer liquors recalculated [Cl [−]] = 0.27 mol kg ^{−1} , [SO ₄ ^{2−}] = 0.25 mol kg ^{−1} , and [CO ₃ ^{2−}] = 0.25 mol kg ^{−1} (Bouzat and Philipponneau, 1991). Dashed lines model predictions with IPs between Al(OH) ₄ [−] , CO ₃ ^{2−} and SO ₄ [−] set to 0;.....	49
Fig. 3–13	Measured (symbols) and model calculated C–S–H solubility using THEREDA, the updated Pitzer dataset and CASH+ model at 25 °C. Si and Ca concentrations in mol kg ^{−1} vs target ratio (a) in water (Kulik et al., 2022); (b) pH; (c) in NaCl (Glasser et al., 1999) (d) KCl (Plusquellec, 2014), (e) NaOH (Yan et al., 2021), and (f) KOH (Yan et al., 2021) solutions	51
Fig. 3–14	Measured (symbols) and model calculated C–S–H solubility using THEREDA, the updated Pitzer dataset and CASH+ model at elevated temperatures. Si and Ca concentrations in mol kg ^{−1} vs target ratio (a) in NaOH solution at 50 °C (Myers et al., 2015) (b) in NaCl solution at 85 °C (Glasser et al., 1999).....	52
Fig. 3–15	Measured (symbols) (Yan et al., 2022) and model calculated aluminium containing C–S–H solubility using THEREDA, the updated Pitzer dataset and CASH+ model at 20 °C 1 molal NaOH and different target Al/Si ratios. Si, Ca, and Al concentrations in mol kg ^{−1} vs target ratio.....	52
Fig. 3–16	Measured (symbols) and calculated aqueous composition. (a) Ca, Al, pH in equilibrium with CAH at different temperatures (Matschei et al., 2007); (b) Ca, Si, Mg as a function of pH varying by addition of MgCl ₂ or MgO. Thermodynamic data for M–S–H and measured values from (Bernard et al., 2018).....	53

List of Acronyms

AFm	hydrated calcium aluminates monosubstituted
C–S–H	calcium silicate hydrate
C–A–S–H	calcium aluminium silicate Hydrate
EDH	extended Debye–Hückel (activity model)
IPs	interaction parameters
HMW	Harvie–Møller–Weare
RMS	root mean square error
SIT	specific ion interaction theory
TDB 2020	update to the Nagra/PSI chemical thermodynamic database (Hummel and Thoenen 2023)
THEREDA	Thermodynamic Reference Database

List of Symbols

$\log_{10}K^\circ$	the equilibrium constant of the reaction, logarithmic	
$\Delta_r G_m^\circ$	the molar Gibbs free energy of reaction	(kJ · mol ⁻¹)
$\Delta_r H_m^\circ$	the molar enthalpy of reaction	(kJ · mol ⁻¹)
$\Delta_r S_m^\circ$	the molar entropy of reaction	(J · K ⁻¹ · mol ⁻¹)
$\Delta_r C_{p,m}^\circ$	the molar heat capacity of reaction	(J · K ⁻¹ · mol ⁻¹)
$\Delta_f G_m^\circ$	the standard molar Gibbs free energy of formation	(kJ · mol ⁻¹)
$\Delta_f H_m^\circ$	the standard molar enthalpy of formation	(kJ · mol ⁻¹)
$\Delta_f S_m^\circ$	the standard molar entropy of formation	(J · K ⁻¹ · mol ⁻¹)
$\Delta_f C_{p,m}^\circ$	the standard molar heat capacity of formation	(J · K ⁻¹ · mol ⁻¹)
S_m°	the standard molar entropy	(J · K ⁻¹ · mol ⁻¹)
$C_{p,m}^\circ$	the standard molar heat capacity	(J · K ⁻¹ · mol ⁻¹)
T_r	the reference temperature of 298.15 K	
P_r	the reference pressure of 1 · 10 ⁵ Pa	
M	molarity	(mol · L ⁻¹ solution)
m	molality	(mol · kg ⁻¹ H ₂ O)
I	ionic strength	(mol · kg ⁻¹ H ₂ O)

Pitzer interaction parameters

Binary

- λ_a (neutral, anion) / λ_c (neutral, cation)
- $\beta^{(0)}$ (cation,anion)
- $\beta^{(1)}$ (cation,anion)
- $\beta^{(2)}$ (cation,anion)
- C^ϕ (cation,anion)
- $\alpha^{(1)}$ (cation,anion)
- $\alpha^{(2)}$ (cation,anion)
- θ_a (anion,anion) / θ_c (cation,cation)

Ternary

- ψ_a (anion,anion,cation) / ψ_c (cation,cation,anion)
- η_a (neutral, anion, anion') / η_c (neutral, cation, cation')
- ζ (neutral, cation, anion)

1 Introduction

To derive a thermodynamic dataset that is internally consistent and that can be applied across a broad range of temperatures and compositions in multicomponent systems, it is essential to obtain the standard state thermodynamic properties (e.g., $\log_{10}K^\circ$, $\Delta_f H_m^\circ$) and activity model parameters (e.g., interaction parameters) of all relevant solids and aqueous species. In the case of aqueous solutes, the standard state is defined as an ideal one molal solution at infinite dilution ($I = 0 \text{ m}$). For solids, the standard state is defined as the unit activity of pure solids. The data should be obtained from well-defined experiments that are processed with consistent chemical system and thermodynamic models. When no measured data were available, estimation methods can be used to provide approximate values for missing data in order to avoid gross errors in calculations. Expert evaluation, often arbitrary, is necessary to decide which estimation method to use, when estimations are needed. These parameters need to be determined while considering their compositional and temperature dependence.

The aqueous phase compositional dependence of the solubility of solids and aqueous species is calculated through the functional dependence expressed by the aqueous activity model. The Pitzer activity model is the main model supported by THEREDA database to account for the properties of aqueous species as a function of composition. The Pitzer model (Pitzer, 1991) allows for calculating thermodynamic properties of aqueous electrolytes in concentrated solutions with high level of accuracy (Rowland et al., 2015). The model expresses the excess Gibbs energy as a three-term virial expansion. The first virial term is a form of the Debye–Hückel equation, the second term accounts for binary interactions and the third term accounts for ternary interactions. The mathematical expressions of the Pitzer equations have been detailed elsewhere (Meyer, 2006; Meyer and Willms, 2008; Pitzer, 1991). They contain several adjustable parameters expressed as interaction parameters. For a binary solution up to four parameters can be used for each cation/anion pair, and one parameter for each cation/cation, anion/anion, cation/neutral, and anion/neutral. For a ternary system, additional parameters can be used to account for each two cations/one anion, two anions/one cation and one cation/one anion/one neutral species ternary interactions. Not all interactions are necessary to describe data and most dominant parameters are the ones accounting for interactions between species of different charge while same charge interactions being relevant only at high concentrations. The Pitzer parameters considered in this study can be found in the list of symbols.

Additionally, the temperature effect on the activity model is accounted for through the polythermal Pitzer interaction parameters. The temperature dependence of the Pitzer interaction parameters is described with the following function (Pitzer–PHREEQC temperature function in THEREDA):

$$P(T) = A + B \cdot \left(\frac{1}{T} - \frac{1}{T_r} \right) + C \cdot \ln \left(\frac{T}{T_r} \right) + D \cdot (T - T_r) + E \cdot (T^2 - T_r^2) + F \cdot \left(\frac{1}{T^2} - \frac{1}{T_r^2} \right) \quad 1-1$$

Where P is the value of a given Pitzer interaction parameter at temperature, T (K) and A to F are the adjustable coefficients. Notice that for this equation A is the value of the Pitzer IP at 25 °C.

Similarly, the temperature dependence of the stability of solids and aqueous complexes is determined by analysing the functional relationship between solubility or formation reaction constants (at standard state) and temperature. In the THEREDA, this relationship is expressed using the NEA–transformed temperature function.

$$\log_{10}K^\circ(T) = A + B \cdot T + C / T + D \cdot \ln(T) + E / T^2 \quad 1-2$$

The two sets of parameters, namely the standard thermodynamic properties and the polythermal Pitzer interaction parameters, are not independent of each other. This is because the equilibrium constants obtained from laboratory experiments are determined in an ionic medium and need to be extrapolated to zero ionic strength ($I = 0$ m) standard state using the activity model and its parameters. In principle different activity models should lead to the same standard state properties but due to differences in their functional dependence the results may differ. Ideally, for consistency, the same methods used for modelling the systems of interest should be employed for generating the database.

For low soluble solids, standard thermodynamic properties are retrieved from experiments typically conducted in water or in binary systems with low medium concentrations, where activity models like SIT, EDH, or Pitzer exhibit consistency within experimental uncertainty. Therefore, the reported $\log_{10}K^\circ(T)$ values or other properties that have been already extrapolated to $I = 0$ m, using different activity models, can be directly used to assess the temperature dependence for a given solid or aqueous species. For highly soluble salts the interdependence between the standard thermodynamic properties and the activity model is more difficult to unwind. In such cases measurements of solution properties (e.g., osmotic coefficient, complexation) in addition to solubility measurements are beneficial.

In the present study, both standard state properties and Pitzer interaction parameters for Si and Al species were reassessed. The standard thermodynamic property values were retained from THEREDA if they already agreed with experimental data. If necessary, the properties were updated based on a re-evaluation of existing experimental data. The new set of polythermal Pitzer interaction parameters for Al and Si species was retrieved to ensure consistency with the oceanic salts system in the THEREDA database. This means that all interactions between ions and complexes from the oceanic salts system were taken as they were set in THEREDA and were used when deriving the interaction parameters for Si and Al aqueous species. The Pitzer interaction parameters for the oceanic salts system have been revised and extended by Voigt et al. (2011), while maintaining consistency with the Harvie et al. parameter datasets for 25 °C (Harvie et al., 1984). The chemical system considered is Al–Si–Ca–Mg–Na–K–Cl–SO₄–CO₃–H₂O.

A comprehensive Pitzer parameter dataset encompasses all potential combinations of binary and ternary interactions among species in the chemical system. However, not all binary and ternary combinations need to be considered since the activity coefficients depend on the interaction parameters and the concentration of interacting species. For instance, there is no need for interaction parameters between Al(OH)₄⁻ and H⁺ because the aluminate species predominates only at high pH levels where H⁺ concentrations are negligible. Therefore, including an interaction parameter involving these species would have no impact on the calculations.

In the current study, the selection of potential interaction parameters was based on the dominant speciation of cations and anions as a function of pH (Fig.1–1) and their relevance to the Si and Al speciation as a function of pH. Fig.1–1 illustrates that carbon speciation changes between CO₂(aq), HCO₃⁻ and CO₃²⁻ from low to high pH, while sulphur is dominated by SO₄²⁻ with HSO₄⁻ playing a role only at pH < 3. The selection of possible interaction parameters is guided by species predominance and is further discussed in the subsequent chapters.

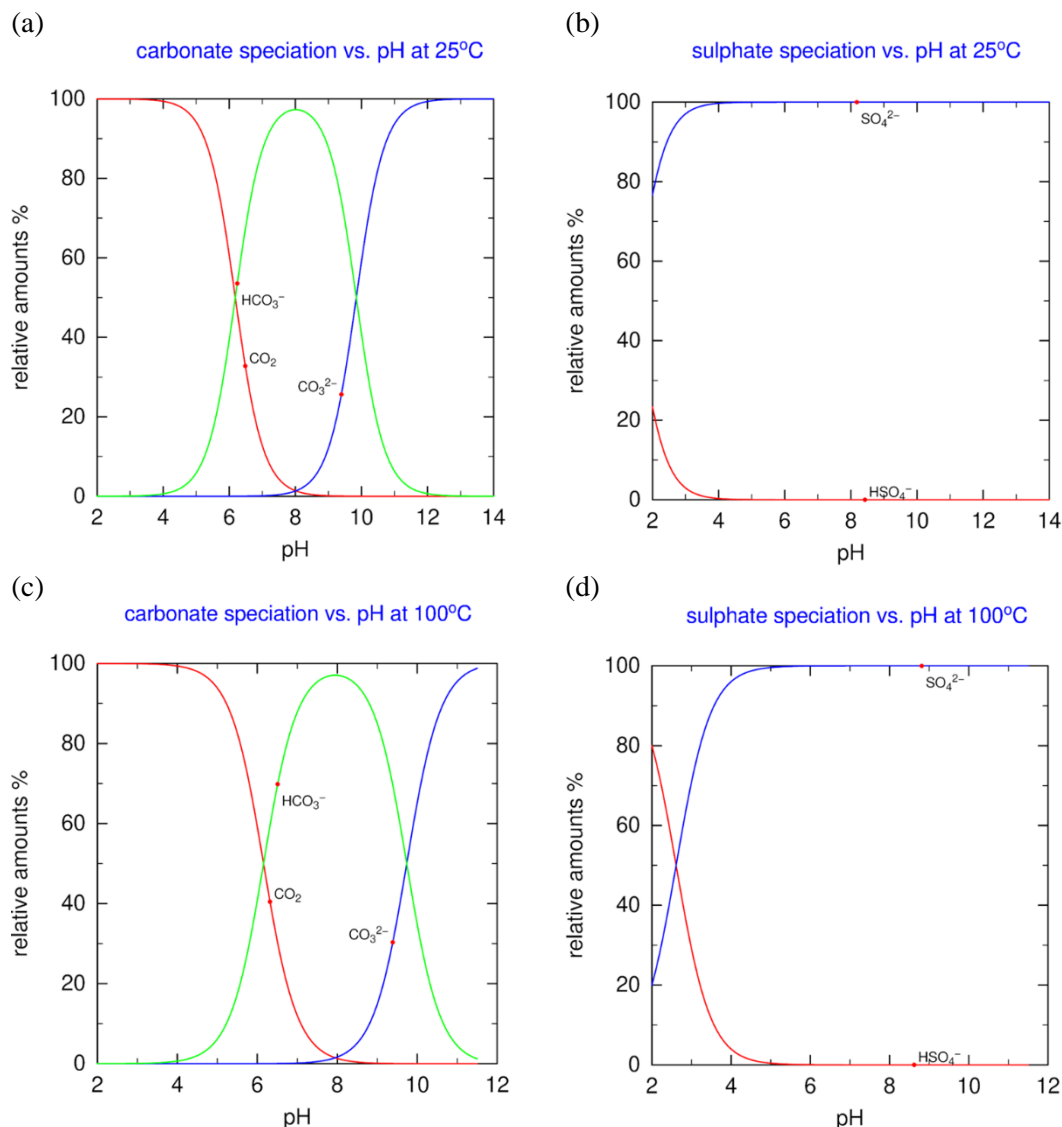


Fig.1–1 Carbon and sulphur aqueous speciation as a function of pH at 25 °C (a,b) and 100 °C (c,d) in 0.1 m NaCl background electrolyte using THEREDA database (v. 2020).

The choice between employing binary or ternary interaction parameters depends on the specific system under investigation and the concentrations of aqueous species that are controlled by the solubility of solids. In cases where the system can be adequately described, binary interaction parameters alone may suffice. Ternary mixing parameters become more significant when dealing with multi-salt mixtures that involve high concentrations of two or more ions but have no effect in systems dominated by one major electrolyte having other solutes in small concentrations.

To retrieve ternary interaction parameters, experiments with ternary mixtures at high concentrations are required. However, at elevated pH conditions in multicomponent systems, several solid phases containing Si, Al, Ca, and Mg become stable. As a result, the concentration of these elements decreases, making it impossible to obtain sufficiently high concentrations of Al and Si species, before the saturation of solids, necessary for retrieving the interaction parameter values. Additionally, the high concentrations needed for these parameters to have an effect are also not reached in calculations due to the predicted precipitation of solids (unless disequilibrium, oversaturated metastable conditions are present).

At elevated pH, the system of interest may have a high concentration of a background electrolyte, such as NaCl, NaOH, KCl, or KOH, while the species of interest, such as aqueous species of Al, Si, Ca, and Mg, are bound in stable solid phases with low solubility. Consequently, their interaction primarily occurs with the ions of the background electrolyte, making binary interaction parameters between species of interest and ions of the background electrolyte relevant and additional ternary interactions not necessary. Ternary interactions would therefore be necessary for conditions of a multicomponent background electrolyte.

For situations where the species of interest are present at low to trace concentrations, in the presence of an ionic medium, the $\beta^{(0)}$ and $\beta^{(1)}$ cation–anion interaction parameters appear to be sufficient in describing their activity coefficients, osmotic coefficients, and reaction constant data. Studies by Plyasunov et al. (1998) and Simoes et al. (2016) have shown that the Pitzer model can adequately describe osmotic coefficient experimental data for single electrolytes using only $\beta^{(0)}$ and $\beta^{(1)}$ parameters, while setting $C^{(\phi)}$, $\beta^{(2)}$, and $\alpha^{(2)}$ to zero. The parameter $C^{(\phi)}$, becomes significant only at high concentrations ($5 \text{ mol} \cdot \text{kg}^{-1}$) (Simoes et al., 2016) and is correlated with $\beta^{(1)}$ according to Plyasunov et al. (1998), while $\beta^{(2)}$, and $\alpha^{(2)}$ are necessary to account for the highly non-ideal behaviour of 2–2, 2–3 electrolytes at low concentrations and the effect of complexation.

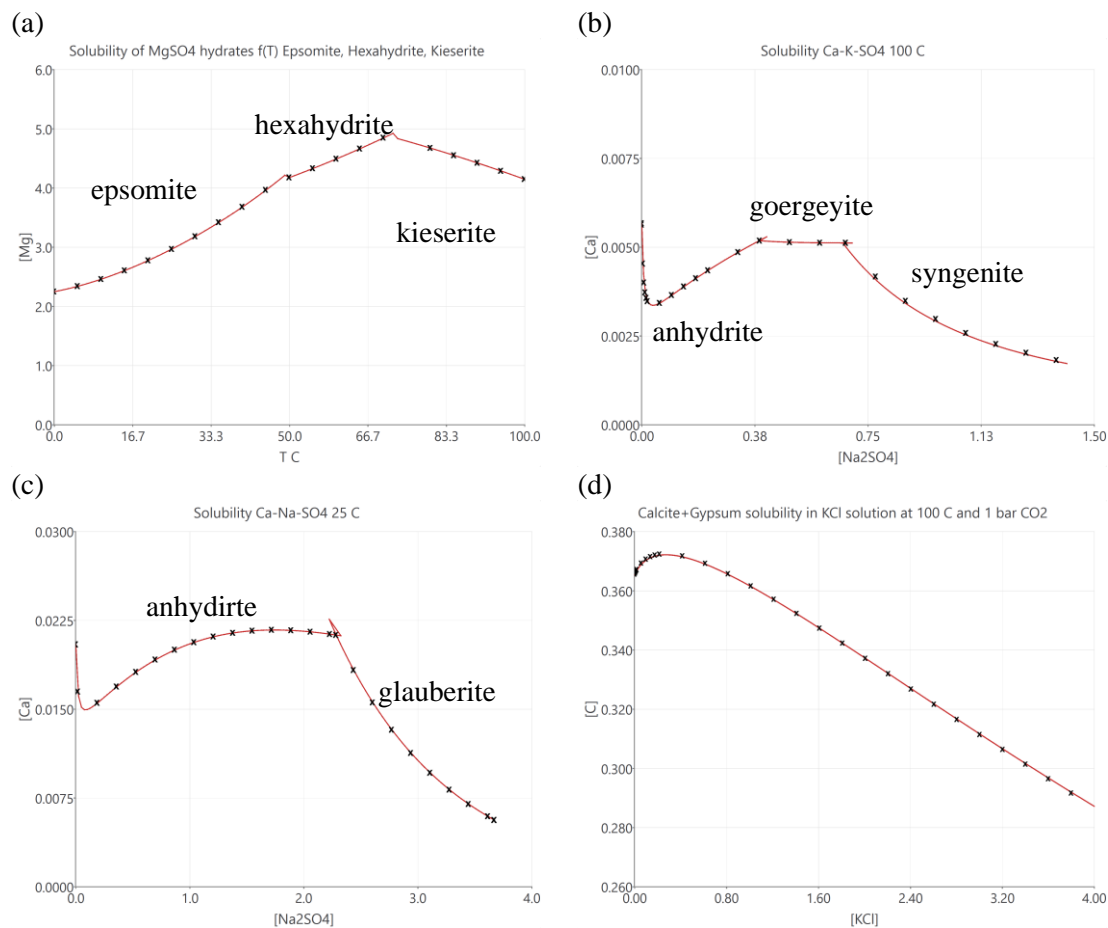


Fig. 1–2 Comparison between calculations using THEREDA database (v. 2020) with GEM–Selektor (curve) and PHREEQC (x)

The Pitzer IPs are retrieved from fitting against experimental data in binary and ternary electrolyte solutions. These are osmotic coefficient, complexation and solubility measurements. For the

present study, the Pitzer IPs were fitted against selected experimental data collected from literature using the GEMSFITS parameter optimization tool (Miron et al., 2015). Each experimental point was calculated in terms of the chemical equilibrium problem (Kulik et al., 2013) based on the input composition and temperature conditions for the defined system speciation, using the Pitzer model when calculating the activity coefficient. This was necessary for modelling each experiment, since it guaranteed consistency with the available data in THEREDA. The chemical system setup was done in GEM–Selektor v.3.9.6 (Kulik et al., 2013) modelling package using the standard state properties and base IPs of major ions and complexes from the THEREDA database. The code has been benchmarked against PHREEQC (interactive 3.7.3) (Parkhurst and Appelo, 2013) using the THEREDA database (v. 2020) so that the implementation of the Pitzer model using the same database produces the same results (Fig. 1–2).

The IPs were adjusted by the optimization algorithm to minimize the sum of squared difference between the measured and calculated data (least squares) of several kinds that were considered simultaneously. To avoid overfitting of the data, only the parameters that are sensitive to the measured values were adjusted. This was done by evaluating the parameter sensitivities and parameter correlation coefficients resulted from the fit (Miron et al., 2015).

In many cases there are not sufficient measurements that cover a wide enough range of temperatures and compositions to retrieve all the possible standard properties of solids and IPs with their temperature dependence within one system. To provide a dataset useful for calculations when experimental data is lacking several estimation methods are employed.

For estimating $\Delta_r S_m^\circ$ and $\Delta_r C_{p,m}^\circ$, necessary for calculating the temperature dependence of solubility and complexation, the chemical reactions are rewritten in isocoulombic / isoelectric form (Gu et al., 1994; Miron et al., 2020). For these reactions, $\Delta_r S_m^\circ$ and $\Delta_r C_{p,m}^\circ$ are small and can be assumed to be equal to zero allowing to estimate the unknown property if the properties of all the other reactants and products are known. This assumption leads to smaller errors when doing calculations at elevated temperatures than in the case of just using non isocoulombic / isoelectric reactions (Gu et al., 1994; Miron et al., 2020).

For estimating Pitzer IPs, the charge analogy (Reardon, 1990) or the relation with the SIT parameters (Plyasunov et al., 1998) can be used. The relation with SIT is especially relevant for NaCl electrolytes for which SIT parameters were available. When no SIT parameters were available, these can be derived from the relation to the species charge proposed by Hummel and Thoenen (2023).

1.1 Parameterization strategy

Depending on the available data and species predominance (Fig.1–1) the following strategy was adopted for deriving a set of polythermal interaction parameters for Si and Al species in the system Al–Si–Ca–Mg–Na–K–Cl–SO₄–CO₃–H₂O from low to high pH.

From all possible binary and ternary IPs combinations between Al and Si species and ions of the oceanic salt system only the ones for which all species are present in significant concentrations at relevant conditions were retained for the dataset. For example, no interaction parameters with species H⁺, HSO₄⁻, CO₂(aq), dominant at low pH, were retained for species dominant at high pH.

For the relevant binary and ternary interactions, initial parameter values were set based on analogy with carbonate and sulphate species of the same charge (Reardon, 1990). Where SIT interaction parameters with Na⁺ and Cl⁻ were available in the Nagra/PSI TDB 2020 (Hummel and Thoenen 2023), these SIT parameters were used to estimate values for the $\beta^{(0)}$ and $\beta^{(1)}$ cation–anion interaction parameters using the relation of Plyasunov et al. (1998) (Table 1-1).

Table 1-1 Relation between SIT and Pitzer parameters for different ion combinations at 25 °C (Plyasunov et al., 1998).

Ion combination	$\beta^{(0)} - \varepsilon_\gamma/2$	$\beta^{(1)}$
M ⁺ , X ⁻	0.035	0.34
M ²⁺ , X ⁻ and M ⁺ , X ²⁻	0.150	1.56
M ³⁺ , X ⁻ and M ⁺ , X ³⁻	0.366	4.29
M ⁴⁺ , X ⁻ and M ⁺ , X ⁴⁻	0.754	8.89

The initial parameter values were refined/refitted against selected experimental data. Only the parameter values which were sensitive to the experimental data were changed while the remaining ones were kept as estimates. Details on the estimations, selection of experimental data and fits results are described in the following sections.

For a special case, parameters describing the interaction with K⁺ values could be estimated assuming an equal difference for:

$$\text{IP}(\text{Na}^+, \text{anion}) - \text{IP}(\text{Na}^+, \text{Si_species}) = \text{IP}(\text{K}^+, \text{anion}) - \text{IP}(\text{K}^+, \text{Si_species}) \quad 1-3$$

THEREDA from fit = THEREDA Unknown?

This relates to the activity of the solutes and their interactions. It was used by Wesolowski (1992) for deriving IPs with K from Na in the system Na–K–Al–OH⁻Cl (see section 3.4.2).

Peer-reviewed papers and published reports were examined for collecting necessary experimental data, mainly solid–liquid equilibria/solubilities and isopiestic measurements of osmotic coefficients. The extensive work of Meyer and Willms (Meyer, 2006; Meyer and Willms, 2008) was evaluated as a basis for building the experimental dataset. Their work contains extensive data for binary and ternary Si and Al-containing systems at ambient and elevated temperatures.

The fitting workflow (Fig. 1–3) involved multiple iterations, wherein different parameter configurations were optimized to identify the ideal set of sensitive parameters capable of reproducing the data. This process might entail the inclusion of new experimental data or adjustments to the model, selecting relevant/sensitive parameters, parameter estimation, setting the fitted parameters and fixed parameters, and changes to the aqueous speciation. These iterations were repeated until an optimal solution was achieved (Fig. 1–3). The result was a set of Pitzer interaction parameters that is consistent with the system speciation and the species of the oceanic salt system in THEREDA.

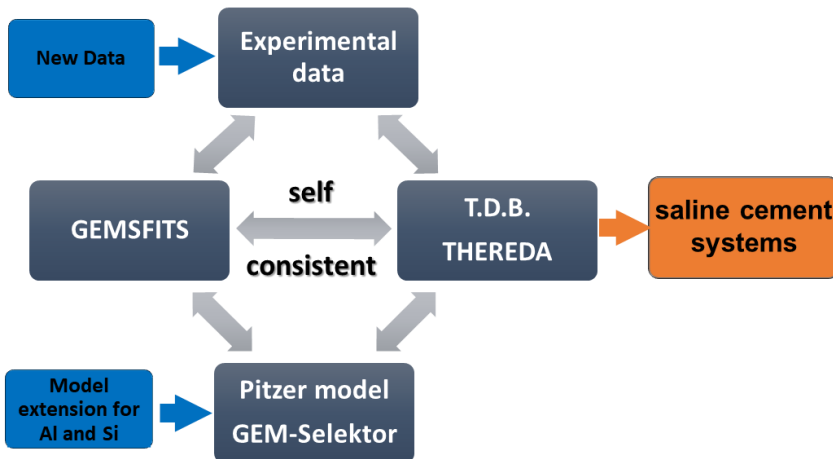


Fig. 1–3 Workflow for extending the Pitzer model with interaction parameters for Al and Si species consistent with the THEREDA database, form modelling of cementitious materials in highly saline systems.

Given the complexity of chemical systems, which involve a multitude of parameters, e.g., IPs, species and their standard thermodynamic properties, it is possible that different equally good datasets can be derived. This explains the existence of various Pitzer parameters datasets derived for similar systems in the literature. Crucially, maintaining internal consistency within a dataset is paramount. Differences could also be found for the available oceanic salt system datasets; therefore, the newly derived dataset of Si and Al is consistent with the base data in THEREDA. The dataset had to demonstrate also its ability to replicate accurately the data across a broad spectrum of conditions, at the very least for those conditions used during the fitting procedure.

In the following, fitted parameter values were marked in **bold** typeface while estimated values were reported in *italic* typeface. Values that were based on convention or that were taken from estimates but were evaluated against measured data (sensitive but kept fixed during the fit) are given in normal typeface.

2 Si

Silicon is a ubiquitous element in the environment occurring in various amorphous, crystalline, and dissolved forms. The aqueous speciation is influenced by the dissolved silica concentration, pH, temperature, and *I*. At concentrations of dissolved silica <0.01m its aqueous speciation is well described by monomeric species such as the ortho silicic acid $\text{H}_4\text{SiO}_4(\text{aq})$, and the deprotonated species H_3SiO_4^- , and $\text{H}_2\text{SiO}_3^{2-}$ that become more important with increasing pH.

To ensure a consistent set of standard thermodynamic data and Pitzer model IPs, the standard thermodynamic properties for Si solids, including α -quartz (THEREDA notation: $\text{SiO}_2\text{-alpha_Qtz(cr)}$) and amorphous silica ($\text{SiO}_2(\text{am})$), were assessed. Additionally, the thermodynamic properties of relevant aqueous species within the pH range from 2 to 14 (Fig. 2–1) were reassessed. These species include $\text{Si}(\text{OH})_4(\text{aq})$, $\text{SiO}(\text{OH})_3^-$, and $\text{SiO}_2(\text{OH})_2^{2-}$, as well as aqueous complexes formed between Si and alkaline metals and alkaline (earth) metals, such as $\text{NaSiO}_2(\text{OH})_2^-$, $\text{KSiO}_2(\text{OH})_2^-$, $\text{CaSiO}(\text{OH})_3^+$, $\text{CaSiO}_2(\text{OH})_2(\text{aq})$, $\text{MgSiO}(\text{OH})_3^+$, and $\text{MgSiO}_2(\text{OH})_2(\text{aq})$. The standard thermodynamic data mentioned above were re-evaluated and, where necessary, revised based on available experimental data. Possible species between Al and Si are discussed in section 3.4.3.

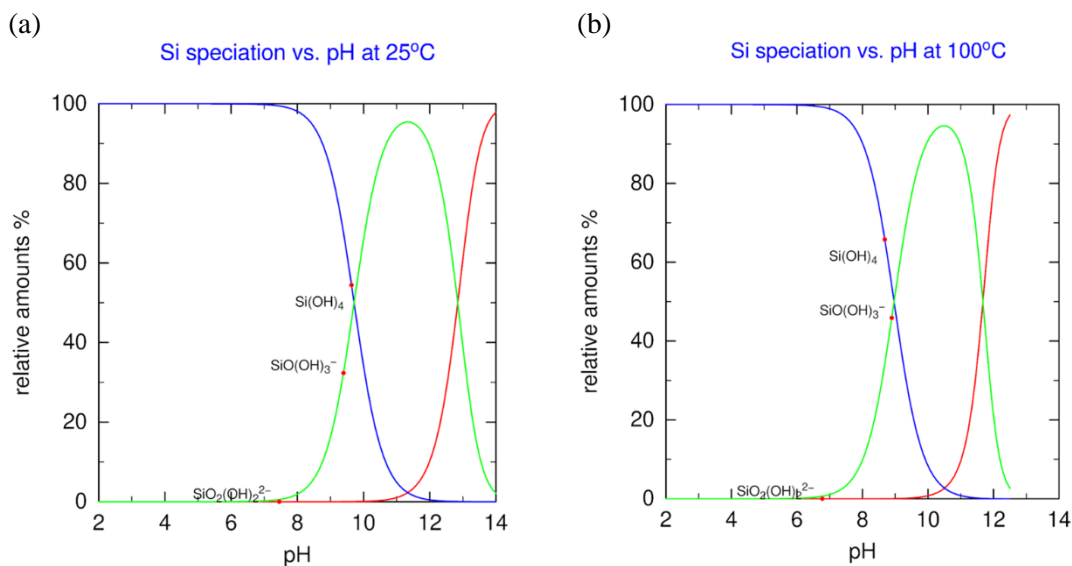


Fig. 2–1 Si aqueous speciation as a function of pH at 25 °C (a) and 100 °C (b) in 0.1 M NaCl background electrolyte using THEREDA database (v. 2020).

2.1 Standard thermodynamic data for the system Si–O–H

The standard state thermodynamic data for the Si–O–H system in THEREDA was previously reviewed by Wilhelm (Wilhelm, 2013). Wilhelm selected the thermodynamic properties of α -quartz, $\text{SiO}_2(\text{am})$, and silica aqueous species ($\text{Si}(\text{OH})_4(\text{aq})$) at the reference temperature and pressure, along with their temperature dependence. α -Quartz from CODATA (Cox et al., 1989) was utilized as an anchor phase to calculate the standard thermodynamic properties of other silica solids and aqueous species. The temperature dependence of α -quartz and $\text{SiO}_2(\text{am})$ solubility in water was parameterized by Gunnarsson & Arnórsson (Gunnarsson and Arnórsson, 2000), based on a thorough review of measured solubility data, and is valid in the temperature

range from 0 to 350 °C. By utilizing these two temperature dependence Eqs. (2–1, 2–2) and the reference thermodynamic properties of Si(cr), α -quartz(cr) from CODATA (Table 2–1), a consistent set of reference thermodynamic properties for $\text{SiO}_2(\text{am})$ and $\text{Si}(\text{OH})_4(\text{aq})$ was derived in THEREDA.

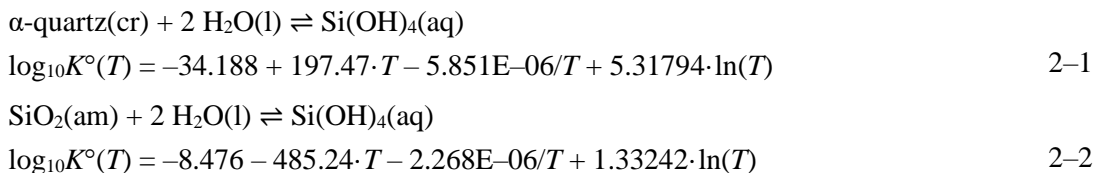


Table 2-1 Reference standard thermodynamic properties for Si element and quartz.

	$\Delta_f H_{298}^\circ$ $\text{J} \cdot \text{mol}^{-1}$	$\Delta_f S_{298}^\circ$ $\text{J} \cdot \text{K}^{-1} \cdot \text{mol}^{-1}$	$\Delta_f C_{p,298}^\circ$ $\text{J} \cdot \text{K}^{-1} \cdot \text{mol}^{-1}$	References
Si(cr)		18.81 ± 0.08	19.789 ± 0.003	(Cox et al., 1989)
α -quartz(cr)	$-(910700 \pm 1000)$	41.46 ± 0.2	44.602 ± 0.3	(Cox et al., 1989)

In the previous data evaluation by Hummel et al. (Hummel et al., 2002), the value for $\Delta_f C_{p,m}^\circ$ of $\text{Si}(\text{OH})_4(\text{aq})$ ($195.204 \text{ J} \cdot \text{K}^{-1} \cdot \text{mol}^{-1}$) was based on an assumption of $\Delta_r C_{p,m}^\circ = 0$ (2–1). However, in the present update, the $\Delta_f C_{p,m}^\circ$ ($237.368 \pm 2 \text{ J} \cdot \text{K}^{-1} \cdot \text{mol}^{-1}$) was calculated to be consistent with the Eq. 2–1 coefficients (Gunnarsson and Arnórsson, 2000), and $\Delta_r C_{p,m}^\circ = 42.066 \pm 2 \text{ K}^{-1} \cdot \text{mol}^{-1}$ (2–1). This revision was also done in the Nagra/PSI TDB 2020 update (Hummel and Thoenen, 2023). Although a significant difference appears in calculations above 200 °C (Wilhelm, 2013) when using either of the two values, the $\Delta_r C_{p,m}^\circ$ value ensures consistency between the thermodynamic properties and the evaluation of Gunnarsson and Arnórsson (2000).

The standard thermodynamic data for the Si acid species, $\text{SiO}(\text{OH})_3^-$, and $\text{SiO}_2(\text{OH})_2^{2-}$ were based on the data of (Busey and Mesmer, 1978) (see section 2.3).

2.2 Polythermal IPs for $\text{Si}(\text{OH})_4(\text{aq})$

At acidic and near-neutral pH conditions (< 9), the dominant species of SiO_2 in solution is the monomer $\text{Si}(\text{OH})_4(\text{aq})$. This species plays a significant role in acidic brines and ordinary groundwaters. To model the influence of electrolyte solutions on the concentration of the neutral silicate species $\text{Si}(\text{OH})_4(\text{aq})$ accurately and perform calculations at different temperatures, a set of IPs and their temperature dependence coefficients are required. Within the framework of the Pitzer model, the relevant parameters for the interaction between neutral aqueous species and charged species include λ_a (neutral, anion), λ_c (neutral, cation), ζ (neutral, cation, anion), η_a (neutral, anion, anion'), and η_c (neutral, cation, cation'). Ternary IPs ζ and η can be relevant in multicomponent systems at very high concentrations.

Various experimental datasets were available for parameterizing the model. These datasets consisted primarily of binary systems, with some including ternary solutions, and covered a wide range of temperatures and compositions (see Table 2–2). For deriving the model parameters, only data up to 300 °C were considered. Beyond this temperature, the density of the water solvent

decreases as it approaches the critical point, resulting in decreased accuracy of thermodynamic functions. Although a limited amount of data exists at higher temperatures, these temperatures are outside the range of interest for THEREDA. During the parameterization process, no inconsistencies within this temperature range were identified between the derived model and the basis oceanic salts system in THEREDA, even though part of the oceanic salt system is parameterized with data of a narrower temperature interval.

Table 2-2 Experimental data on $\text{SiO}_2(\text{am})$ solubility in electrolyte solutions. * only data up to 300 °C were used in the fit.

Reference	System	T (°C)	Concentration range (m)
(Marshall and Warakomski, 1980)	NaCl	25	0–6.14
	KCl		0–4.81
	LiCl		0–19.19
	MgCl ₂		0–5.78
	CaCl ₂		0.43–6.03
	Na ₂ SO ₄		0–1.97
	NaHCO ₃		0–1.29
	KNO ₃		0–3.76
	LiNO ₃		0–12.08
	MgSO ₄		0–3.03
(Marshall, 1980)	NaNO ₃	25–300	0–6.12
(Meyer, 2006)	NaCl	25	0–5.61
	KCl		0–4.57
	MgCl ₂		0–5.82
	CaCl ₂		0–4.57
	K ₂ SO ₄		0–0.7
	NaCl + CaCl ₂		0–4.5 + 0–3.5
	NaCl + MgCl ₂		0–4 + 0–1.5
	KCl + CaCl ₂		0–3.5 + 0–3
	KCl + MgCl ₂		0–3 + 0–1.6
	Na ₂ SO ₄ + K ₂ SO ₄		0–2 + 0–0.6
(Gallup, 1989)	CaCl ₂ + MgCl ₂		0–2 + 0–2
	NaCl	25–250	3.18–5.8
	MgCl ₂		1.02–5.8
	CaCl ₂		1.02
(Chen and Marshall, 1982)	KCl		0–3.31
	NaCl	25–350*	0.19–6.4
	Na ₂ SO ₄		0.1–3.1
	MgCl ₂		0.5–7
	MgSO ₄		0.06–3.61

Reference	System	T (°C)	Concentration range (m)		
(Meyer and Willms, 2008)	NaCl	25–90	0–5.8		
	KCl		0–4.5		
	MgCl ₂		0–5.8		
	CaCl ₂		0–4.8		
	Na ₂ SO ₄ + K ₂ SO ₄		0–1.8	+	0–0.7
	NaCl + CaCl ₂		0.1–1.0	+	0.1–2
	KCl + CaCl ₂		0.1–0.7	+	0.3–1.8
	NaCl + KCl		0.1–0.84	+	0.1–0.3
	NaCl + MgCl ₂		0.1–0.9	+	0.07–1.4
	KCl + MgCl ₂		0.1–0.65	+	0.07–1.5
	CaCl ₂ + MgCl ₂		0.3–1.3	+	0.1–1.4
(Felmy et al., 1994)	HCl	22–47	0–2.1		
	NaNO ₃		0–4.6		
(Elmer and Nordberg, 1958)	HNO ₃	36–95	0–15		

The $\lambda(\text{Si(OH)}_4\text{(aq)}, \text{cation or anion})$ IPs, representing the interaction of $\text{Si(OH)}_4\text{(aq)}$ with cations and anions of the oceanic salt systems, were previously estimated by Reardon (Reardon, 1990) based on the analogy with $\text{CO}_2\text{(aq)}$. Experimental data from Marshall and collaborators (Chen and Marshall, 1982; Marshall, 1980; Marshall and Warakomski, 1980) on the solubility of $\text{SiO}_2\text{(am)}$ in various electrolyte solutions at different temperatures (Table 2-2) were used by Felmy et al. (1994), Azaroual et al. (1997), and Meyer (Meyer, 2006; Meyer and Willms, 2008) to derive different polythermal λ IP sets that accurately describe the solubility data. Meyer conducted additional measurements with $\text{SiO}_2\text{(am)}$ in electrolyte solutions at different temperatures, including ternary mixed electrolyte common ion solutions (Table 2-2), and utilized all available data to derive a comprehensive polythermal λ IP set. Gallup (1989) contributed additional experimental data points that overlapped with the measurements by Marshall et al. (Table 2-2). For acidic conditions, the solubility of $\text{SiO}_2\text{(am)}$ was determined by Felmy et al. (1994) in HCl and by Elmer & Nordberg (1958) in HNO₃ solutions, respectively.

Measurements conducted in common ion salt solutions, such as $\text{MgSO}_4\text{--CaSO}_4$, can provide valuable data for deriving binary IPs between ions of the same charge, such as θ_c (e.g., Mg^{2+} – Ca^{2+}), or ternary IPs. When considering the neutral species $\text{Si(OH)}_4\text{(aq)}$, ζ (e.g., $\text{Si(OH)}_4\text{(aq)}$, Mg^{2+} , SO_4^{2-}) or η_c (e.g., $\text{Si(OH)}_4\text{(aq)}$, Na^+ , K^+) IPs can be evaluated from such experiments. Azaroual et al. (1997) suggest that $\text{SiO}_2\text{(am)}$ solubility experiments in electrolyte solutions with $I < 7 \text{ m}$ can be described well without introducing ternary IPs. However, Meyer (2006; 2008) and Felmy et al. (1994) utilized ternary (ζ) IPs when deriving their parameter sets. The need for employing ternary IPs was evaluated in this work.

It is important to note that measurements of $\text{SiO}_2\text{(am)}$ solubility can be subject to systematic errors arising from differences in the batches of $\text{SiO}_2\text{(am)}$ used in the experiments. Factors such as grain size, surface effects, and sample preparation methods can contribute to these variations (Marshall, 1980; Marshall and Warakomski, 1980). The measured data was scaled to the same solubility in water using the reported measured value and the calculated reference $\log_{10}K^\circ(T)$ values of the $\text{SiO}_2\text{(am)}$ solubility in water (Eq. 2–2). The values from one set of measurements conducted at a

given temperature and various electrolyte concentrations were multiplied by the ratio of the measured $\text{SiO}_2(\text{am})$ solubility in water for that specific experimental set to the calculated solubility in pure water (based on the standard thermodynamic properties of $\text{SiO}_2(\text{am})$ and $\text{Si}(\text{OH})_4(\text{aq})$ as selected in THEREDA). This was needed for deriving a consistent polythermal set of λ IPs that were not affected by discrepancies in $\text{SiO}_2(\text{am})$ batches and refer to the same standard state properties of $\text{Si}(\text{OH})_4(\text{aq})$ and $\text{SiO}_2(\text{am})$. The resulted IPs were determined only by the interactions of $\text{Si}(\text{OH})_4(\text{aq})$ with the electrolyte.

Previously published parameter sets were fitted to match selected experimental data, but inconsistencies arise from the use of different conventions and parameter values, as well as temperature coefficients, for the interactions within the hexary system of oceanic salts. In the derived IP set by Meyer & Willms (2008), the HMW (Harvie et al., 1984) parameter values for the basis major electrolyte interactions were employed. It is important to note that $\lambda(\text{Si}(\text{OH})_4(\text{aq}), \text{cation or anion})$ can only be derived in pair combinations, dissolved cation and anion, and thus, conventionally, one ion's IP in the dataset needs to be set to zero. This choice affects only the formal ion activity coefficient, while the mean activity coefficient and equilibrium calculations remain unaffected (Clegg et al., 2022). Different studies have made different choices regarding which ion to set to zero. For instance, Wilhelm (2013) set the IPs with H^+ to zero, while Azaroual et al. (1997) set the IPs with Cl^- to zero. THEREDA does not provide specific guidelines for this choice, leaving it to expert judgment. In THEREDA, for example, $\lambda(\text{O}_2(\text{aq}), \text{Cl}^-)$ and $\lambda_a(\text{CO}_2(\text{aq}), \text{H}^+)$ were set to 0, respectively. The limited measured data in HCl solutions would not allow to derive accurate polythermal coefficients for $\lambda(\text{Si}(\text{OH})_4(\text{aq}), \text{Cl}^-)$. The influence of interactions with H^+ is significant only at very low pH (< 2), while Cl^- is a common ion in natural and experimental systems across a wide range of temperature and concentrations and affects the IPs values for all other cations of chloride salts. Therefore, λ was set to zero for the interaction of $\text{Si}(\text{OH})_4(\text{aq})$ with Cl^- , and the remaining parameters were derived by fitting them to the experimental data.

After several trial fits, it was observed that all experimental data in binary solutions could be fitted using just two temperature coefficients, A and B, (Eq. 1–1). Coefficient A represents the value of the IP at 25 °C, while coefficient B describes a linear temperature dependence against the inverse of temperature. Further attempts to incorporate additional temperature coefficients did not result in improved fits. The coefficients from Eq. 1–1 are correlated. Precise experimental data describing subtle changes of the IP with temperature were necessary for accurate fitting. Within the variability of the selected data the use of A and B was sufficient.

Azaroual and Meyer (Azaroual et al., 1997; Meyer and Willms, 2008) noted that the solubility of $\text{SiO}_2(\text{am})$ in CaCl_2 and MgCl_2 solutions exhibits minimal differences and falls within the range of experimental scatter. During the fitting process, it was observed that the temperature dependence of the interactions between $\text{Si}(\text{OH})_4(\text{aq})$ and Na^+ as well as K^+ was very similar. Additionally, the experimental data in sulphate solutions could be satisfactorily described by setting the B temperature coefficients (Eq. 1–1) for the interaction between $\text{Si}(\text{OH})_4(\text{aq})$ and SO_4^{2-} to zero. With these insights, the fitting procedure incorporated the following constraints:

since $\lambda(\text{Si}(\text{OH})_4(\text{aq}), \text{Ca}^{2+}) = \lambda(\text{Si}(\text{OH})_4(\text{aq}), \text{Mg}^{2+})$, temperature coefficients

B of $\lambda(\text{Si}(\text{OH})_4(\text{aq}), \text{Na}^+)$ = B of $\lambda(\text{Si}(\text{OH})_4(\text{aq}), \text{K}^+)$ and

B of $\lambda(\text{Si}(\text{OH})_4(\text{aq}), \text{SO}_4^{2-}) = 0$

Several trial fits were conducted to determine the optimal values for these parameters individually. However, it was found that the quality of the fit could not be significantly improved by adjusting them independently.

The absolute values of the IPs are influenced by the choice of which IP was arbitrarily set to zero (in this case, $\lambda(\text{Si}(\text{OH})_4(\text{aq}), \text{Cl}^-) = 0$). It is worth noting that the effect of individual ions on the

activity coefficient (γ) of $\text{Si}(\text{OH})_4(\text{aq})$ is additive, similar to the findings of Clegg and Brimblecombe (1990) for $\text{O}_2(\text{aq})$. As a result, additive relations can be employed to convert the IPs to different conventions, such as setting $\lambda(\text{Si}(\text{OH})_4(\text{aq}), \text{H}^+)$ to zero, by using the following constraints:

$$\begin{aligned} A \lambda(\text{Si}(\text{OH})_4(\text{aq}), \text{Na}^+) + A \lambda(\text{Si}(\text{OH})_4(\text{aq}), \text{Cl}^-) &= 0.1 \\ B \lambda(\text{Si}(\text{OH})_4(\text{aq}), \text{Na}^+/\text{K}^+/\text{H}^+) + B \lambda(\text{Si}(\text{OH})_4(\text{aq}), \text{Cl}^-) &= 40 \\ A \lambda(\text{Si}(\text{OH})_4(\text{aq}), \text{H}^+) + A \lambda(\text{Si}(\text{OH})_4(\text{aq}), \text{Cl}^-) &= 0.146 \\ A \lambda(\text{Si}(\text{OH})_4(\text{aq}), \text{K}^+) + A \lambda(\text{Si}(\text{OH})_4(\text{aq}), \text{Cl}^-) &= 0.04 \\ A \lambda(\text{Si}(\text{OH})_4(\text{aq}), \text{Ca}^{2+}/\text{Mg}^{2+}) + 2*A \lambda(\text{Si}(\text{OH})_4(\text{aq}), \text{Cl}^-) &= 0.35 \\ B \lambda(\text{Si}(\text{OH})_4(\text{aq}), \text{Ca}^{2+}/\text{Mg}^{2+}) + 2*B \lambda(\text{Si}(\text{OH})_4(\text{aq}), \text{Cl}^-) &= 144 \\ 2*A \lambda(\text{Si}(\text{OH})_4(\text{aq}), \text{Na}^+) + A \lambda(\text{Si}(\text{OH})_4(\text{aq}), \text{SO}_4^{2-}) &= 0.1 \\ 2*B \lambda(\text{Si}(\text{OH})_4(\text{aq}), \text{Na}^+) + B \lambda(\text{Si}(\text{OH})_4(\text{aq}), \text{SO}_4^{2-}) &= 80 \\ A \lambda(\text{Si}(\text{OH})_4(\text{aq}), \text{Na}^+) + A \lambda(\text{Si}(\text{OH})_4(\text{aq}), \text{HCO}_3^-) &= 0.095 \\ B \lambda(\text{Si}(\text{OH})_4(\text{aq}), \text{Na}^+) + B \lambda(\text{Si}(\text{OH})_4(\text{aq}), \text{HCO}_3^-) &= 40 \text{ (assumed the same as with Cl⁻)} \end{aligned}$$

There is no available experimental data at elevated temperatures to determine the temperature dependence of $\lambda(\text{Si}(\text{OH})_4(\text{aq}), \text{HCO}_3^-)$. However, based on the assumption that the B coefficient for this interaction is similar to that of $\lambda(\text{Si}(\text{OH})_4(\text{aq}), \text{Cl}^-)$ (which is 0), we could estimate that $B \lambda(\text{Si}(\text{OH})_4(\text{aq}), \text{Na}^+) + B \lambda(\text{Si}(\text{OH})_4(\text{aq}), \text{HCO}_3^-)$ equals 40. Additionally, there is no measured data for evaluating $\lambda(\text{Si}(\text{OH})_4(\text{aq}), \text{CO}_3^{2-})$. Nevertheless, the CO_3^{2-} species becomes significant at higher pH levels where $\text{Si}(\text{OH})_4(\text{aq})$ is less dominant. Consequently, the impact of this interaction on solubility calculations should be minimal. We can assume an IP equal to that with SO_4^{2-} and with the same temperature dependence. The final A and B coefficients of Eq. 1–1 for $\lambda(\text{Si}(\text{OH})_4(\text{aq}), \text{cation or anion})$ can be found in Table 2-3.

Table 2-3 Coefficients for the temperature function (Eq. 1–1) of ion IPs with $\text{Si}(\text{OH})_4(\text{aq})$.

IP coefficients Eq. 1–1	A	B	T (°C)	Concentration range (m)
$\lambda(\text{Si}(\text{OH})_4(\text{aq}), \text{Cl}^-)^*$	0	0	25–300	
$\lambda(\text{Si}(\text{OH})_4(\text{aq}), \text{H}^+)$	0.146	40	25–95	0–4.6
$\lambda(\text{Si}(\text{OH})_4(\text{aq}), \text{Na}^+)$	0.100	40	25–300	0–6.4
$\lambda(\text{Si}(\text{OH})_4(\text{aq}), \text{K}^+)$	0.040	40	25–300	
$\lambda(\text{Si}(\text{OH})_4(\text{aq}), \text{Ca}^{2+})$	0.350	144	25–300	
$\lambda(\text{Si}(\text{OH})_4(\text{aq}), \text{Mg}^{2+})$	0.350	144	25–300	0–7
$\lambda(\text{Si}(\text{OH})_4(\text{aq}), \text{SO}_4^{2-})$	–0.15	0	25–300	
$\lambda(\text{Si}(\text{OH})_4(\text{aq}), \text{HCO}_3^-)$	–0.05	0	25–100	
$\lambda(\text{Si}(\text{OH})_4(\text{aq}), \text{CO}_3^{2-})^{**}$	–0.15	0	25	<i>n.a.</i>

* by convention; ** estimated as analogue to IP with SO_4^{2-}

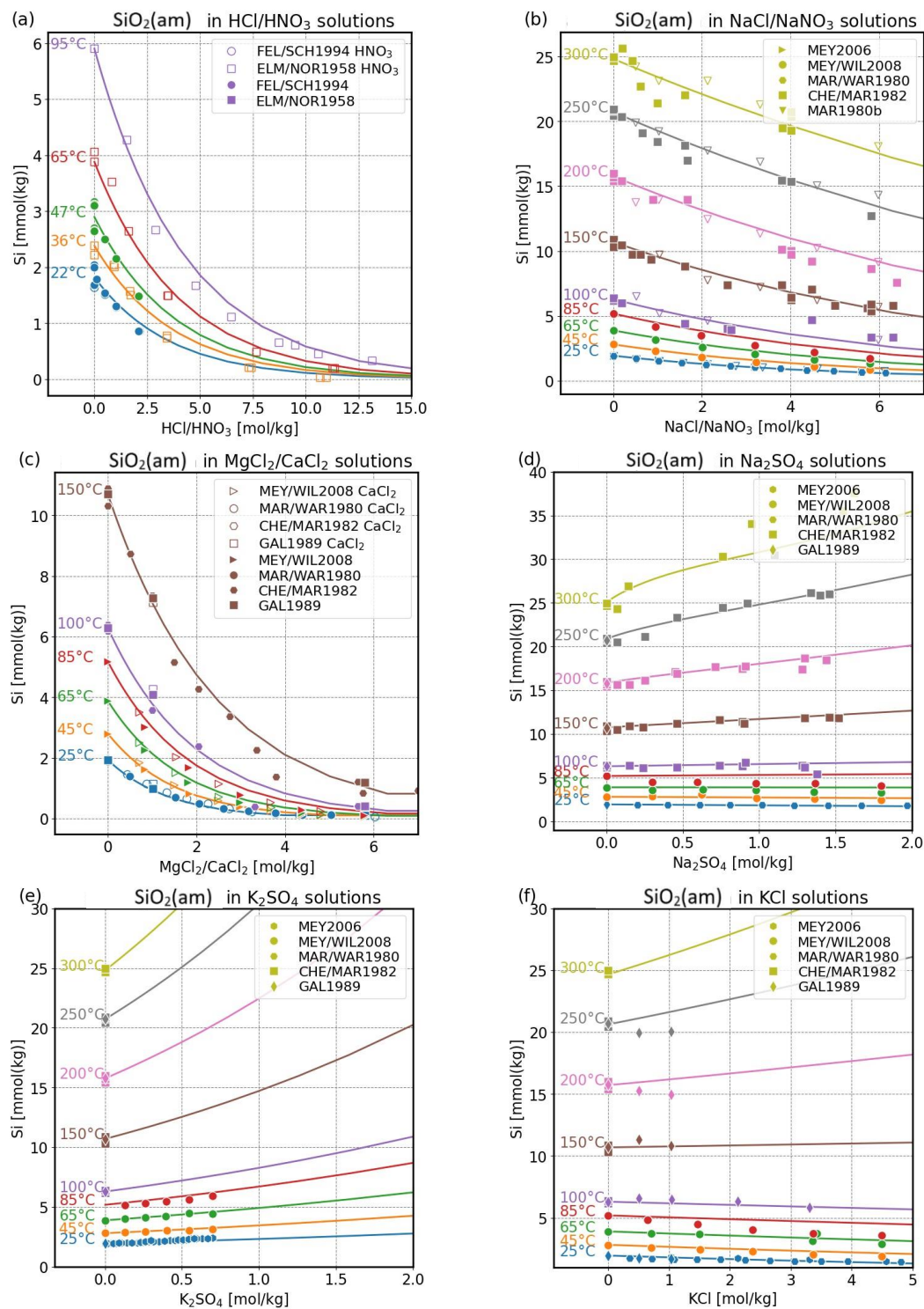


Fig. 2–2 Comparison between measured (symbols) and calculated (lines) $\text{SiO}_2(\text{am})$ solubility in different binary electrolyte solutions at different temperatures. Empty symbols in a, and b are experiments done in HNO_3 and NaNO_3 solutions but modelled assuming HCl and NaCl solutions of equivalent concentrations.

The experimental data in binary electrolyte solution could be fitted well using λ binary IPs (Fig. 2–2). Furthermore, the addition of ternary $\zeta(\text{Si(OH)}_4\text{(aq)}, \text{cation}, \text{anion})$ IPs was tested, but it did not result in any improvement to the fit (there was no change in the mean squared error). Therefore, it is concluded that additional ζ ternary parameters are not necessary to accurately describe the experimental data in binary electrolyte solutions.

The $\lambda(\text{Si(OH)}_4\text{(aq)}, \text{H}^+)$ was fitted based on measured data in HCl solutions. Marshall and Warakomski (1980) showed that NaCl and NaNO₃ solutions have indistinguishable effect on the SiO₂(am) solubilities at investigated temperatures and concentrations. This makes it possible to complement the available data in HCl solutions with analogous measurements in nitric acid solutions at 36, 65, and 95 °C (Elmer and Nordberg, 1958) and better constrain the temperature dependence of the IP. The experimental data in HNO₃ and NaNO₃ can be modelled using the equivalent concentrations of HCl and NaCl (Fig. 2–2 a, b).

The calculated solubilities in ternary systems were compared to the measured values using the binary IPs obtained from the solubilities in binary electrolyte solutions. This comparison aimed to determine if the model, based on the binary systems, could reproduce the ternary data within the experimental uncertainty without the need of additional parameters such as the such as the $\eta_c(\text{Si(OH)}_4\text{(aq)}, \text{cation}, \text{cation}')$ and $\zeta(\text{Si(OH)}_4\text{(aq)}, \text{cation}, \text{anion})$.

The ternary systems investigated by Meyer & Willms (2006; 2008) involved the presence of a shared anion and different cations. Comparisons between model calculated and measured values show fairly good agreement (Fig. 2–3). Trial fits were made with the addition of $\eta_c(\text{Si(OH)}_4\text{(aq)}, \text{cation}, \text{cation}')$ and $\zeta(\text{Si(OH)}_4\text{(aq)}, \text{cation}, \text{anion})$ IPs.

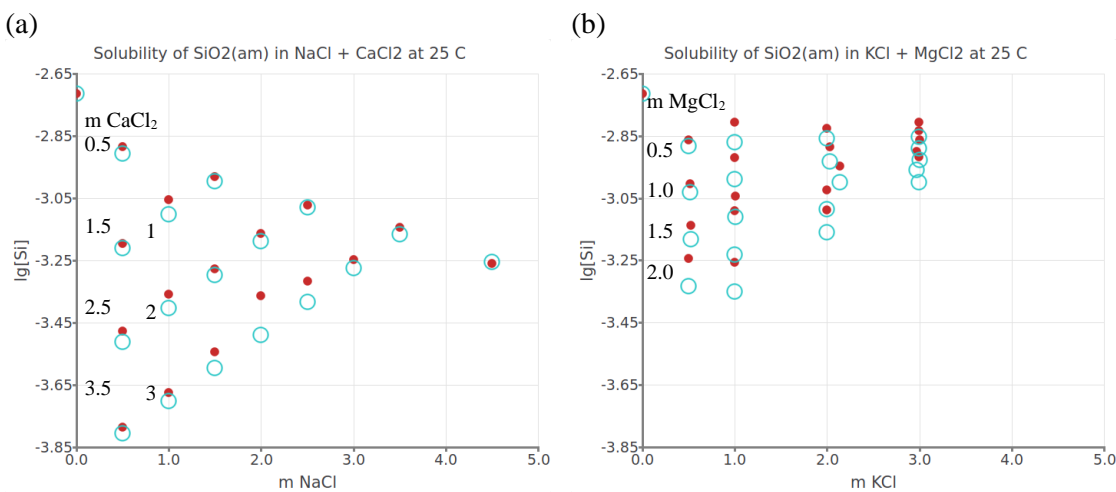


Fig. 2–3 Comparison between measured (full circles) and calculated (empty circles) SiO₂(am) solubility in ternary electrolyte solutions at 25 °C.

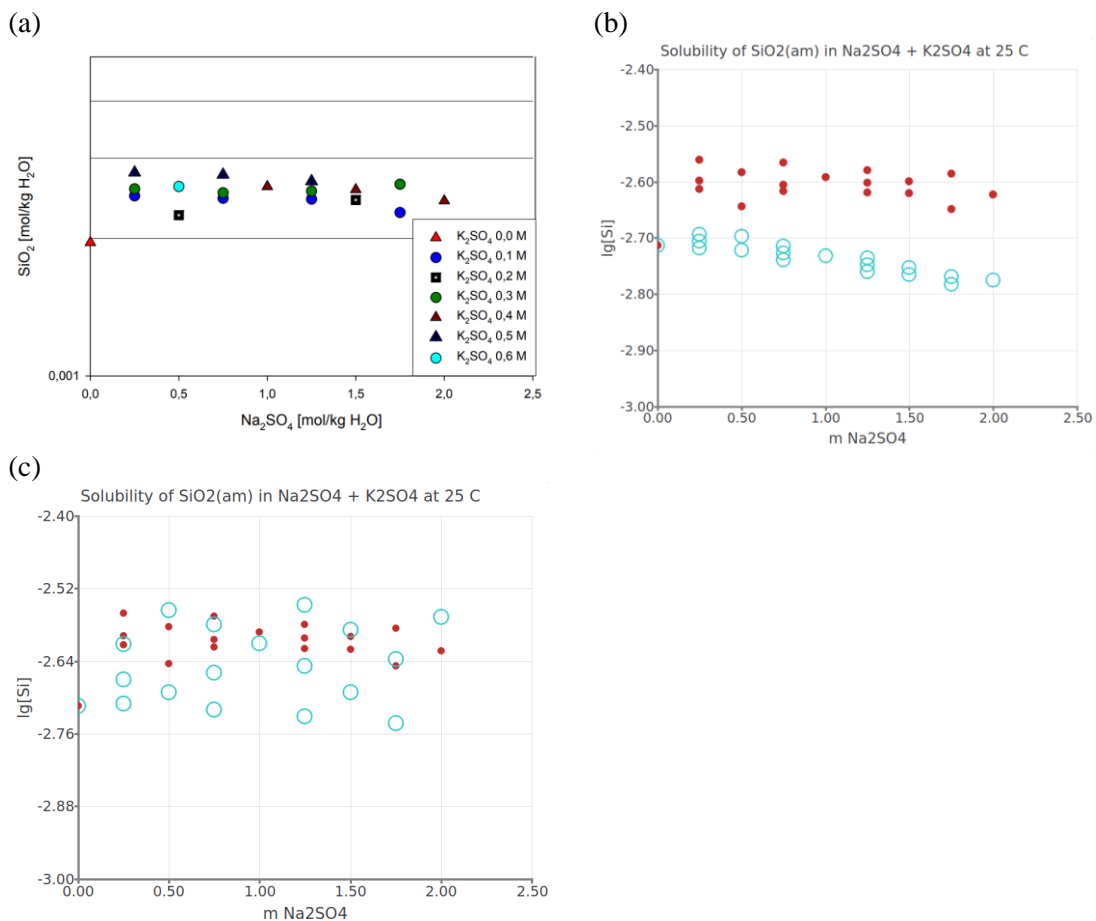


Fig. 2-4 Solubility of $\text{SiO}_2(\text{am})$ in $\text{Na}_2\text{SO}_4-\text{K}_2\text{SO}_4$ solutions at 25 °C from Meyer (2006) (a), measured (full circles) compared with model calculated (empty circles) (b). (c) calculated using $\zeta(\text{Si}(\text{OH})_4(\text{aq})-\text{K}^+-\text{SO}_4^{2-}) = 0.25$

In the comparison between the model predictions and experimental measurements in the ternary systems, a good agreement was achieved at 25 °C (Fig. 2-3). However, discrepancies were observed in the $\text{Na}_2\text{SO}_4-\text{K}_2\text{SO}_4$ solutions, where the model consistently underpredicts the measured solubilities by 0.1–0.18 log units (Fig. 2-4b). This discrepancy can be partially addressed by introducing a $\zeta(\text{Si}(\text{OH})_4(\text{aq}), \text{K}^+, \text{SO}_4^{2-})$ parameter of 0.25 (Fig. 2-4c). Similarly, an $\eta_c(\text{Si}(\text{OH})_4(\text{aq}), \text{K}^+, \text{Na}^+)$ parameter could also have a similar effect. The discrepancy between the model and measurements in the $\text{Na}_2\text{SO}_4-\text{K}_2\text{SO}_4$ solutions could be attributed to systematic errors in the measurements if we compare solubility in water to solubility in solution (Fig. 2-4a). This increase in measured solubility occurs between 0 and 0.2 M Na_2SO_4 , while at higher concentrations, the values remain relatively constant within the scatter of the data. Another possible explanation is a difference in the batch of $\text{SiO}_2(\text{am})$ used, which could result in systematically higher solubility. The measured $\text{SiO}_2(\text{am})$ solubility in water was not from the same batch as the one done in Na_2SO_4 solution and there is no way to know what would be the extent of this effect. Considering the good agreement in other ternary systems and the relatively large ternary parameter needed for only a minimal improvement, no additional ternary parameter was selected for this system.

However, when comparing the calculations with the data reported in the tables of Meyer & Willms (2008) at elevated temperatures (45, 65, and 85 °C), large discrepancies were observed for the ternary systems that show god agreement for 25 °C. These discrepancies were particularly

suspicious when comparing the data at 25 °C with 45 °C (Fig. 2–5). Upon reassessing the data in the tables, it was found that the reported concentrations of electrolytes contain an error. By accessing the lab-archived Excel files containing the original data, it was discovered that the concentrations reported in the "Target Concentration" column of original files significantly differ from the values present in the tables of Meyer & Willms's (2008) report. The electrolyte concentrations were calculated for a mixture of stock solutions based on their mass, which were then supposedly used in the solubility experiments. Taking the reported Target Concentration values as the actual solution concentrations used in the experiments significantly improves the agreement between the measured and calculated values (Fig. 2–6). Therefore, it appears that the Target Concentration values were the correct salt concentrations, rather than the values reported in the tables of Meyer & Willms (2008). The ternary data is well represented by the calculated values as a function of temperature and concentration using just binary IPs (Fig. 2–6).

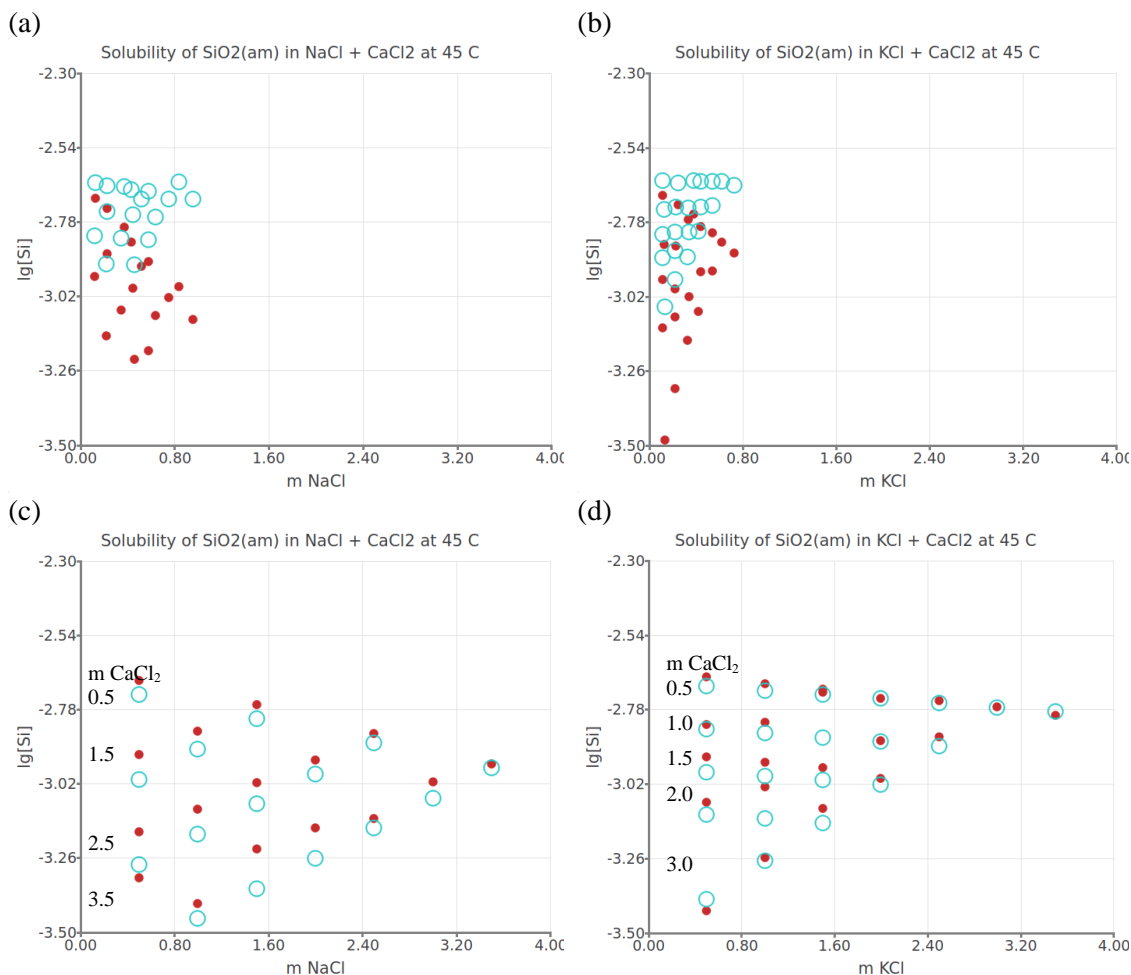


Fig. 2–5 Comparison between measured (full circles) and calculated (empty circles) $\text{SiO}_2(\text{am})$ solubility in ternary electrolyte solutions at elevate temperatures. (a, b) Datasets of Meyer & Willms (2008) before correction (see text). (b, c, d) Datasets of Meyer & Willms (2008) after correction (see text).

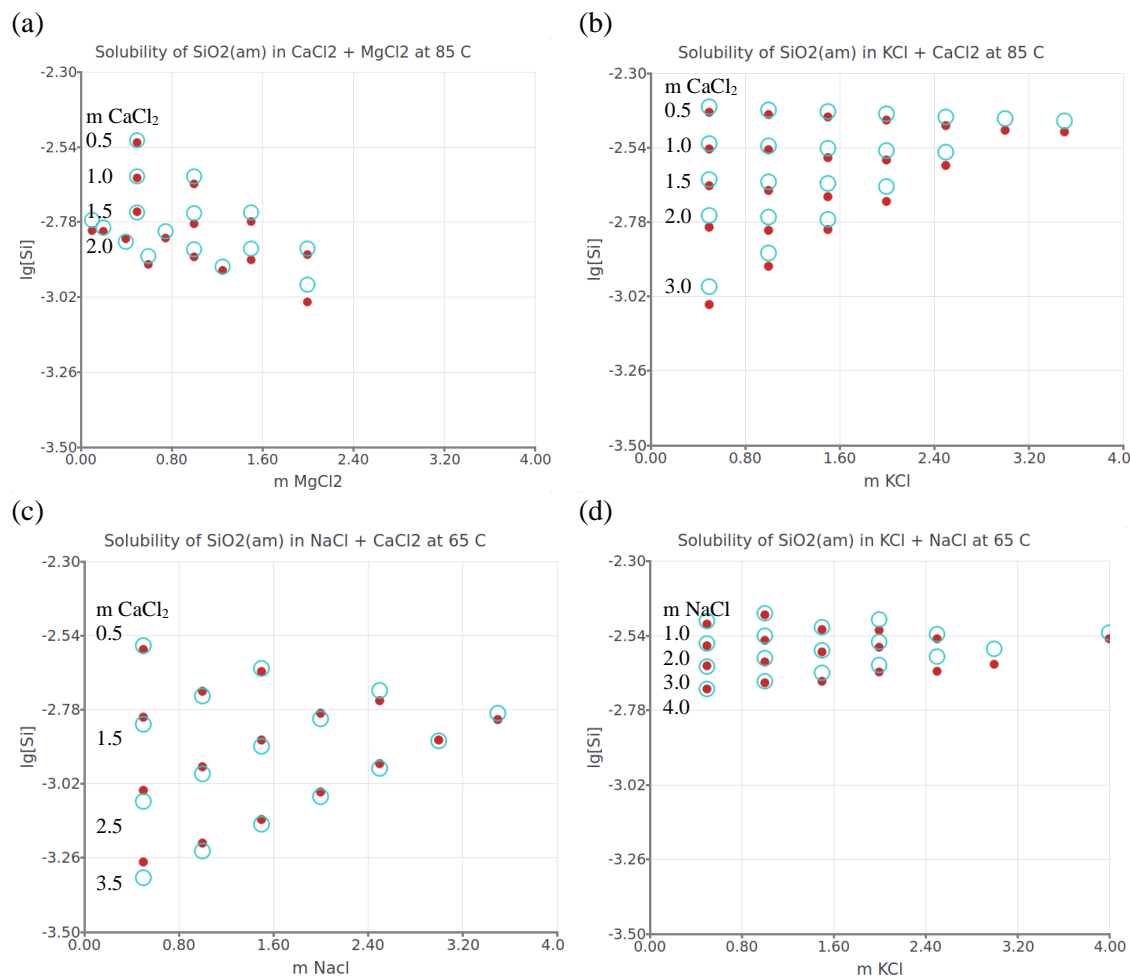


Fig. 2–6. Comparison between measured (full circles) and calculated (empty circles) $\text{SiO}_2(\text{am})$ solubility in ternary electrolyte solutions at elevate temperatures. Datasets of Meyer & Willms (2008) after correction (see text).

2.3 Hydrolysis of silicic acid

For the first and second hydrolysis of the silicic acid, the $\log_{10}K^\circ(T)$ temperature dependence previously available in THEREDA was based on the parameterization of Hummel et al. (Hummel et al., 2002) which is valid up to 100 °C.

The experimental data of Busey & Mesmer (1977) in NaCl solution covers a wider range of temperatures and can be used to derive a consistent set of $\log_{10}K^\circ(T)$, standard thermodynamic properties and polythermal Pitzer IPs in NaCl solutions. The coefficients for $\log_{10}K^\circ(T)$ function (2–3) were therefore selected from Busey & Mesmer (1977) and are valid up to 300 °C, these are consistent with the experiments in NaCl solutions and allowed in the next step to derive a consistent set of polythermal IPs. The reaction was reformulated in terms of THEREDA base species (2–4)

$\text{Si(OH)}_4(\text{aq}) + \text{OH}^- \rightleftharpoons \text{SiO(OH)}_3^- + \text{H}_2\text{O(l)}$	
$\log_{10}K^\circ(T) = -18.4014 + 2.34669\text{E+03}/T + 2.57979 \cdot \ln(T)$	2-3
$\text{Si(OH)}_4(\text{aq}) \rightleftharpoons \text{SiO(OH)}_3^- + \text{H}^+$ (using THEREDA base species)	
$\log_{10}K^\circ(T) = 45.0097 - 3.58254\text{E+03}/T - 7.51672 \cdot \ln(T)$	2-4
$\text{SiO(OH)}_3^- + \text{OH}^- = \text{SiO}_2(\text{OH})_2^{2-} + \text{H}_2\text{O(l)}$ (assuming $\Delta_r C_{p,m}^\circ = 0$)	2-5
$\log_{10}K^\circ(T) = -4.6227 + 1.56965\text{E+03}/T$	
$\text{Si(OH)}_4(\text{aq}) \rightleftharpoons \text{SiO}_2(\text{OH})_2^{2-} + 2 \text{H}^+$ (using THEREDA base species)	2-6
$\log_{10}K^\circ(T) = 103.7980 - 7.94213\text{E+03}/T - 17.61322 \cdot \ln(T)$	

Due to lack of data to independently derive the standard state properties and Pitzer IPs for the second hydrolysis formation reaction ($\text{SiO}_2(\text{OH})_2^{2-}$) in NaCl solution at 25 °C, along with their temperature dependence, some approximations were necessary. First, the change in heat capacity, $\Delta_r C_{p,m}^\circ$, for the reaction (2-5) was estimated to be close to zero since it is isoelectric. Second, the entropy of reaction (2-5) was adjusted to reproduce the second hydrolysis constant data in 1 M NaCl solutions measured at different temperatures (Busey & Mesmer, 1977). This adjustment was performed while considering the selected Pitzer IPs, details in Chapter 2.4. The reaction (2-5) was then converted into terms of the THEREDA master species (2-6) to be used in the database and further calculations.

It is important to note that these approximations and adjustments were necessary due to the lack of measured data, and further experimental investigations would be beneficial to accurately determine the standard state properties and Pitzer IPs for the second hydrolysis species at different temperatures and electrolyte concentrations (e.g. NaCl, KCl).

2.4 IPs for SiO(OH)_3^- and $\text{SiO}_2(\text{OH})_2^{2-}$

The stability of silicate ions and the hydrolysis of silicic acid ($\text{Si(OH)}_4(\text{aq})$) have been experimentally studied using the potentiometric method in NaCl and NaClO_4 mediums (Busey and Mesmer, 1978; Ingri, 1959; Lagerström, 1959; Santschi and Schindler, 1974; Sjöberg et al., 1983). The experimental data is described in terms of the average number of hydroxide ions ($[\text{OH}^-]$) bound per $\text{Si(OH)}_4(\text{aq})$, referred to as "Z." To avoid interference from Si polymeric species, the concentration in the experiments was kept below 0.008 M. The data obtained at $0 \leq Z \leq 0.95$ could be used to derive the ionization constant of SiO(OH)_3^- and the binary IPs ($\beta^{(0)}, \beta^{(1)}, C^{(\phi)}$) with Na^+ , while data at $Z \geq 0.95$ can be used to retrieve the parameters for the second hydrolysis species, $\text{SiO}_2(\text{OH})_2^{2-}$.

The reported hydrolysis constants for SiO(OH)_3^- at 25 °C (Ingri, 1959; Lagerström, 1959; Santschi and Schindler, 1974; Sjöberg et al., 1983) and at elevated temperatures (Busey and Mesmer, 1977) at different NaCl concentrations were used to derive a set of polythermal binary IPs ($\text{SiO(OH)}_3^-, \text{Na}^+$). During trial fits, it was observed that the data up to 3 M NaCl was well described by using IPs values that were equal to those of $(\text{HCO}_3^-, \text{Na}^+)$ (Fig. 2-7a) (RMS 0.099). The temperature dependence for these parameters was assumed to be zero. An improved fit could be obtained by adjusting four parameters, the $C^{(\phi)}(\text{SiO(OH)}_3^-, \text{Na}^+)$ at 25 °C, A coefficient, its temperature dependence B coefficient (Eq. 1-1), and the temperature dependence B coefficient value of $\beta^{(0)}(\text{SiO(OH)}_3^-, \text{Na}^+)$ and $\beta^{(1)}(\text{SiO(OH)}_3^-, \text{Na}^+)$ (RMS 0.074, Fig. 2-7B). The remaining IPs were assumed to be the same as those for HCO_3^- (Table 2-4).

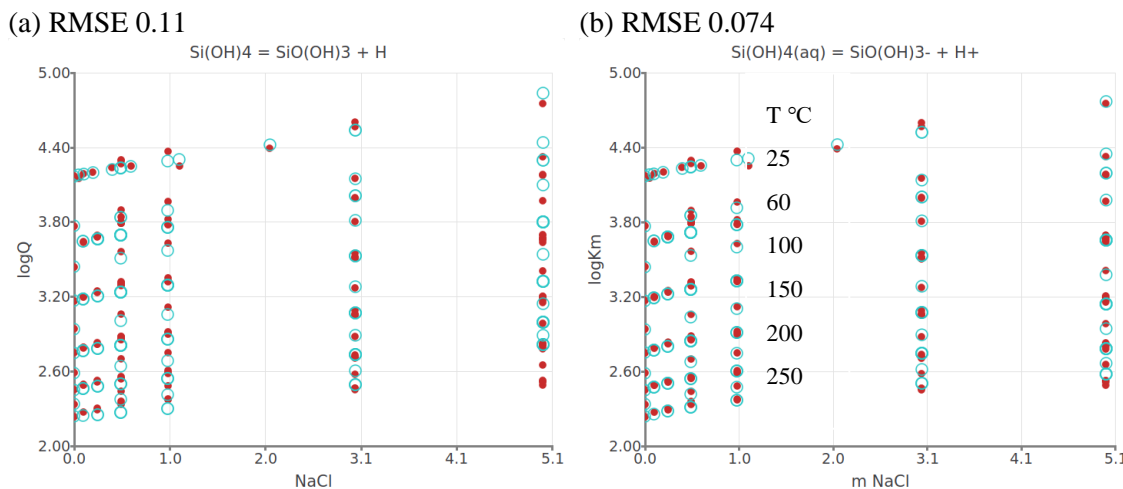


Fig. 2-7 Comparison between measured (full red circles) and calculated (empty blue circles) and ionization constant data, at different temperatures, with initial IPs values from HCO_3^- (a), and adjusted IPs from Table 2-4 (b).

There were no experimental data available to evaluate the IPs of $\text{SiO}(\text{OH})_3^-$ with K^+ , Ca^{2+} , and Mg^{2+} . At alkaline conditions in the presence of Ca and Mg it is expected that silicate hydrate solid phases will precipitate keeping Si concentration low. In addition, the effect of these ions is accounted through the complexes between Si and Ca^{2+} , and Mg^{2+} (section 2.5). In order to avoid wrongly combining the effect of IPs and aqueous complexation at low concentrations no IPs with Ca and Mg were selected in the dataset.

To estimate some of the missing IP values, the differences between IPs of ion pairs with the same charge can be used due to the additivity of the electrolyte medium effect on activity coefficients. For example, for the interaction with K^+ , we can assume that the difference between the IPs coefficients in Eq. (1-1) follows the constraint:

$$\text{IP}(\text{SiO}(\text{OH})_3^-, \text{Na}^+) - \text{IP}(\text{HCO}_3^-, \text{Na}^+) = \text{IP}(\text{SiO}(\text{OH})_3^-, \text{K}^+) - \text{IP}(\text{HCO}_3^-, \text{K}^+). \quad 2-7$$

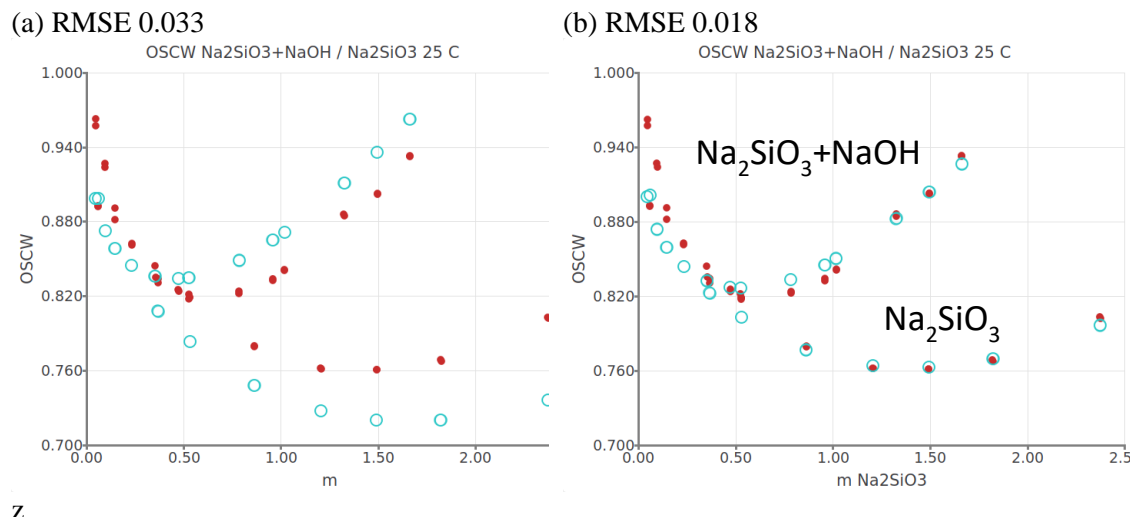
The same assumption can be applied to both binary and ternary IPs. If there were experimental data available to adjust the IPs for Na then the adjustment would be propagated to IPs with K based on a constraint defined by 2-7. If no experimental data was available (i.e., for adjusting interactions with Na^+), the value of the chosen analogue was taken as the estimated for the missing IP (e.g. $(\text{SiO}(\text{OH})_3^-, \text{K}^+) = (\text{HCO}_3^-, \text{K}^+)$). The resulted parameters that were mostly based on the analogy with HCO_3^- , are given in Table 2-4, and reproduce well the ionization constant data (Fig. 2-7) at different NaCl concentrations and temperatures (Busey and Mesmer, 1978).

Table 2-4. Coefficients for the temperature function (Eq. 1-1) of ion IPs with $\text{SiO}(\text{OH})_3^-$. Values in bold were fitted against experimental data. In round brackets are initial values from (HCO_3^-) before the fit.

IP coefficients Eq. 1-1	A	B	T (°C)	Concentration range (m)
$\beta^{(0)}(\text{SiO}(\text{OH})_3^-, \text{Na}^+)$	0.0277*	50 (0)	25–300	0–5
$\beta^{(1)}(\text{SiO}(\text{OH})_3^-, \text{Na}^+)$	0.0411*	50 (0)	25–300	0–5

IP coefficients Eq. 1–1	A	B	T (°C)	Concentration range (m)
$C^{(\phi)}(\text{SiO(OH)}_3^-, \text{Na}^+)$	0.0060 (0)	-33 (0)	25–300	0–5
$\beta^{(0)}(\text{SiO(OH)}_3^-, \text{K}^+)$	0.0296*	50**		
$\beta^{(1)}(\text{SiO(OH)}_3^-, \text{K}^+)$	-0.0130*	50**		
$C^{(\phi)}(\text{SiO(OH)}_3^-, \text{K}^+)**$	-0.0020	-33		
$\theta(\text{SiO(OH)}_3^-, \text{OH}^-)*$	0.0000	0	25	
$\theta(\text{SiO(OH)}_3^-, \text{Cl}^-)*$	0.0300	0	25–300	0–5
$\theta(\text{SiO(OH)}_3^-, \text{HCO}_3^-)*$	0.0000	0		
$\theta(\text{SiO(OH)}_3^-, \text{SO}_4^{2-})*$	0.0100	0		
$\theta(\text{SiO(OH)}_3^-, \text{CO}_3^{2-})*$	-0.0400	0		
$\psi(\text{Cl}^-, \text{SiO(OH)}_3^-, \text{Na}^+)*$	-0.0150	0	25–300	0–5
$\psi(\text{CO}_3^{2-}, \text{SiO(OH)}_3^-, \text{Na}^+)*$	0.0020	0		
$\psi(\text{CO}_3^{2-}, \text{SiO(OH)}_3^-, \text{K}^+)*$	0.0120	0		
$\psi(\text{SO}_4^{2-}, \text{SiO(OH)}_3^-, \text{Na}^+)*$	-0.0050	0		
$\psi(\text{SO}_4^{2-}, \text{SiO(OH)}_3^-, \text{K}^+)*$	-0.0050	0		
$\psi(\text{Na}^+, \text{K}^+, \text{SiO(OH)}_3^-)*$	-0.003	0		

* from (HCO_3^-) , ** from $(\text{SiO(OH)}_3^-, \text{Na}^+) - (\text{HCO}_3^-, \text{Na}^+) = (\text{SiO(OH)}_3^-, \text{K}^+) - (\text{HCO}_3^-, \text{K}^+)$



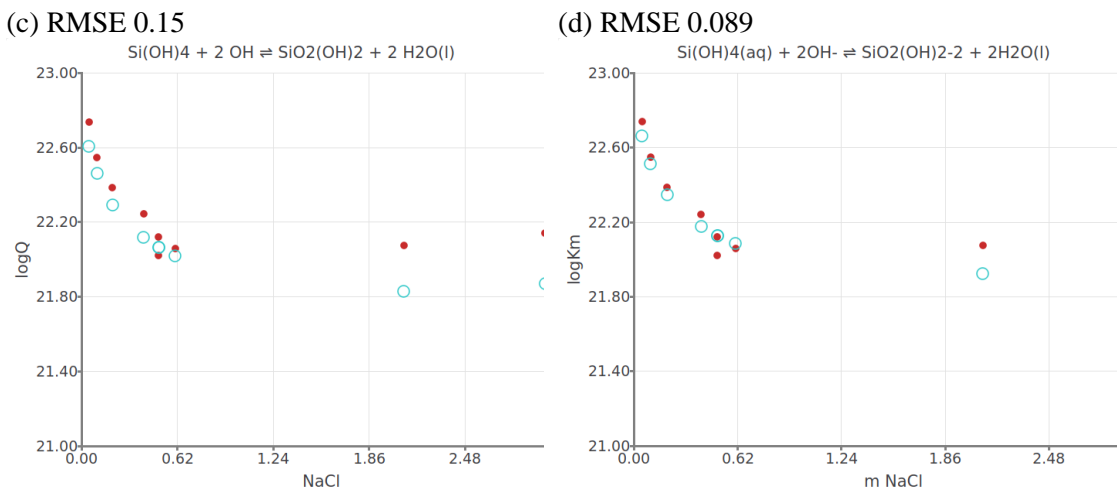


Fig. 2-8. Comparison between measured (full red circles) and calculated (empty blue circles) osmotic coefficient (a, b, m represents the Na_2SiO_3 mol kg^{-1} H_2O) and ionization constant data (C, D), at 25 °C, with initial IPs values from CO_3^{2-} (A, C), and adjusted IPs from Table 2-5 (B, D).

Room temperature (25 °C) experimental measurements conducted at $Z \geq 0.95$ in NaCl solutions (Ingrı, 1959; Lagerström, 1959; Sjöberg et al., 1983), and osmotic coefficient (OSCW) measurements in NaSiO_3 and $\text{NaSiO}_3\text{+NaOH}$ solutions (Park and Englezos, 1998) were used to evaluate the IPs for the interactions of $\text{SiO}_2(\text{OH})_2^{2-}$ in the $\text{SiO}_2\text{-NaCl-NaOH}$ system. The initial guesses for the IPs were based on the IPs of CO_3^{2-} with the respective cations. However, when using just the initial guesses estimates, systematic differences were observed between the measured OSCW and the ionization constants at all concentrations and > 1 m NaCl (Fig. 2-8a,c).

To improve the agreement with the experimental data, four IPs were further adjusted: the $\beta^{(0)}(\text{SiO}_2(\text{OH})_2^{2-}, \text{Na}^+)$, $\beta^{(1)}(\text{SiO}_2(\text{OH})_2^{2-}, \text{Na}^+)$, $\theta_a(\text{SiO}_2(\text{OH})_2^{2-}, \text{OH}^-)$ and $\theta_a(\text{SiO}_2(\text{OH})_2^{2-}, \text{SiO}(\text{OH})_3^-)$ Table 2-5, and standard $\log_{10}K^\circ(298.15)$ for 2-5. The remaining IPs were fixed to the values taken from CO_3^{2-} . The discrepancy from the measured OSCW was reduced to less than 2% at concentrations > 0.25 m Na_3SiO_3 (Fig. 2-8b). It should be noted that the accuracy of measured OSCW data tends to decrease at low concentrations. Different combinations of parameters were tested, and the final set provided the best results in terms of reducing the root mean square error (RMSE) while also having the lowest number of adjusted parameters and maintaining analogy to CO_3^{2-} for the remaining ones. The agreement between measured and calculated data using the selected parameters is shown in Fig. 2-8b,d.

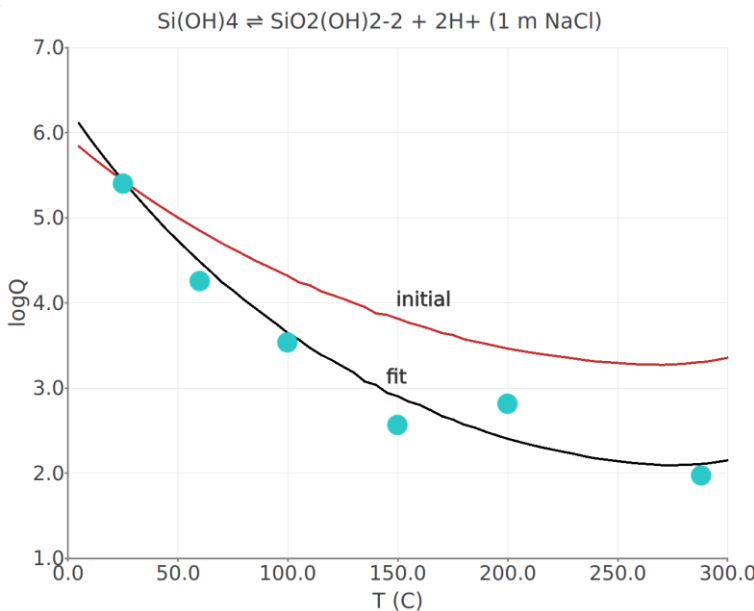


Fig. 2-9. Comparison between measured (circles) (Busey and Mesmer, 1977) and calculated (lines) second hydrolysis constants at 1 m NaCl as a function of temperature.

Values for the second ionization constant at elevated temperatures are only reported in the work of Busey & Mesmer (Busey and Mesmer, 1977) at 1 m NaCl concentration. These data are not sufficient to evaluate the temperature dependence of the IPs due to the lack of information on the standard entropy and heat capacity for the second hydrolysis constant. However, these data (Fig. 2-9) can be used to estimate the value of $\Delta_r S_m^\circ$ for the formation reaction (written in an isoelectric form 2-5) by assuming $\Delta_r C_{p,m}^\circ = 0$ and that the IPs ($\text{SiO}_2(\text{OH})_2^{2-}, \text{Na}^+$) were constant with temperature. The $\Delta_r S_m^\circ = -88.5 \text{ J} \cdot \text{K}^{-1} \cdot \text{mol}^{-1}$ for reaction 2-5 was obtained.

It is important to note that these values should be considered as qualitative estimates since it is not possible to separate the effect of the standard state properties from the IPs without systematic measurements at different temperatures and electrolyte concentrations. For example, a similar agreement could be obtained by leaving $\Delta_r S_m^\circ$ and $\Delta_r C_{p,m}^\circ$ at their initial values but setting a strong temperature dependence on $\beta^{(0)}(\text{SiO}_2(\text{OH})_2^{2-}, \text{Na}^+)$ (Eq. 1-1 B ~1500). However, such a strong temperature dependence is rather unusual, although the contribution from the change of IPs with temperature cannot be excluded. Based on the available range of experimental data, the independent evaluation of this contribution between different parameters was not possible.

There were no experimental data available that would allow for estimating possible IPs between $\text{SiO}_2(\text{OH})_2^{2-}$ and Ca^{2+} and Mg^{2+} . At high pH in the Ca–Mg–Si–OH system it is expected that the aqueous solution will contain relatively low concentrations of either Ca–Mg or Si due to the rapid precipitation of C–S–H, M–S–H, or other Ca, Mg silicate or hydroxide phases. And the effect at low concentrations is accounted for by the formation of Si and alkali earth metals complexes, therefore no IPs with these cations were selected.

Table 2-5. Coefficients for the temperature function (Eq. 1-1) of ion IPs with $\text{SiO}_2(\text{OH})_2^{2-}$.

IP coefficients Eq. 1-1	A	B	T (°C)	Concentration range (m)
$\beta^{(0)}(\text{SiO}_2(\text{OH})_2^{2-}, \text{Na}^+)$	0.0520 (0.0400)	0*	25	0–3
$\beta^{(1)}(\text{SiO}_2(\text{OH})_2^{2-}, \text{Na}^+)$	1.5500 (1.3890)	0*	25	0–3
$C^{(\phi)}(\text{SiO}_2(\text{OH})_2^{2-}, \text{Na}^+)*$	0.0044	0	25	0–3
$\beta^{(0)}(\text{SiO}_2(\text{OH})_2^{2-}, \text{K}^+)**$	0.1610 (0.1490)	0		
$\beta^{(1)}(\text{SiO}_2(\text{OH})_2^{2-}, \text{K}^+)*$	1.5910 (1.4300)	0		
$C^{(\phi)}(\text{SiO}_2(\text{OH})_2^{2-}, \text{K}^+)*$	-0.0015	0		
$\theta_a(\text{SiO}_2(\text{OH})_2^{2-}, \text{Cl}^-)*$	-0.0200	0	(25–275)	1
$\theta_a(\text{SiO}_2(\text{OH})_2^{2-}, \text{OH}^-)$	0.0000 (0.1000)	0*	25	0–3
$\theta_a(\text{SiO}_2(\text{OH})_2^{2-}, \text{SO}_4^{2-})*$	0.0200	0		
$\theta_a(\text{SiO}_2(\text{OH})_2^{2-}, \text{HCO}_3^-)*$	-0.0400	0		
$\theta_a(\text{SiO}_2(\text{OH})_2^{2-}, \text{CO}_3^{2-})*$	0.0000	0		
$\theta(\text{SiO}_2(\text{OH})_2^{2-}, \text{SiO}(\text{OH})_3^-)$	0.2000 (-0.0400)	0*	25	0–3
$\psi_a(\text{Cl}^-, \text{SiO}_2(\text{OH})_2^{2-}, \text{Na}^+)*$	0.0085	0	(25–275)	1
$\psi_a(\text{Cl}^-, \text{SiO}_2(\text{OH})_2^{2-}, \text{K}^+)*$	0.0040	0		
$\psi_a(\text{OH}^-, \text{SiO}_2(\text{OH})_2^{2-}, \text{Na}^+)*$	-0.0170	0	25	0–3
$\psi_a(\text{OH}^-, \text{SiO}_2(\text{OH})_2^{2-}, \text{K}^+)*$	-0.0100	0		
$\psi_a(\text{SO}_4^{2-}, \text{SiO}_2(\text{OH})_2^{2-}, \text{Na}^+)*$	-0.0050	0		
$\psi_a(\text{SO}_4^{2-}, \text{SiO}_2(\text{OH})_2^{2-}, \text{K}^+)*$	-0.0090	0		
$\psi_a(\text{HCO}_3^-, \text{SiO}_2(\text{OH})_2^{2-}, \text{Na}^+)*$	0.0020	0		
$\psi_a(\text{HCO}_3^-, \text{SiO}_2(\text{OH})_2^{2-}, \text{K}^+)*$	0.0120	0		
$\psi_a(\text{SiO}(\text{OH})_3^-, \text{SiO}_2(\text{OH})_2^{2-}, \text{Na}^+)*$	0.0020	0	25	0–3
$\psi_a(\text{SiO}(\text{OH})_3^-, \text{SiO}_2(\text{OH})_2^{2-}, \text{K}^+)*$	0.0120	0		
$\psi_c(\text{K}^+, \text{Na}^+, \text{SiO}_2(\text{OH})_2^{2-})*$	0.0030	0		

* (CO_3^{2-}), ** from $(\text{SiO}_2(\text{OH})_2^{2-}, \text{Na}^+) - (\text{CO}_3^{2-}, \text{Na}^+) = (\text{SiO}_2(\text{OH})_2^{2-}, \text{K}^+) - (\text{CO}_3^{2-}, \text{K}^+)$

2.5 Metal silicate complexes

Previous studies evaluating the solubility of $\text{SiO}_2(\text{am})$ in different electrolytes indicate that there is no complexation with silica under neutral conditions. Therefore, all solute effects were accounted for through IPs (chapter 2.2). Seward (Seward, 1974) proposed the formation of a Na–silica complex at alkaline pH to explain his measured data. However, this interpretation was challenged by Busey and Mesmer (Busey and Mesmer, 1978), who demonstrated that such a Na–Si complex was not required to explain the solubility measurements under highly alkaline conditions. They argued that the electrolyte effect can be adequately accounted for by considering the interaction between Na and Si species alone.

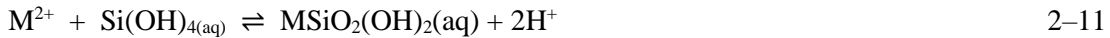
The potentiometric data presented by Busey and Mesmer (Busey and Mesmer, 1978) for alkaline conditions up to 5 m NaCl can be well-described without invoking complexation. In a recent study, Miron et al. (2022) compared the measured solubility of calcium silicate hydrate (C–S–H) in NaCl solutions with calculated results. The findings revealed that when considering the $\text{NaHSiO}_3(\text{aq})$ species proposed by Seward (1974), an increase in Si concentration is predicted. However, this contradicted the measured data. On the other hand, calculations performed without considering this species showed a relatively constant to slightly decreasing Si concentration, which aligned more closely with the experimental observations. Therefore, it is not expected that complexes between Si and alkali metals form in cementitious systems and are not necessary to explain the measured data.

Alkaline earth metal silicate complexes have been proposed by Santschi and Schindler (Santschi and Schindler, 1974), who conducted potentiometric titration experiments involving H_4SiO_4 in the presence of Ca and Mg ions in 1 M NaClO_4 solutions at pH values up to 9 and a temperature of 25 °C. The results of their experiments were interpreted as the formation of two weak complexes, $\text{MSiO}(\text{OH})_3^+$ and $\text{MSiO}(\text{OH})_2(\text{aq})$ (where M represents Ca^{2+} or Mg^{2+} , described by reactions 2–8 and 2–9).



$$\log_{10}K^\circ(T) = -2.58301\text{E+03} / T \quad (\text{M} = \text{Ca}^{2+})$$

$$\log_{10}K^\circ(T) = -2.52636\text{E+03} / T \quad (\text{M} = \text{Mg}^{2+})$$



$$\log_{10}K^\circ(T) = -5.72239\text{E+03} / T \quad (\text{M} = \text{Ca}^{2+})$$

$$\log_{10}K^\circ(T) = -5.26920\text{E+03} / T \quad (\text{M} = \text{Mg}^{2+})$$

Hummel and Thoenen (2023) selected reaction constants based on the data provided by Santschi and Schindler (Santschi and Schindler, 1974). Additional experimental data on the formation of these complexes were presented by Nicoleau and Schreiner (Nicoleau and Schreiner, 2017). Their results indicated complexes that were approximately one order of magnitude weaker than those chosen by Hummel and Thoenen (2021).

The neutral complex involving Ca^{2+} was found to have a significant influence on the calculated concentration of Si in equilibrium with C–S–H (calcium silicate hydrate), as reported by Kulik et al. (2022) and Walker et al. (2016), and it is necessary to accurately describe the solubility measurements. The updated value for the formation constant (2–9) (Kulik et al., 2022; Walker et al., 2016) is 0.5 \log_{10} units less stable than the value selected by Hummel and Thoenen (2023), and 1.1 \log_{10} units more stable than the value derived by Nicoleau and Schreiner (2017). There exists some disagreement regarding the stability of these complexes due to the challenging nature

of the experiments in this system, as noted by Nicoleau and Schreiner (2017). However, including these complexes in the THEREDA database with the updated value for $\text{CaSiO}(\text{OH})_2(\text{aq})$ from Kulik et al. (2022) is essential for accurately describing the solubility of C–S–H.

There were no available experiments that provide information on the temperature and electrolyte concentration dependence of these species, making it impossible to extract values for $\Delta_r S_m^\circ$, $\Delta_r C_{p,m}^\circ$, and Pitzer IPs for these species from measured data. As an approximation, it was assumed that the values for $\Delta_r S_m^\circ$, $\Delta_r C_{p,m}^\circ$ in reactions 2–10 and 2–11 were both 0, considering that these reactions are isoelectric and the temperature effect on the reactions may be close to zero (Gu et al., 1994; Miron et al., 2020). Binary Pitzer IPs for $\text{MSiO}(\text{OH})_3^+$ interacting with Cl^- were estimated using the method outlined by Plyasunov et al. (Plyasunov et al., 1998) with SIT $\epsilon = 0.05$ (Hummel and Thoenen, 2023) which leads to a value of 0.06 for $\beta^{(0)}$ and 0.34 for $\beta^{(1)}$. IPs for $\text{MSiO}_2(\text{OH})_2(\text{aq})$ with Na^+ , K^+ , Cl^- , HCO_3^- , and SO_4^{2-} were assumed to be the same as those for $\text{Si}(\text{OH})_4(\text{aq})$ (Table 2-3).

The Pitzer model can potentially account for the effects of weak complexes by utilizing IPs between Ca^{2+} , Mg^{2+} , and Si hydrolysed species. The $\beta^{(2)}$ parameter (with $\alpha^{(2)} = 50$) can be fitted to capture the anomalous behaviour of 2–2 electrolytes at low concentrations used to describe the weak complexation between $\text{SiO}_2(\text{OH})_2^{2-}$ and Ca^{2+} . Trial calculations of C–S–H solubility in H_2O revealed that $\beta^{(2)}$ values on the order of –5000 were necessary to get similar results for the concentration of Si in equilibrium with C–S–H at high Ca/Si ratios, comparable to using the $\text{CaSiO}_2(\text{OH})_2(\text{aq})$ complex instead of the IP. It is worth noting that the $\beta^{(2)}$ value (–5000) required for the interaction between $\text{SiO}_2(\text{OH})_2^{2-}$ and Ca^{2+} has a similar order of magnitude as the value (–2700) reported for the $\text{Al}_2(\text{SO}_4)_3$ electrolyte by Pitzer and Silvester (Pitzer & Silvester, 1978) or the value (–2330) derived in section 3.3.3. In the case of $\text{Al}_2(\text{SO}_4)_3$, this value is related to the formation of Al–sulphate complexes as discussed by Reardon (Reardon, 1988). Because the concentrations of these silicate species are low and are mainly influenced by the solubility of solids, the choice of complexes and not IPs was preferred for the updated THEREDA dataset, as it is also consistent with the solubility data for C–S–H and the development of thermodynamic data for cement phases (Lothenbach et al., 2019).

2.6 Si polymeric species

At low concentrations of dissolved silica (< 0.01 m), the aqueous speciation is primarily dominated by monomeric species. As the Si concentration increases, various Si polymeric species such as dimeric, trimer, tetrameric, and hexameric and their deprotonated counterparts may start to form. However, distinguishing between different types of species based on solubility and potentiometric data is challenging. As a result, several datasets proposing overlapping or different polymeric species have been put forward (Felmy et al., 2001; Guillaumont et al., 2003; Provis et al., 2005; Sjöberg and Öhman, 1985). The actual speciation at high pH and high dissolved silica concentration is still debated and cannot be unequivocally solved by solubility experiments alone but additional experimental methods are needed. A combination of solubility, osmotic coefficient determination (electromotive force emf, isopiestic measurements), potentiometry, and [^{29}Si] NMR can be used to analyse the species present in the system, their protonation state and extract the thermodynamic parameters (Felmy et al., 2001; Park and Englezos, 1999a, 1998; Sjöberg et al., 1985, 1981).

In natural environments, the concentration of dissolved silicon is typically below 0.01 m and seldom exceeds 0.1 m. This is primarily due to the precipitation of various silicate minerals (Sjöberg, 1996). However, the solubility of $\text{SiO}_2(\text{am})$ sharply increases above pH 9 due to the formation of ionized species of silicic acid and potential polymeric species. This phenomenon is particularly relevant in highly alkaline solutions where silicate minerals are present (alkali activated materials), resulting in high concentrations of dissolved silica and the possibility of

polysilicate species being present in the solution. The general conditions at which the polysilicate species form are characterized by highly alkaline solutions, high silica concentrations (> 0.001 m), and high $\text{SiO}_2/\text{Na}_2\text{O}$ ratios (concentrated alkali metal silicate solutions). These are relevant for glass dissolution, zeolite synthesis, silicate and aluminosilicate binders (geopolymers) (Phair et al., 2001; Provis et al., 2005; Sefcik and McCormick, 1997) and for looking at conditions related to polymerisation and silicate precipitation. In the context of cementitious pore water, the presence of C–S–H, along with other cement hydrate phases, help maintain the Si concentration below 0.01 m, making the polymers not relevant for the bulk pore solution composition.

In the review by Hummel and Thoenen (2023), the available data on Si polymeric species were examined. They concluded that the solubility of $\text{SiO}_2(\text{am})$ can be adequately reproduced by considering a single Si tetramer species, $\text{Si}_4\text{O}_8(\text{OH})_{44}^-$. This simplified representation provides a satisfactory description of $\text{SiO}_2(\text{am})$ solubility.

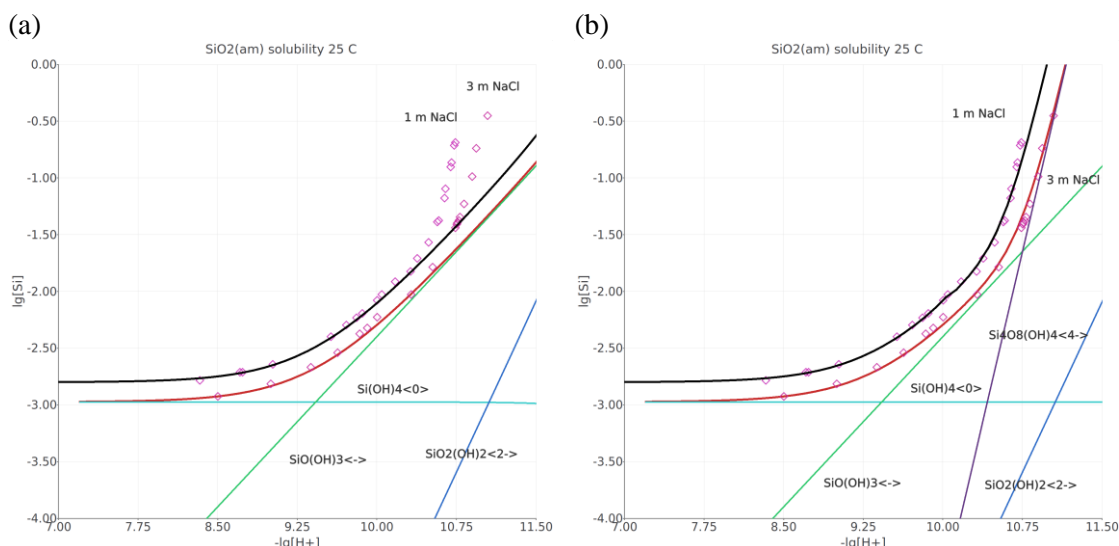
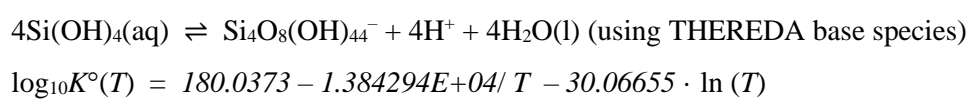


Fig. 2–10 Solubility of $\text{SiO}_2(\text{am})$ in NaCl media at 25°C . Measured data points from (Zarubin and Nemkina, 1990), calculated line using the data for species revised in this study. (a) only monomeric species; (b) with the $\text{Si}_4\text{O}_8(\text{OH})_{44}^-$ added (slope of 4) and derived $\log_{10}K(298.15) = -36.812$, $\beta^{(0)} 1.35$, and $\beta^{(1)} 11.0$ as given in Felmy et al. (2001).

When comparing the measured and calculated solubility of $\text{SiO}_2(\text{am})$ using only the monomeric species (Fig. 2–10a), it becomes evident that the data at 1 and 3 m NaCl were underestimated above 0.01 m Si. To address this discrepancy, a similar approach as suggested by Hummel and Thoenen (2023) was adopted in this study. The approach considers the contribution of a single Si tetramer species, $\text{Si}_4\text{O}_8(\text{OH})_{44}^-$, and adjusting two parameters, its stability constant and the $\beta^{(0)}$ binary IP, to fit the data from Zarubin and Nemkina (1990). The resulted $\log_{10}K(298.15)$ value is -36.695 , similar the one selected by (Grenthe et al., 1992) of -36.3 ± 0.5 , and by (Hummel and Thoenen, 2023) of -36.28 ± 0.16 . The resulted $\beta^{(0)}$ is 1.35 , a value close to 1.1 selected by (Felmy et al., 2001).

This choice of using a Si tetramer species satisfactorily reproduces the data (Fig. 2–10b) because the slope of the measured data was approximately 4.3 and 3.7 at 1 and 3 m NaCl , respectively. These values suggest that a polymeric species with a charge around -4 , could account for the observed data. However, it should be noted that NMR studies (Felmy et al., 2001; Provis et al., 2005) have demonstrated the formation of several different polymeric species under varying Si concentrations, pH levels, and electrolyte concentrations. While the present simplification of

considering a single tetramer species was sufficient for describing measured Si solubility data, further investigations are needed to establish a consistent set of polymeric species and determine their temperature and electrolyte concentration dependence.



There were no available investigations that describe the stability of $\text{Si}_4\text{O}_8(\text{OH})_{44}^-$ at different temperatures. The study from Busey and Mesmer (1978) provides $\log_{10}K^\circ(T)$ values for a different tetramer, $\text{Si}_4\text{O}_6(\text{OH})_6^{2-}$, in 1 M NaCl solutions at various temperatures. To minimize errors at elevated temperatures, it was reasonable to assume a $\Delta_rS_m^\circ$ and $\Delta_rC_{p,m}^\circ$ of 0 for the isoelectric reaction (2-12). The formation reaction with temperature dependence was then rewritten in terms of THEREDA master species (2-13).

No measurements were available in order to derive IPs with K^+ . To avoid gross errors the values of the binary IPs with K^+ were taken as analogue to Na^+ ones.

3 Al

3.1 Standard thermodynamic data for the system Al–O–H

Thermodynamic properties of gibbsite ($\text{Al(OH)}_3(\text{cr})$) were used as anchor to derive a consistent set of standard thermodynamic properties (at $I = 0$) in the system Al–O–H (Table 3-1). Properties of Al(cr) were taken from CODATA (Cox et al., 1989). Values for $\Delta_f H_{298}^\circ$, $\Delta_f S_{298}^\circ$, and $\Delta_f C_{p,298}^\circ$ of gibbsite were taken from (Robie and Hemingway, 1995) and were based on thermochemical measurements of (Hemingway et al., 1977; Hemingway and Robie, 1977). In addition the measured $\Delta_f C_{p,298}^\circ$ of boehmite was taken as anchor value for the heat capacity.

Table 3-1 Reference standard thermodynamic properties for Al element and gibbsite. * from solubility as a function of temperature.

	$\Delta_f H_{298}^\circ$ $\text{J} \cdot \text{mol}^{-1}$	$\Delta_f S_{298}^\circ$ $\text{J} \cdot \text{K}^{-1} \cdot \text{mol}^{-1}$	$\Delta_f C_{p,298}^\circ$ $\text{J} \cdot \text{K}^{-1} \cdot \text{mol}^{-1}$	References
Al(cr)		28.3 ± 0.1	24.2 ± 0.07	(Cox et al., 1989)
$\text{Al(OH)}_3(\text{cr}) /$ gibbsite	$-(1293130 \pm 1190)$	68.44 ± 0.3	91.7 ± 0.3	(Robie and Hemingway, 1995)
$\text{AlOOH}(\text{cr}) /$ boehmite	*	*	54.24 ± 0.1	(Hemingway et al., 1991)

Brown and Ekberg, 2016 (Brown and Ekberg, 2016) reviewed the available data on the solubility of aluminium hydroxides and the formation of aluminium hydrolysed species. These data were used to derive a consistent reference thermodynamic dataset for Al–O–H.

When plotted against the inverse of the absolute temperature, the values of the gibbsite and boehmite solubility reaction constants show a linear trend (Fig. 3–1a). The temperature dependence of such reactions can be estimated using 2-term extrapolation method where heat capacities of the reaction can be assumed to be zero. The temperature dependence coefficients (1–1) of the reactions (3–1, 3–2) were derived by fitting the reaction constant data by (Brown and Ekberg, 2016):



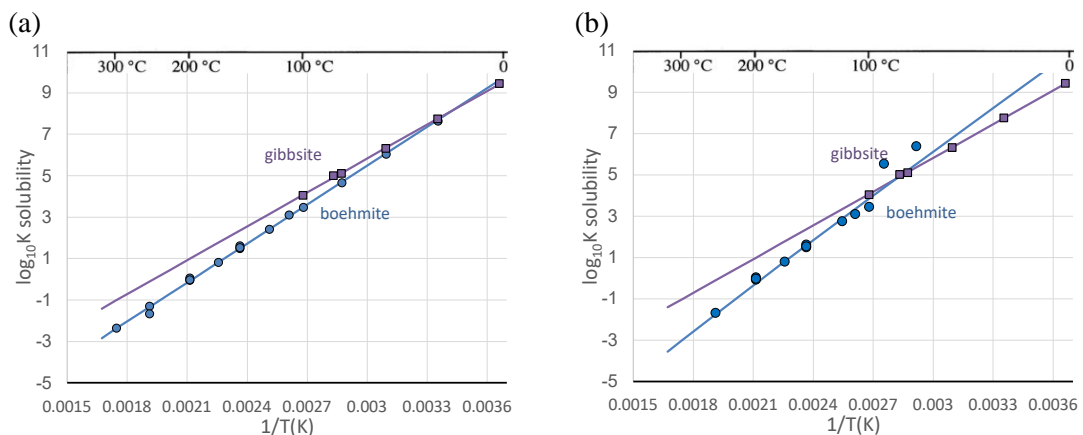
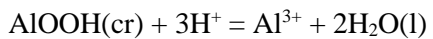


Fig. 3-1 (a) Comparison between calculated (3-1, 3-2) and selected model extrapolated solubility data (symbols) by (Brown and Ekberg, 2016); (b) Comparison between calculated (3-1, 3-3) and measured data for boehmite selected in this study from (Bénézeth et al., 2001; Palmer et al., 2001) and from (Verdes et al., 1992).

Accepting these data for the two Al solids results that gibbsite is predicted to be stable only at temperatures below 19 °C. This is in contradiction with statements that boehmite becomes the stable phase only at around > 80–100 °C (Brown and Ekberg, 2016; Ruff et al., 2008; Wesolowski, 1992; Zhang et al., 2021, 2019). Experiments on boehmite solubility below 100 °C may be problematic and could be affected by dissolution and reprecipitation of aluminium hydroxide. Data for the solubility of boehmite below 100 °C selected by (Brown and Ekberg, 2016) from (Bénézeth et al., 2001; Palmer et al., 2001) were based on model extrapolation and were not individual measurements. By selecting only the data reported by (Bénézeth et al., 2001; Palmer et al., 2001) at experimental conditions and adding the two measurements at 90 and 70 °C from (Verdes et al., 1992) that were not selected by (Brown and Ekberg, 2016) new coefficients for boehmite solubility were determined (Fig. 3-1b).



$$\log_{10} K^\circ(T) = -1.63639 + 6419.87/T - 1.97834 \cdot \ln(T)$$

3-3

A small heat capacity of reaction ($-37.88 \text{ J} \cdot \text{K}^{-1} \cdot \text{mol}^{-1}$) was needed to maintain the consistency with the measured $\Delta_f C_{p,298}^\circ$ of boehmite (Table 3-1). There is a large discrepancy with the low temperature data for boehmite but the trend of boehmite being less stable than gibbsite is apparent (Fig. 3-1b). The new dataset maintains a good agreement with the high temperature data for boehmite and results in a transition temperature between gibbsite and boehmite of 82 °C. More additional investigations are needed to better determine the transition temperature between gibbsite and boehmite. Using the revised reaction properties, standard thermodynamic data for $\text{H}_2\text{O(l)}$, Al(cr) , $\text{H}_2(\text{g})$ and $\text{O}_2(\text{g})$, a consistent set of standard properties $\Delta_f H_{298}^\circ$, $\Delta_f S_{298}^\circ$, and $\Delta_f C_{p,298}^\circ$ of Al^{3+} ion were retrieved.

In aqueous solution aluminium hydrolyses to form a series of species of the form Al(OH)_n^{3-n} with n ranging from 0 to 4. Data for the formation reactions of these species have been reviewed by Brown and Ekberg, 2016 (Brown and Ekberg, 2016) and were used to derive temperature coefficients for their formation reactions (1-1). The formation reactions can be written as isoelectric reactions:



The $\log_{10}K^\circ$ of these reactions vary linearly with respect to the inverse of absolute temperature across the range 0 – 300 °C, with the exception of Al(OH)_4^- that has a curvilinear trend in the same temperature range (Brown and Ekberg, 2016). A linear trend exists if we limit the data to the 0 – 200 °C range, which is within the applicability range of THEREDA. The coefficients derived by (Brown and Ekberg, 2016) were accepted in the present study while for Al(OH)_4^- new ones were retrieved assuming linear dependence in the 0 – 200 °C range.

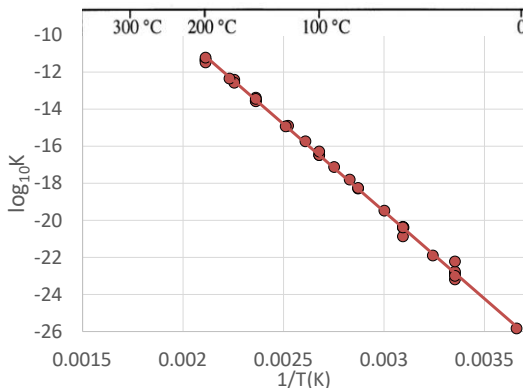
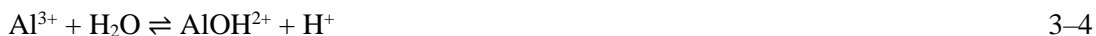
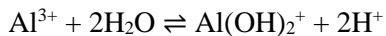


Fig. 3-2 Measured (symbols) data for $\text{Al}^{3+} + 4\text{H}_2\text{O} \rightleftharpoons \text{Al}(\text{OH})_4^- + 4\text{H}^+$ in the range 0 – 200 °C range selected by (Brown and Ekberg, 2016) and calculated model (3–7).



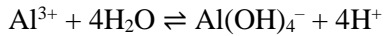
$$\log_{10}K^\circ(T) = 4.83 - 2983/T$$



$$\log_{10}K^\circ(T) = 8.78 - 5788/T$$



$$\log_{10}K^\circ(T) = 8.02 - 7061/T$$



$$\log_{10}K^\circ(T) = 8.74 - 9424/T$$

The hydrolysed $\text{Al}(\text{OH})_4^-$ was used in THEREDA for defining other reaction dependent aluminium species. Original reactions in this study were redefined by adding subtracting reaction 3–7 from corresponding reactions to have $\text{Al}(\text{OH})_4^-$ as master species. The coefficients of the new reactions were selected and entered in the database.



$$\log_{10}K^\circ(T) = 1.78 + 3976/T$$



$$\log_{10}K^\circ(T) = 7.1036 - 3004.13/T - 1.97834 \cdot \ln(T)$$



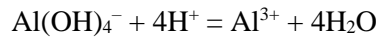
$$\log_{10}K^\circ(T) = -3.91 + 6501/T$$



$$\log_{10}K^\circ(T) = 0.04 + 3636/T$$



$$\log_{10}K^\circ(T) = -0.72 + 2363/T$$



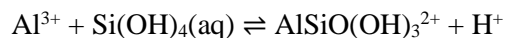
3–13

$$\log_{10}K^\circ(T) = -8.74 + 9424/T$$

3.2 Al polymeric species and interactions with Si at low pH

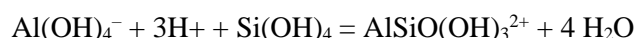
Several Al polymeric species have been described in the literature, e.g., $\text{Al}_2(\text{OH})_2^{4+}$, $\text{Al}_3(\text{OH})_4^{5+}$ and $\text{Al}_{13}(\text{OH})_{32}^{7+}$ (Brown and Ekberg, 2016). These species form at very high aluminium concentrations and in acidic conditions. Including them in the database would require to introduce respective binary and possibly ternary IPs with all major anions. Based on the experimental measurements evaluated below such species were not found necessary to describe the data and therefore were not selected for THEREDA.

The $\text{AlSiO}(\text{OH})_3^{2+}$ complex has been described in studies of the acidic region pH range $3.5 < \text{pH} < 5.5$ at milli molar Al and Si concentrations. (Hummel and Thoenen, 2023) retrieved standard thermodynamic properties for the formation of these species from studies at 25 °C and at different temperatures up to 150 °C (Pokrovski et al., 1996). These standard thermodynamic data (Pokrovski et al., 1996) were selected in THEREDA. Pitzer IPs for this species with Cl^- , $\beta^{(0)}$ 0.225 and $\beta^{(0)}$ 1.56, were estimated based on correlation with SIT (Table 1-1), ε 0.15 (Hummel and Thoenen, 2023). No data were available to retrieve or estimate IPs with HCO_3^- and SO_4^{2-} anions. Care should be taken if this complex is predicted above milli molar concentrations in calculations of concentrated electrolyte solutions. Solubility data on aluminosilicates minerals in different electrolyte solutions at various temperatures are needed to better constrain this complex and derive a consistent set of polythermal Pitzer IPs.



3–14

$$\log_{10}K^\circ(T) = 9.25 - 3473/T$$



3–15

$$\log_{10}K^\circ(T) = 0.51 + 5951/T$$

A different procedure for Al–Si at low pH, would have been to disregard the Al–Si complex formation and derive IP between $\text{Si}(\text{OH})_4(\text{aq})$ and Al^{3+} . The concentration of these species in the available experiments is too low to be able to derive Pitzer IPs. (Accornero and Marini, 2009) proposed a correlation between λ IPs of $\text{Si}(\text{OH})_4(\text{aq})$ and different ions and derived an $\lambda(\text{Si}(\text{OH})_4(\text{aq}), \text{Al}_2^{3+})$ of 0.4. A similar correlation using the data derived in the present study leads to $\lambda(\text{Si}(\text{OH})_4(\text{aq}), \text{Al}_2^{3+})$ of 0.8. No measured data were available at high enough concentrations to test these values and only using $\text{AlSiO}(\text{OH})_3^{2+}$ allows the reproduction of measured data at low concentrations of Si–Al in the acidic region of (Pokrovski et al., 1996).

3.3 IPs in the Al–Ca–Mg–Cl–OH– SO_4^{2-} – CO_2 system at low pH

At low pH conditions where Al^{3+} is the dominant species the binary and ternary IPs between Al^{3+} anions and cations, of the system Al–Ca–Mg–Cl–OH– SO_4^{2-} , were evaluated based on available experimental data. Limited experimental data in the presence of carbonate were used to evaluate possible interactions with $\text{CO}_2(\text{aq})$ species that is dominant at low pH.

3.3.1 Al–Cl–H₂O

The Pitzer IPs in this system were retrieved based on the available solubility of AlCl₃·6H₂O and osmotic coefficient data at different temperatures and concentrations. Several parameter sets were previously reported in the literature and were derived using different datasets. The parameter set of Pitzer & Mayorga (1973), for 25 °C, was derived from fitting the osmotic coefficient data reported in (Robinson and Stokes, 1965). Christov et al. (2007) in their study evaluated the data on aluminum in the acidic system and produced an updated set of parameters that contains also polythermal coefficients. Both parameter sets reproduce the osmotic coefficient data but diverged when were used to calculate the solubility of AlCl₃·6H₂O(cr) (Chloraluminite) (Fig. 3–3). The parameterization of Christov et al. (2007) agrees with the dataset of (Wang et al., 2016) that shows a steeper slope. It was not clear as to why there is this difference between the experiments, but it may be related to the starting material (AlCl₃·6H₂O(cr)) and experimental setup. In addition, the standard thermodynamic properties of the AlCl₃·6H₂O(cr) were not derived independently from the IPs and the temperature effect may be fitted either in the standard properties of the solid phase or in the IP temperature coefficients. Therefore, different sets of IPs, with their temperature coefficients, as well as standard thermodynamic properties of AlCl₃·6H₂O(cr) and their temperature dependence can be derived to describe the experimental data.

In the present evaluation a good agreement with the experimental data was obtained up to 100 °C without the need for introducing temperature dependence coefficients for the IPs (Table 3-2). This was done by taking the parameters of Pitzer & Mayorga (1973) as such and accepting the agreement with the lower slope in the solubility of the AlCl₃·6H₂O(cr) as a function of temperature (Fig. 3–3b). The only necessary adjustment that improved the agreement with the osmotic coefficient data above 2 m AlCl₃ was to set the $C^{(\phi)}(Al^{3+}, Cl^-)$ to zero (compared to 0.00273 reported in Pitzer & Mayorga (1973)).

The values of the selected IPs for the Al–Cl–H₂O were important because they propagate to the derived values for interactions in ternary systems containing other electrolytes. In the subsequent evaluations of ternary systems, it was found that not using temperature coefficients for the interactions in Al–Cl–H₂O has the positive consequence of fewer or no temperature coefficients to be needed to describe the ternary electrolyte systems at different temperatures. This greatly reduces the number of parameters while keeping good agreement with the measured data.

Table 3-2 Pitzer IP coefficients (Eq. 1–1) in the system Al–Cl–H₂O. Bold values were evaluated in this study.

IP coefficients Eq. 1-1	A	B	T (°C)	Maximum concentration (m)
$\beta^{(0)}(Al^{3+}, Cl^-)$	0.6993*	0	0–100	3.5
$\beta^{(1)}(Al^{3+}, Cl^-)$	5.845*	0	0–100	3.5
$C^{(\phi)}(Al^{3+}, Cl^-)$	0.000 (0.00273*)	0	0–100	3.5
$\theta_c(Al^{3+}, H^+)$	0.185*	0	0–100	3.5
$\psi_c(Al^{3+}, Cl^-, H^+)$	0.013*	0	0–100	3.5

* (Pitzer and Mayorga, 1973)

The selected thermodynamic data for AlCl₃·6H₂O(cr) formation reaction given as log₁₀K°(T) function (0–100 °C):

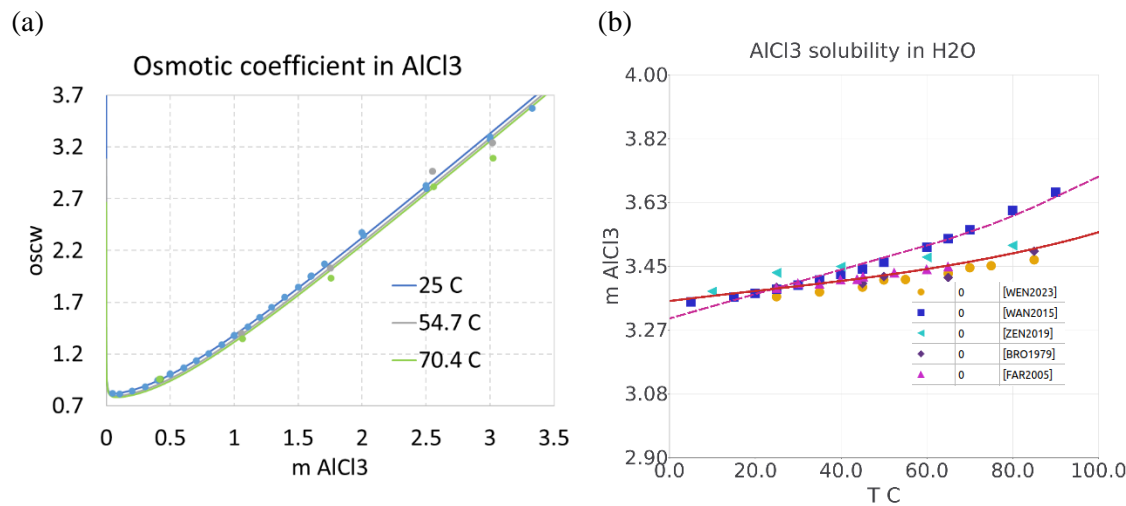
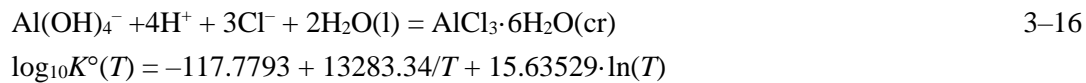


Fig. 3-3 (a) Data from (Robinson and Stokes, 1965) at 25 and at elevated temperatures from (Richter et al., 2000) (b) circle (Cheng et al., 2023), square (Wang et al., 2016), left arrow (Zeng et al., 2019), diamond (Brown et al., 1979), and triangle (Farelo et al., 2005), dashed line calculated with the model from (Christov et al., 2007).

3.3.2 Al–Na–K–Ca–Mg–Cl–H₂O

The binary and ternary IPs and their temperature dependence coefficients for this system were evaluated based on solubility measurements in ternary and quaternary systems (Table 3-3). Although the interactions of Al³⁺, with Cl⁻ and H⁺ Although the interactions of Al³⁺ with Cl⁻ and H⁺ were previously established, trial tests for adjusting these parameters did not lead to any improvements in test calculations.

Table 3-3 Experimental data used to asses the IPs in the system Al–Na–K–Ca–Mg–Cl–H₂O.

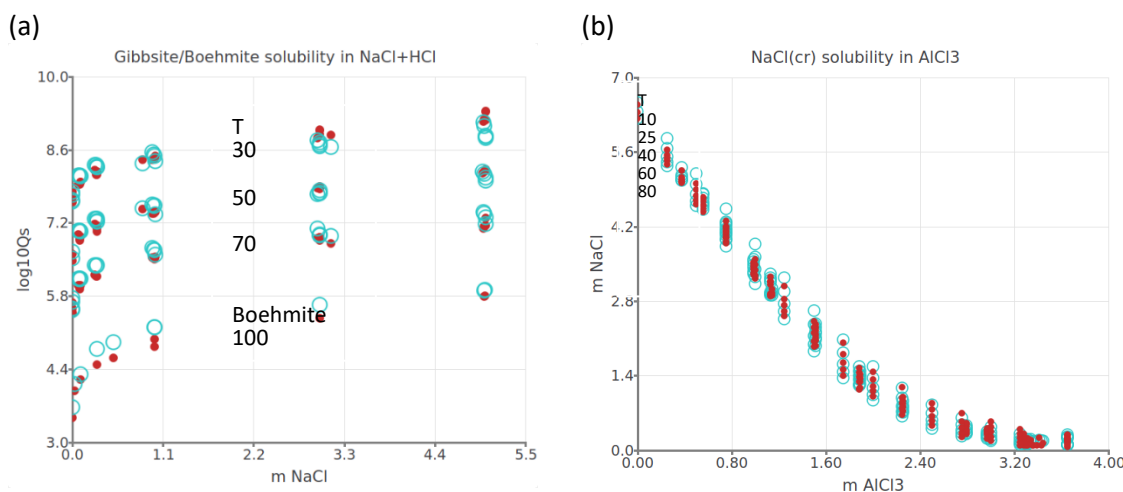
References	System	T (°C)	Maximum concentration (m)
Reported in (Christov et al., 2007) (Linke, 1965; Patel K. and Seshardi S., 1966)	KCl–AlCl ₃ MgCl ₂ –AlCl ₃	0–80	Solubility limit of KCl(cr), AlCl ₃ ·6H ₂ O(cr) and MgCl ₂ ·6H ₂ O
(Farelo et al., 2005)	NaCl–AlCl ₃ KCl–AlCl ₃	25–60	Solubility limit of KCl(cr), NaCl(cr) and AlCl ₃ ·6H ₂ O(cr)
(Zeng et al., 2019)	NaCl–AlCl ₃ NaCl–CaCl ₂ –AlCl ₃	10–80	Solubility limit of NaCl(cr), AlCl ₃ ·6H ₂ O(cr), and CaCl ₂ hydrates
(Cheng et al., 2023)	AlCl ₃ –KCl AlCl ₃ –CaCl ₂	25–70	0.9 KCl 1.5 CaCl ₂

References	System	T (°C)	Maximum concentration (m)
(Palmer and Wesolowski, 1992)	Gibbsite–NaCl–HCl	30–70	5 NaCl
(Palmer et al., 2001)	Boehmite–NaCl	100*	5 NaCl
(Liu et al., 2022)	MgCl ₂ –AlCl ₃	10–80	Solubility limit of AlCl ₃ ·6H ₂ O(cr), MgCl ₂ ·6H ₂ O
(Gao et al., 2013)	AlCl ₃ –KCl AlCl ₃ –MgCl ₂ AlCl ₃ –CaCl ₂	10–90	Solubility limit of KCl(cr), 5 m CaCl ₂ /MgCl ₂

*Contains measurements up to 250 °C

Final parameters are found in Table 3–4. The $\theta_c(\text{Al}^{3+}, \text{Na}^+)$ and $\psi_c(\text{Al}^{3+}, \text{Cl}^-, \text{Na}^+)$ IPs were constrained on solubility measurements of gibbsite in NaCl–HCl solutions (Palmer and Wesolowski, 1992) (30–70 °C), boehmite in NaCl at 100 °C (Palmer et al., 2001), and solubility of NaCl(cr) in AlCl₃ solutions up to the solubility limit of AlCl₃·6H₂O, temperatures 25–60 °C (Farelo et al., 2005), and 5–90 °C (Zeng et al., 2019).

Palmer & Wesolowski (Palmer and Wesolowski, 1992) derived values of 0.335 and –0.065 for the binary and ternary IP with Na⁺ based slowly on the gibbsite solubility data. In the present study the value of θ_c for 25 °C is the same as in (Palmer and Wesolowski, 1992) but has a temperature dependence and the ternary ψ_c is –0.039 with temperature dependence over the 0–100 temperature range. A good agreement could be obtained with the measured data in the Al–NaCl system (Fig. 3–4). Test calculations were done to set the $\theta_c(\text{Al}^{3+}, \text{Na}^+)$ to a value close to 0, similar to the IP values for the other ions of metals, but this leads to a worse agreement with the gibbsite solubility at increased NaCl concentrations.



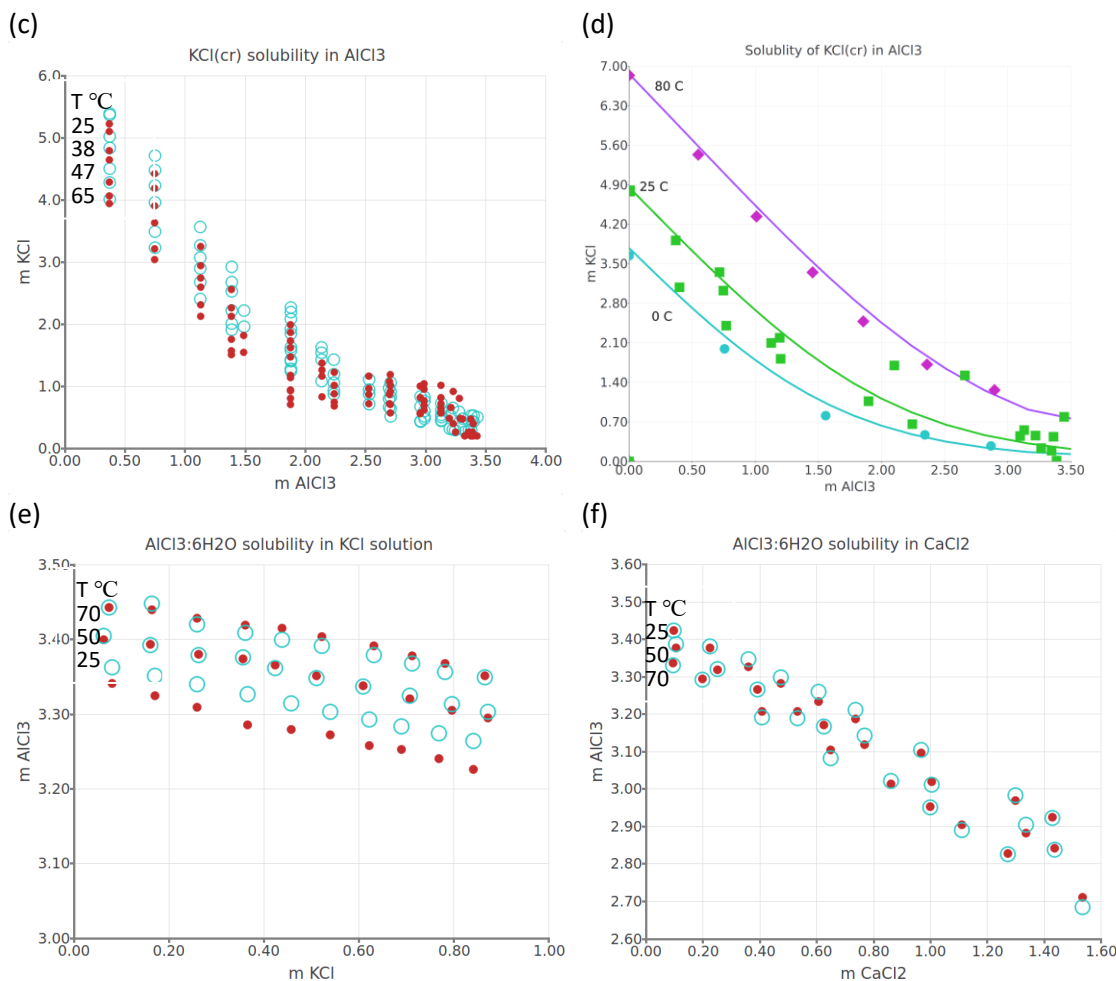


Fig. 3-4 Comparison between calculated (empty circles) and measured experimental data (full circles) for (a) gibbsite and boehmite solubility $\log_{10}Q_s(T) = [\text{Al}^{3+}]/[\text{H}^+]^3$ (Palmer et al., 2001; Palmer and Wesolowski, 1992); (b) NaCl(cr) in AlCl₃ (Farelo et al., 2005; Zeng et al., 2019); KCl(cr) solubility in AlCl₃ (c) (Farelo et al., 2005) (d) (Christov et al., 2007; Linke, 1965; Patel K. and Seshardi S., 1966); (e) AlCl₃·6H₂O solubility in KCl (Cheng et al., 2023); (f) AlCl₃·6H₂O solubility in CaCl₂ (Cheng et al., 2023).

The calculated data for the solubility of KCl(cr) shows worse agreement with measured values for some datasets at lower temperatures (Fig. 3-4c). The agreement could not be improved when considering all datasets and adjusting the IPs. No temperature dependence coefficients (1–1) were necessary for the IPs with K⁺.

In the Al–Ca–Cl–H₂O system the value for the derived binary IP with Ca²⁺ is 0 with a ternary IP $\psi_c(\text{Al}^{3+}, \text{Cl}^-, \text{Ca}^{2+})$ having a value similar to the one for Na⁺ and K⁺. Calculated values using the derived parameters for the solubility of NaCl(cr) in CaCl₂+AlCl₃ solution (not shown) and of AlCl₃·6H₂O at different temperatures were in agreement with the measured data (Fig. 3-4f).

When evaluating the data in chloride and sulphate aluminium containing systems, different authors (André et al., 2018; Christov, 2001; Reardon, 1988) derived values for the binary aluminium metal (M) interaction $\theta_c(\text{Al}^{3+}, M)$ that were zero or close to 0, and values for the ternary IPs $\psi_c(\text{Al}^{3+}, \text{Cl}^-, \text{SO}_4^{2-}, M)$ that were between –0.1 to 0.1. This is in accordance with the values derived in the present study for the ternary parameters (ψ_c). The binary parameters derived here

(Table 3-4) were close to 0 with the exception of $\theta_c(\text{Al}^{3+}, \text{Na}^+)$. This large value was necessary to keep the agreement with the aluminium hydroxide solubility, measurements that were characterized by relatively low concentrations of aluminium (milli moles) in the NaCl solution.

Table 3-4 Pitzer IP coefficients (Eq. 1-1) in the system Al–Na–K–Ca–Mg–Cl–H₂O. Bold values were evaluated in this study.

IP coefficients Eq. 1-1	A	B	T (°C)	Maximum concentration (m)
$\theta_c(\text{Al}^{3+}, \text{Na}^+)$	0.335	35	0–100	Solubility limit of NaCl(cr), AlCl ₃ ·6H ₂ O(cr)
$\psi_c(\text{Al}^{3+}, \text{Cl}^-, \text{Na}^+)$	-0.039	14	0–100	Solubility limit of NaCl(cr), AlCl ₃ ·6H ₂ O(cr)
$\theta_c(\text{Al}^{3+}, \text{K}^+)$	-0.002	0	0–90	Solubility limit of KCl(cr), AlCl ₃ ·6H ₂ O(cr)
$\psi_c(\text{Al}^{3+}, \text{Cl}^-, \text{K}^+)$	-0.020	0	0–90	Solubility limit of KCl(cr), AlCl ₃ ·6H ₂ O(cr)
$\theta_c(\text{Al}^{3+}, \text{Ca}^{2+})$	0.000	0	0–70	1.6 CaCl ₂
$\psi_c(\text{Al}^{3+}, \text{Cl}^-, \text{Ca}^{2+})$	-0.058	0	0–70	1.6 CaCl ₂
$\theta_c(\text{Al}^{3+}, \text{Mg}^{2+})$	0.000	0	0–80	Solubility limit of MgCl ₂ ·6H ₂ O(cr), AlCl ₃ ·6H ₂ O(cr)
$\psi_c(\text{Al}^{3+}, \text{Cl}^-, \text{Mg}^{2+})$	0.000	0	0–80	Solubility limit of MgCl ₂ ·6H ₂ O(cr), AlCl ₃ ·6H ₂ O(cr)

For the Al–Mg–Cl–H₂O, measured solubility data in the two salts MgCl₂·6H₂O – AlCl₃·6H₂O system gathered between 10 to 80 °C was compared with the calculated data (Fig. 3–5) using zero values for the θ_c , ψ_c IPs (Table 3-4). Within the scatter of the data no adjustment could produce a significant improvement between measured and calculated data.

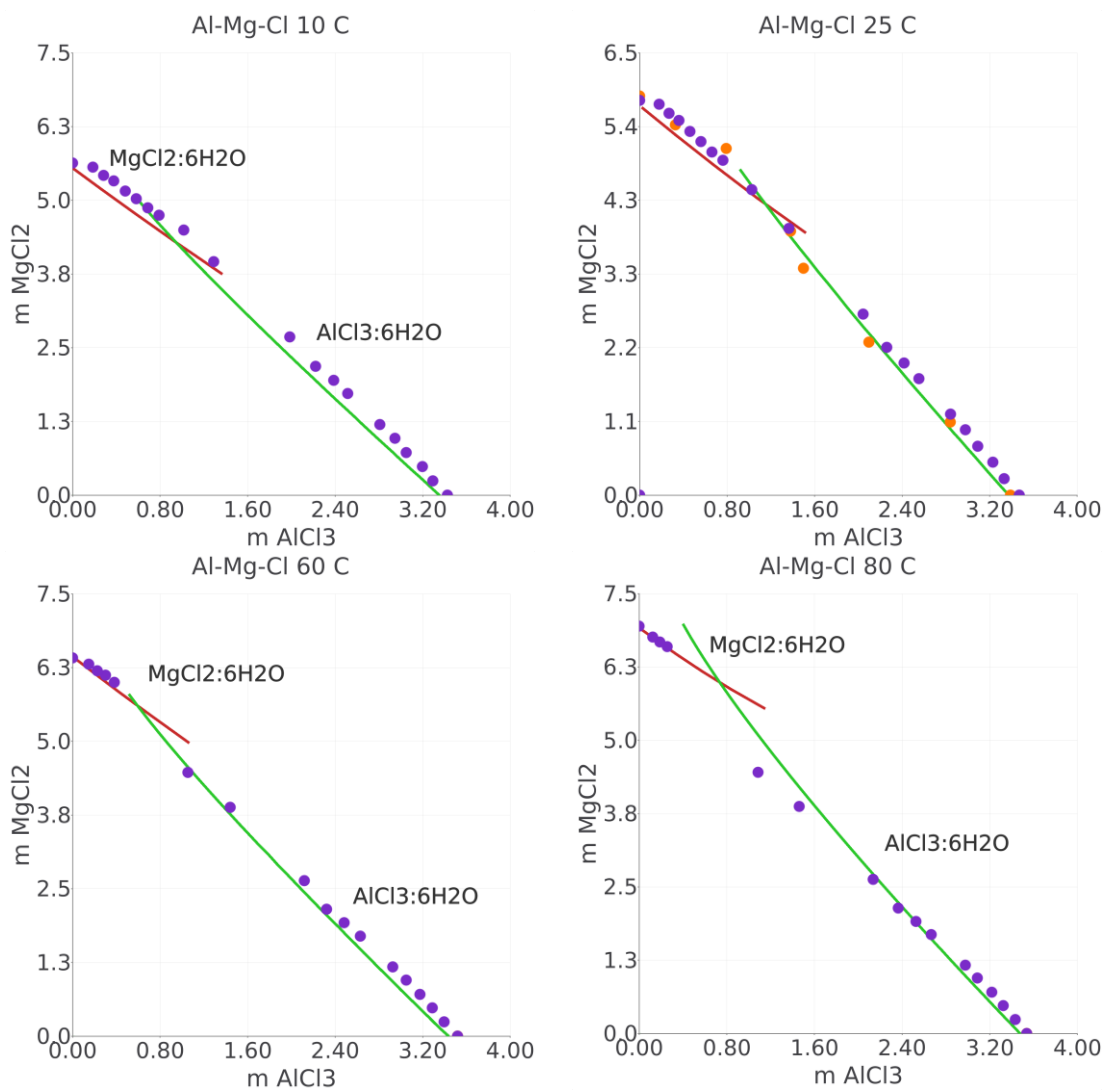


Fig. 3–5 Comparison between calculated (lines) and measured experimental data (full circles) for the binary salt system $\text{MgCl}_2 \cdot 6\text{HO}$ (Bischofite, red line in equilibrium) – $\text{AlCl}_3 \cdot 6\text{H}_2\text{O}$ (green line in equilibrium). Measured data from (Patel K. and Seshardi S., 1966) (orange), and (Liu et al., 2022) (purple).

3.3.3 Al–SO₄–H₂O and Al–Na–K–Mg–SO₄–H₂O systems

Osmotic coefficient in $\text{Al}_2(\text{SO}_4)_3$ solutions at 25 °C was used in various research works to derive different Pitzer parameter sets for the aluminium metal sulphate system (Christov, 2001; Pitzer and Silvester, 1978; Reardon, 1988). The challenges in this system primarily arise from the strong tendency for complexation between aluminium and sulphate ions (e.g., AlSO_4^+ and $\text{Al}(\text{SO}_4)_2^-$). The Pitzer model is most suitable for systems with fully dissociated electrolytes. Describing the chemical systems using complexes between Al and sulphate requires the inclusion of additional interactions for these species with other solutes, significantly increasing the number of parameters, which can lead to difficulties when parameterizing such systems. In this study, we address this issue by adjusting the IPs values without explicitly including any aluminum sulphate complexes in the dataset. However, in other activity models, like Davies or Debye–Hückel, these species were needed when modelling such systems because such models cannot account for such effects through IPs.

Table 3-5 Experimental data used to asses the IPs in the system Al–Na–K–Ca–Mg–SO₄–H₂O.

References	System	T (°C)	Maximum concntration (m)
(Mosgovykh et al., 1984)	CaSO ₄ –Al ₂ (SO ₄) ₃	25	1.1 Al ₂ (SO ₄) ₃ , solubility limit of gypsum
(Li and Demopoulos, 2006)	CaSO ₄ –AlCl ₃	25–80	1.6 AlCl ₃ , solubility limit of gypsum
(Robinson, 1937)	Al ₂ (SO ₄) ₃	25	1.2
(Burge, 1963)	Al ₂ (SO ₄) ₃	25	0.4
(Dobbins and Addleston, 1931)	Na ₂ SO ₄ –Al ₂ (SO ₄) ₃	25	solubility limit of mirabilite and alunogen
(Bassett and Watt, 1950)	MgSO ₄ –Al ₂ (SO ₄) ₃	25	solubility limit of epsomite and alunogen
(Reardon and Stevens, 1991)	K ₂ SO ₄ –Al ₂ (SO ₄) ₃	25	1.1 Al ₂ (SO ₄) ₃
(Britton, 1922)	K ₂ SO ₄ –Al ₂ (SO ₄) ₃	25	0.14 Al ₂ (SO ₄) ₃ , solubility limit of arcanite
(Druzhinin et al., 1961)	Na ₂ SO ₄ –Al ₂ (SO ₄) ₃	25	solubility limit of mirabilite and alunogen

Different available Pitzer datasets (Christov, 2001; Pitzer and Silvester, 1978; Reardon, 1988), were derived without using Al sulphate speciation. These datasets significantly differ in their approach to setting the alpha parameters and determining the value of the $\beta^{(2)}$ IP. The alpha parameters ($\alpha^{(1)}$ and $\alpha^{(2)}$) were used to account for the I dependence of binary interactions of $\beta^{(1)}$ and $\beta^{(2)}$ IPs. Based on empirical fits to experimental data, the values for $\alpha^{(1)}$ and $\alpha^{(2)}$ were in most cases set to 1.4 and 12 for 2:2 electrolytes and 2.0 and 50 for 3:2 and 2:3 electrolytes, respectively. However, relying solely on these values may hinder the ability to achieve improved fits to experimental data of different types, as perfect fits to osmotic coefficient data might not correspond to accurate predictions of mineral solubility.

Reardon (1988) encountered difficulties obtaining good agreement with the osmotic coefficient data in Al₂(SO₄)₃ solutions of intermediate concentrations, although achieving good agreement with solubilities in mixed metal sulphate systems, while at the same time keeping the $\alpha^{(1)}$ and $\alpha^{(2)}$ values for 2:3 electrolytes. In contrast, Christov (2001) proposed to adjust the values of $\alpha^{(1)}$ and $\alpha^{(2)}$ parameters to resolve the discrepancy between osmotic coefficient and solubility data, ultimately settling on a value of 1 for the $\alpha^{(2)}$ and 2 for $\alpha^{(1)}$ parameter. Another challenge in this system is determining the $\beta^{(2)}$ parameter. (Pitzer and Silvester, 1978) suggest to constrain the value based on reported stability constants of the AlSO₄⁺ species, while others rely on fitting this parameters against experimental data (Christov, 2001; Reardon, 1988).

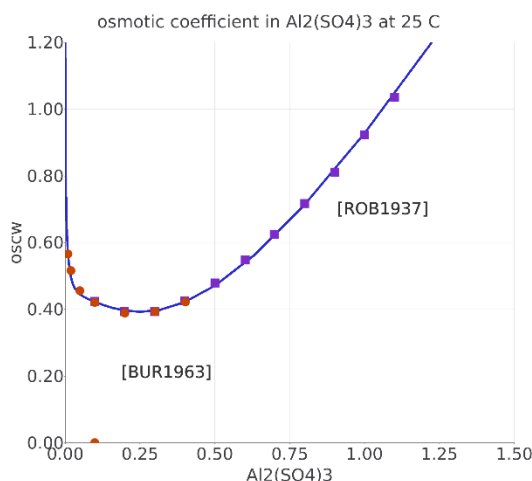


Fig. 3–6 Measured stoichiometric osmotic coefficient in $\text{Al}_2(\text{SO}_4)_3$ solution at 25 °C (Robinson, 1937) (squares) and (Burge, 1963) (circles)

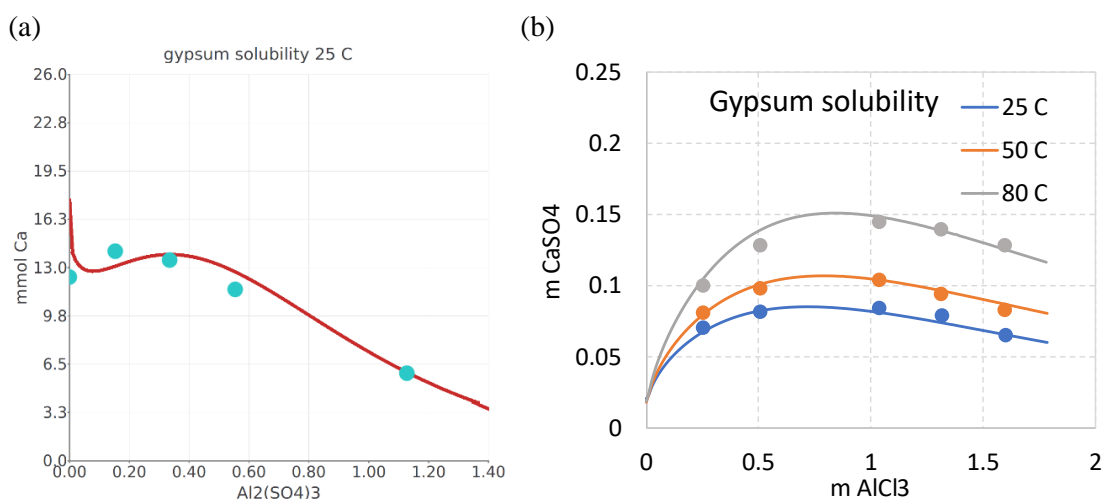


Fig. 3–7 Calculated (lines) and measured (symbols) gypsum solubility $\text{Al}_2(\text{SO}_4)_3$ (a) solution at 25 °C (Mosgovykh et al., 1984) and in AlCl_3 solutions at various temperatures (b) (Li and Demopoulos, 2006).

In the present study, the aim was to achieve the best agreement with measured data for both osmotic coefficient and gypsum solubility in $\text{Al}_2(\text{SO}_4)_3$ and AlCl_3 solutions. To do so, the IPs in the binary $\text{Al}-\text{SO}_4$ and ternary $\text{Al}-\text{M}-\text{SO}_4$ systems were simultaneously fitted, including the $\beta^{(2)}$ parameter and its temperature coefficients, while exploring different combinations of $\alpha^{(1)}$ and $\alpha^{(2)}$ parameters. The $\beta^{(2)}$ and its temperature dependence implicitly accounts for the effect of Al sulphate speciation. After careful analysis, we found that the best agreement with experimental data was obtained by setting the $\alpha^{(1)}$ parameter to 1.4 and leaving the $\alpha^{(2)}$ parameter at 50 (Table 3–6). This approach allows us to better model the osmotic coefficient data (Fig. 3–6) and the solubility of gypsum in $\text{Al}_2(\text{SO}_4)_3$ and AlCl_3 solutions (Fig. 3–7). The temperature dependence of the dataset was evaluated based on limited data on gypsum solubility in AlCl_3 solutions (Li and Demopoulos, 2006) and with the exception of $\beta^{(2)}$ the temperature coefficients of the other IPs were estimated to be 0 for the 25–80 °C interval. Additional experimental data would be

needed for better constraining the temperature coefficients in the system Al–Na–K–Ca–Mg–SO₄–H₂O.

Table 3-6 Pitzer IP coefficients (Eq. 1–1) in the system Al–Na–K–Ca–Mg–SO₄–H₂O. Bold values were evaluated in this study.

IP coefficients Eq. 1-1	A	D	E	T (°C)	Maximum concentration (m)
$\beta^{(0)}(\text{Al}^{3+}, \text{SO}_4^{2-})$	0.577	0	0	25–80	1.1 Al ₂ (SO ₄) ₃ ; 1.6 AlCl ₃
$\beta^{(1)}(\text{Al}^{3+}, \text{SO}_4^{2-})$	10.30	0	0	25–80	1.1 Al ₂ (SO ₄) ₃ ; 1.6 AlCl ₃
$\beta^{(2)}(\text{Al}^{3+}, \text{SO}_4^{2-})$	-2330	480	-0.8	25–80	1.1 Al ₂ (SO ₄) ₃ ; 1.6 AlCl ₃
$C^{(\phi)}(\text{Al}^{3+}, \text{SO}_4^{2-})$	0.007	0	0	25–80	1.1 Al ₂ (SO ₄) ₃ ; 1.6 AlCl ₃
$\alpha^{(1)}(\text{Al}^{3+}, \text{SO}_4^{2-})$	1.400	0	0	25–80	1.1 Al ₂ (SO ₄) ₃ ; 1.6 AlCl ₃
$\alpha^{(2)}(\text{Al}^{3+}, \text{SO}_4^{2-})$	50.00	0	0	25–80	1.1 Al ₂ (SO ₄) ₃ ; 1.6 AlCl ₃
$\psi_c(\text{Al}^{3+}, \text{SO}_4^{2-}, \text{H}^+)$	0	0	0	25	–
$\psi_c(\text{Al}^{3+}, \text{SO}_4^{2-}, \text{Na}^+)$	-0.090	0	0	25	solubility limit of mirabilite and alunogen
$\psi_c(\text{Al}^{3+}, \text{SO}_4^{2-}, \text{K}^+)$	0	0	0	25	1.1 Al ₂ (SO ₄) ₃ , solubility limit of arcanite
$\psi_c(\text{Al}^{3+}, \text{SO}_4^{2-}, \text{Ca}^{2+})$	0	0	0	25–80	1.1 Al ₂ (SO ₄) ₃ , solubility limit of gypsum
$\psi_c(\text{Al}^{3+}, \text{SO}_4^{2-}, \text{Mg}^{2+})$	0	0	0	25	solubility limit of epsomite and alunogen

The binary IPs of Al³⁺ with the metal cations were consistent in both chlorine and sulphate systems. For assessing the ternary IPs $\psi_c(\text{Al}^{3+}, \text{SO}_4^{2-}, \text{metal})$, solubility data for mirabilite (Na₂(SO₄)·10H₂O), epsomite (Mg(SO₄)·7H₂O) and arcanite (K₂(SO₄)) measured at 25 °C were used (Table 3-5). With the exception of the ternary IP with Na⁺, having 0 values for all the other parameters (Table 3-6) lead to good agreement with the measured data (Fig. 3–8). The discrepant value for Na⁺ is related to the value for the binary $\theta_c(\text{Al}^{3+}, \text{Na}^+)$, constrained by the gibbsite solubility, that is also different when compared with the other metals. This shows the relation between different Pitzer parameters in binary and ternary systems and the reason why non unique parameter sets can be derived to achieve similar agreement with the experimental data.

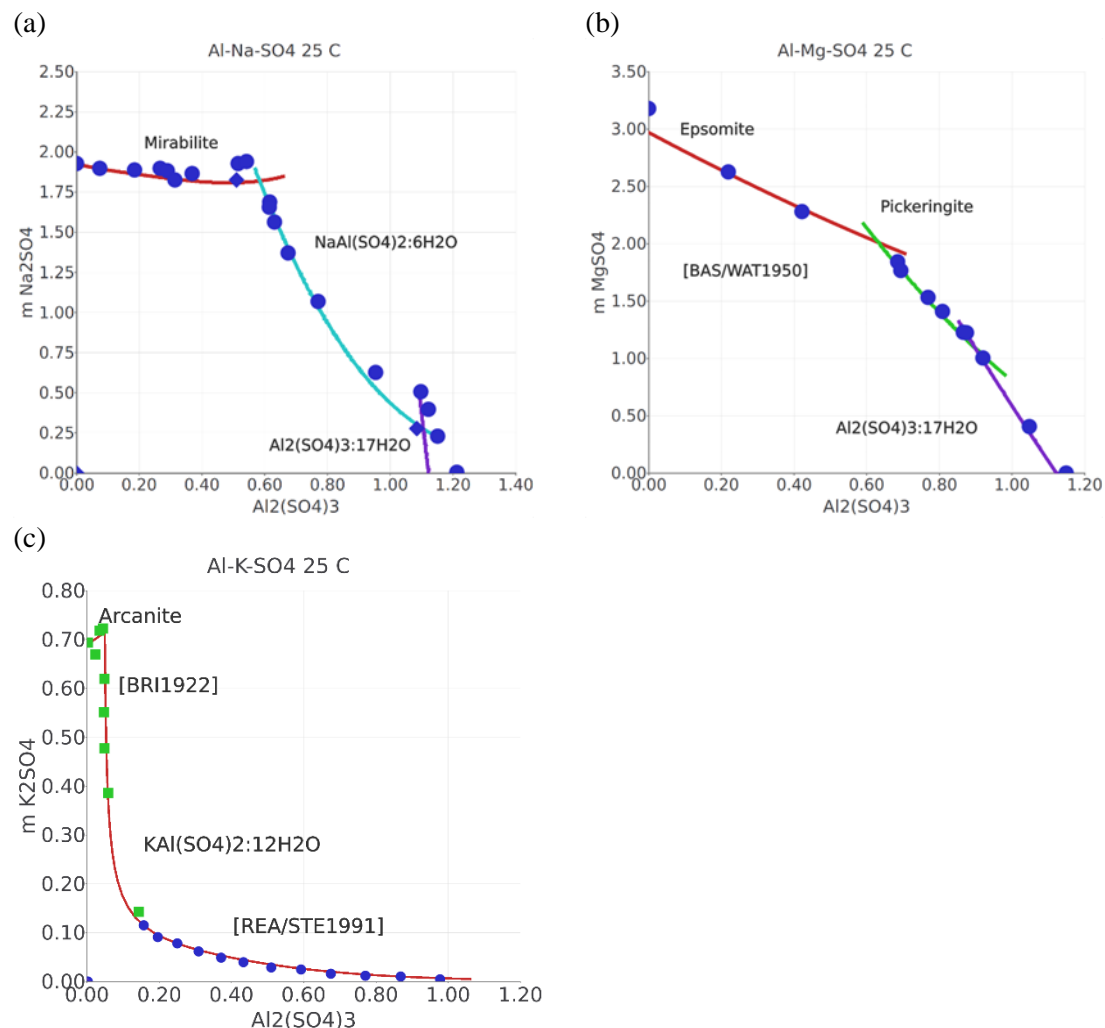
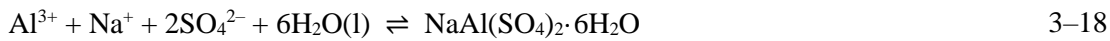
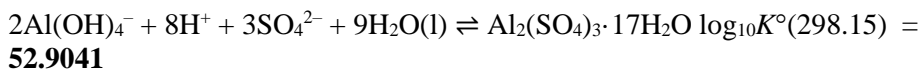


Fig. 3-8 Calculated (lines) and measured (symbols) solubilities in ternary salt systems: (a) $\text{Na}_2\text{SO}_4\text{-Al}_2(\text{SO}_4)_3$ circles (Dobbins and Addleston, 1931), diamonds (DRUZHININ et al., 1961); (b) $\text{MgSO}_4\text{-Al}_2(\text{SO}_4)_3$ (Bassett and Watt, 1950); (c) $\text{K}_2\text{SO}_4\text{-Al}_2(\text{SO}_4)_3$ squares (Britton, 1922), circles (Reardon and Stevens, 1991).

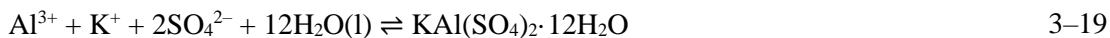
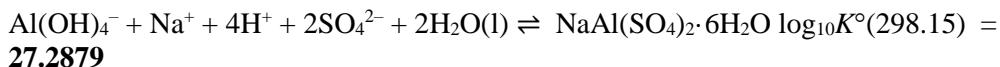
Thermodynamic data for mirabilite, epsomite and arcanite were available in the THEREDA database from previous reviews. No data were available for Na-alum ($\text{NaAl}(\text{SO}_4)_2\cdot 6\text{H}_2\text{O}$), K-alum ($\text{KAl}(\text{SO}_4)_2\cdot 12\text{H}_2\text{O}$), pickeringite ($\text{MgAl}_2(\text{SO}_4)_4\cdot 22(\text{H}_2\text{O})$) and alunogen ($\text{Al}_2(\text{SO}_4)_3\cdot 17\text{H}_2\text{O}$) aluminium salts. Values for the $\log_{10}K^\circ(298.15)$ for these solids were retrieved in the present review based on solubility data at 25 °C that were consistent with the selected Pitzer IPs (Table 3-4, Table 3-6):



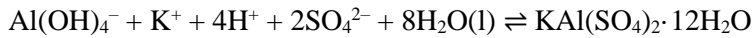
$$\log_{10}K^\circ(298.15) = 7.1676$$



$$\log_{10}K^\circ(298.15) = 4.4197$$



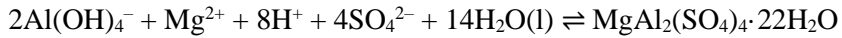
$$\log_{10}K^\circ(298.15) = 6.8431$$



$$\log_{10}K^\circ(298.15) = \mathbf{29.7113}$$



$$\log_{10}K^\circ(298.15) = 9.2338$$



$$\log_{10}K^\circ(298.15) = \mathbf{54.9703}$$

3.3.4 Al–CO₂–H₂O

Yasunishi and Yoshida (1979) measured the solubility of CO₂(g) in the presence of Al₂(SO₄)₃ and AlCl₃ solutions at 25 °C. The data were reported in terms of Oswald coefficients $L = V_{\text{gas}}/V_{\text{solution}}$ (ratio between the volume of the gas and that of the solution) that were converted to molality through the following relation:

$$m_{\text{CO}_2} = \frac{L \cdot (10^3 + m_{\text{electrolyte}} * M_{\text{electrolyte}})}{\rho_{\text{solution}} \cdot (V_{\text{CO}_2(g)}^\circ - L \cdot V_{\text{CO}_2(aq)}^\circ)}, \quad 3-21$$

Where $m_{\text{electrolyte}}$ is the electrolyte concentration, $M_{\text{electrolyte}}$ is the solute molar mass, $V_{\text{CO}_2(g)}^\circ = 24343 \text{ cm}^3$ is the CO₂ gas molar volume, and $V_{\text{CO}_2(aq)}^\circ = 35 \text{ cm}^3$ (Yasunishi and Yoshida, 1979) is the molar volume of aqueous CO₂. The solubility data was then used to retrieve the $\lambda(\text{CO}_2(\text{aq}), \text{Al}^{3+}) = \mathbf{0.24}$

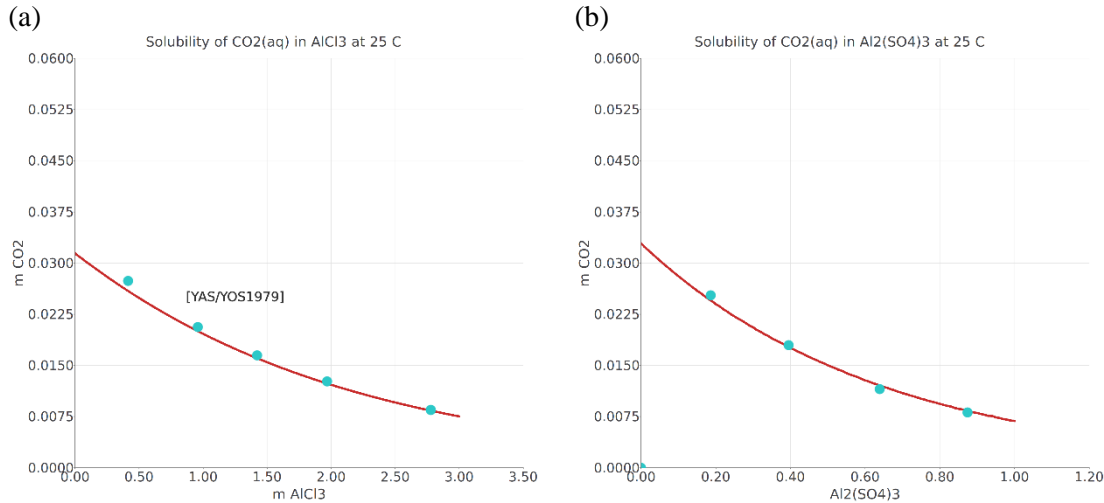


Fig. 3-9 Calculated (lines) and measured (symbols) (Yasunishi and Yoshida, 1979) solubility of CO₂ (mol·kg⁻¹ H₂O) in (a) AlCl₃ and (b) Al₂(SO₄)₃ solutions.

3.4 IPs in the Al–Ca–Mg–Cl–OH[−]SO₄^{2−}CO₂ system at intermediate to high pH

From low to high pH Al³⁺ hydrolyses to form a series of species of the form Al(OH)_n^{3−n} where n ranges from 0 to 4. Available data to derive standard thermodynamic properties (section 3.1) and IPs were solubility and osmotic coefficient measurements (Table 3-7). Most data were available at high pH, where the Al(OH)₄[−] species dominates. Potentiometric data were available for the first aluminium hydrolysis (AlOH²⁺) at various temperatures in NaCl solutions (Palmer and Wesolowski, 1993). Only for these two species could IPs be obtained from experimental data in NaCl systems. For the intermediate hydrolysed species Al(OH)₂⁺ IPs with Cl[−] were estimated from SIT correlations (Table 1-1) from ε 0.05 (Hummel and Thoenen, 2023). For Al(OH)₃(aq) IPs were assumed to be the same by analogy with Si(OH)₄(aq). No data or estimation methods were available to be able to derive IPs for AlOH²⁺, Al(OH)₂⁺ with HCO₃[−] and SO₄^{2−}.

Table 3-7 Experimental data used to asses the IPs in the system Al–Na–K–Cl–H₂O.

Reference	System	T (°C)	Concentration interval (m)
(Wesolowski, 1992)	gibbsite, NaOH, KOH, NaCl, KCl	0–80	0.01–5
(Palmer and Wesolowski, 1993)	AlOH ²⁺ , NaCl	25–125	0.1–5
(Russell et al., 1955)	gibbsite, NaOH	40–100	0.5–11
(Luo et al., 2020)	K ₂ O–Al ₂ O ₃ –H ₂ O	50–80	0.5–20
(Zhou et al., 2003)	NaOH–NaAl(OH) ₄ [−] H ₂ O	40	0.05–12
(Königsberger et al., 2006) reported in (Sipos et al., 1998)	NaOH–NaAl(OH) ₄ [−] H ₂ O	125	0.8–6.5
(Bénédith et al., 2001; Palmer et al., 2001)	boehmite, NaCl	100–290	0.03–5
(Park and Englezos, 1999b)	NaOH AlCl ₃ ·6H ₂ O	25	1–4 0.05–0.35

3.4.1 IPs for aluminium hydrolysed species

At intermediate pH Al hydrolysed species play a role in the dissolved concentration of aluminium. Data for the first hydrolysed species have been collected in NaCl solutions from 25 to 100 °C (Palmer and Wesolowski, 1993). The initial values for the IPs were estimated based on the correlation with SIT (Table 1-1) ε 0.15 (Hummel and Thoenen, 2023) and further adjusted to the measured data (Fig. 3–10). IPs for the second hydrolysis constant were estimated using ε 0.05 (Hummel and Thoenen, 2023). For Al(OH)₃(aq) the IPs were assumed to be the same as for Si(OH)₄(aq).

This should be a reasonable approximation for the salting out effect of the background electrolyte (e.g., NaCl) has on the neutral species. Other IPs that may be required for the positively charged hydrolysis species with SO_4^{2-} and HCO_3^- cannot be determined due to the lack of experimental data where these species were present at significant concentrations. Additional experimental data are required for the solubility of aluminium hydroxides in sulphate and carbonate solutions at intermediate pH.

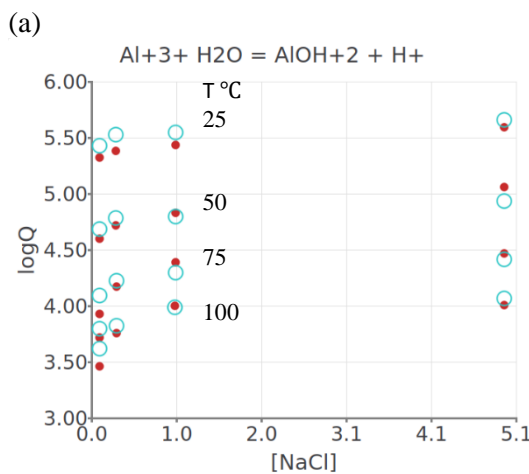


Fig. 3–10 Measured (Palmer and Wesolowski, 1993), full, and calculated, empty, symbols of first aluminium hydrolysis formation constant as a function of I at different temperatures.

Table 3-8 Pitzer IP coefficients (Eq. 1-1) for first and second Al hydrolysis species.

IP coefficients Eq. 1-1	A	B	T (°C)	Concentration interval (m)
$\beta^{(0)}(\text{AlOH}_2^+, \text{Cl}^-)$	0.41	-35	25–100	0–5 NaCl
$\beta^{(1)}(\text{AlOH}_2^+, \text{Cl}^-)$	1.56	0	25–100	0–5 NaCl
$\beta^{(0)}(\text{Al(OH)}_2^+, \text{Cl}^-)$	0.06	0		
$\beta^{(1)}(\text{Al(OH)}_2^+, \text{Cl}^-)$	0.34	0		

3.4.2 IPs for Al(OH)_4^-

3.4.2.1 System Na–K–Cl–OH– Al(OH)_4^-

Extensive data sets on the solubility of aluminium hydroxides (gibbsite and boehmite) have been published. Measurements have been made up to high concentrations of Na/K–OH–Cl solutions and over wide range of temperatures (Table 3-7) allowing a polythermal set of Pitzer IPs to be derived. (Wesolowski, 1992) derives a Pitzer model in the system Na–K–Cl–OH– Al(OH)_4^- using his own data and published data (Russell et al., 1955), and finds that the system can be described by a number of approximations:

$$\beta^{(0)}(\text{Na}^+, \text{OH}^-) - \beta^{(0)}(\text{Na}^+, \text{Al(OH)}_4^-) = \beta^{(0)}(\text{K}^+, \text{OH}^-) - \beta^{(0)}(\text{K}^+, \text{Al(OH)}_4^-) = 0.0356 \quad 3-22$$

$$\beta^{(1)}(\text{Na}^+, \text{OH}^-) - \beta^{(1)}(\text{Na}^+, \text{Al(OH})_4^-) = \beta^{(1)}(\text{K}^+, \text{OH}^-) - \beta^{(1)}(\text{K}^+, \text{Al(OH})_4^-) = 0.0 \quad 3-23$$

$$C^{(\phi)}(\text{Na}^+, \text{OH}^-) - C^{(\phi)}(\text{Na}^+, \text{Al(OH})_4^-) = C^{(\phi)}(\text{K}^+, \text{OH}^-) - C^{(\phi)}(\text{K}^+, \text{Al(OH})_4^-) = 0.00526 \quad 3-24$$

$$\psi_a(\text{Al(OH})_4^-, \text{Na}^+, \text{OH}^-) = \psi_a(\text{Al(OH})_4^-, \text{K}^+, \text{OH}^-) \quad 3-25$$

Such approximations have been used in the present work to derive missing IPs with K^+ from those with Na^+ (e.g., section 2.4). Not explicitly mentioned by (Wesolowski, 1992) the additional approximation can be considered:

$$\psi_a(\text{Cl}^-, \text{Na}^+, \text{OH}^-) - \psi_a(\text{Cl}^-, \text{Na}^+, \text{Al(OH})_4^-) = (\text{Cl}^-, \text{K}^+, \text{OH}^-) - \psi_a(\text{Cl}^-, \text{K}^+, \text{Al(OH})_4^-) = 0.0 \quad 3-26$$

From relations 3–22 to 3–26 and the values for the respective IPs of Na^+ , and K^+ with OH^- and Cl^- , part of the oceanic salt system in THEREDA, the corresponding IPs (Table 3-9) for $\text{Al(OH})_4^-$ were obtained. The differences between the polythermal Pitzer IP coefficients were 0.0. An improvement between the modelled and experimental data could be obtained by further optimizing $\theta_a(\text{Al(OH})_4^-, \text{Cl}^-)$ **-0.045**, $\theta_a(\text{Al(OH})_4^-, \text{OH}^-)$ **0.0**, compared to 0.014 in (Wesolowski, 1992), and $\psi_a(\text{Al(OH})_4^-, \text{Na}^+/\text{K}^+, \text{OH}^-)$ **-0.003**, compared to -0.0048 in (Wesolowski, 1992). The agreement between measured and modelled data is within the experimental uncertainty for gibbsite solubility in NaOH , KOH , NaOH-NaCl , and NaCl-KCl-KOH solutions of different concentrations up to 100 °C (Fig. 3–11). Discrepancies can be observed in KOH solutions above 5 M KOH with data from (Luo et al., 2020). In this case the agreement can be further improved by setting a value of -0.007 for $C^{(\phi)}(\text{Al(OH})_4^-, \text{K}^+)$. In addition, there is excellent agreement with the osmotic coefficient measurements in $\text{NaOH-NaAl(OH})_4$ solutions made at 40 and 125 °C. Systematic over-predictions of the osmotic coefficient measurements in NaOH-AlCl_3 solutions of (Park and Englezos, 1999b) were observed but can't be explained. The same discrepancy was mentioned by (Königsberger et al., 2006) that this data set can't be reproduced by the Pitzer model and seems to be inconsistent with other measurements.

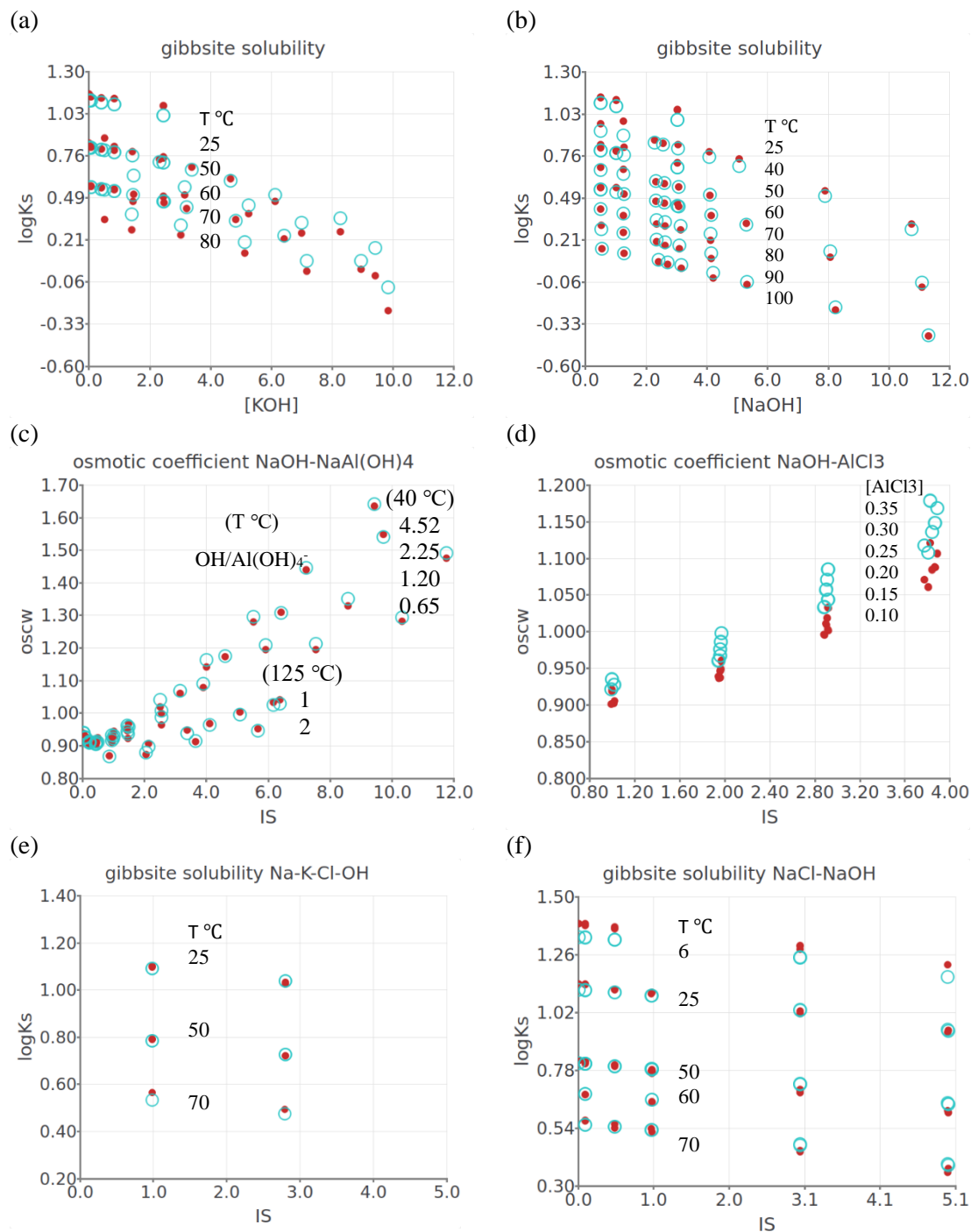


Fig. 3–11 Measured, full, and calculated, empty, symbols: (a) gibbsite solubility at different T in KOH solutions (Wesolowski, 1992) and (Luo et al., 2020); (b) gibbsite solubility at different T in NaOH solutions (Wesolowski, 1992) and (Russell et al., 1955); (c) osmotic coefficient of NaAl(OH) solutions at different T (Sipos et al., 1998); (d) osmotic coefficient of NaOH–AlCl₃ solutions at 25 °C (Park and Englezos, 1999b); (e) gibbsite solubility in NaCl–KCl solutions (Wesolowski, 1992); (f) gibbsite solubility in NaCl–NaOH (m) solutions at different temperatures (Wesolowski, 1992).

Table 3-9 Pitzer IP coefficients (Eq. 1-1) in the system Al–Na–K–Cl–H₂O at elevated pH. Bold values were evaluated in this study. Values in regular font were derived from equivalent IPs of OH[−] and corresponding cations and anions (see text for details). Al concentrations in solution up to 1.5 mol·kg^{−1} H₂O.

IP coefficients Eq. 1-1	A	B	D	T (°C)	Maximum concentr. (m)
$\beta^{(0)}(\text{Al(OH)}_4^-, \text{Na}^+)$	0.0679	−9.8888E+01	−1.0479E−03	0–150	0–12 NaOH
$\beta^{(1)}(\text{Al(OH)}_4^-, \text{Na}^+)$	0.1246	−2.0611E+02	−1.2958E−03	0–150	0–12 NaOH
$C^{(\phi)}(\text{Al(OH)}_4^-, \text{Na}^+)$	−0.0031	1.7300E+01	1.1827E−04	0–150	0–12 NaOH
$\beta^{(0)}(\text{Al(OH)}_4^-, \text{K}^+)$	0.1008	1.4701E+02	7.8788E−04	0–150	0–10 KOH
$\beta^{(1)}(\text{Al(OH)}_4^-, \text{K}^+)$	0.3349	−2.1511E+03	−1.7131E−02	0–150	0–10 KOH
$C^{(\phi)}(\text{Al(OH)}_4^-, \text{K}^+)$	−0.0035	−2.2316E+01	−2.0222E−04	0–150	0–10 KOH
$\theta(\text{Al(OH)}_4^-, \text{OH}^-)$	0	0	0	0–150	0–10 KOH 0–12 NaOH
$\theta(\text{Al(OH)}_4^-, \text{Cl}^-)$	−0.045	−49	0	0–150	0–5 NaCl
$\psi(\text{Al(OH)}_4^-, \text{Na}^+, \text{OH}^-)$	−0.003	0	0	0–150	0–12 NaOH
$\psi(\text{Al(OH)}_4^-, \text{K}^+, \text{OH}^-)$	−0.003	0	0	0–150	0–10 KOH
$\psi(\text{Al(OH)}_4^-, \text{Na}^+, \text{Cl}^-)$	−0.0043	C D E	8.2841E−01 −4.7316E−03 3.3739E−06	0–150	0–5 NaCl
$\psi(\text{Al(OH)}_4^-, \text{K}^+, \text{Cl}^-)$	−0.0032	−1.7041E+00	2.02194E−05	0–150	0–5 KCl

3.4.2.2 System Ca–Mg–CO₃–SO₄–Al(OH)₄

No measured data were available to derive potential IPs between Al(OH)₄[−], Ca²⁺, and Mg²⁺. At elevated pH conditions it is expected that calcium and magnesium hydroxides will precipitate (e.g. portlandite, brucite) and other calcium and magnesium cementitious phases are expected to precipitate, keeping these elements at millimolar concentrations, making the effect of IPs insignificant compared to other possible background electrolytes such as the alkali metals. Interactions between Al(OH)₄[−] and other negatively charged species such as CO₃^{2−} and SO₄^{2−} may become relevant in concentrated solutions. Using the observations from the NaOH–Al(OH)₄ system these IPs and their temperature coefficients were estimated to be equal to those with OH[−] as analogous for Al(OH)₄[−] (Table 3-10). An independent test of the derived model predictions against measurements of gibbsite solubility in solutions containing varying amounts of Na₂CO₃ and in synthetic Bayer liquors (containing Cl–CO₃–SO₄) shows good agreement with the derived Pitzer IPs set (Fig. 3–12). The solution concentration reported in (Bouzat and Philipponneau, 1991) was approximated to molality using the density of NaOH solutions at 60 and 50 °C. Therefore the measured data may not represent the true values although a large difference having the correct solutions densities is not expected. (Königsberger et al., 2006) got good agreement with these measurements and predictions using a very similar Pitzer model.

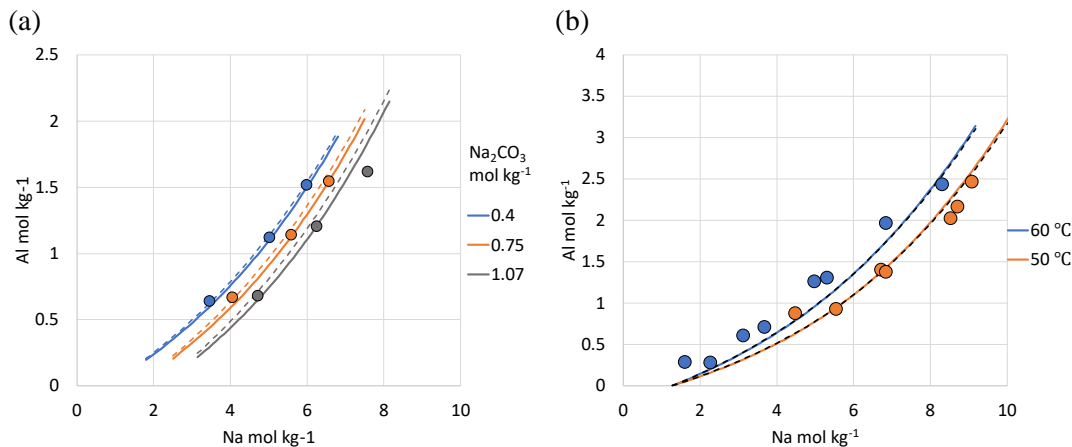


Fig. 3-12 Comparison between measured (symbols) and model calculated gibbsite solubility in (a) Na₂CO₃ solutions at 60 °C (Königsberger et al., 2006), (b) synthetic Bayer liquors recalculated [Cl⁻] = 0.27 mol kg⁻¹ H₂O, [SO₄²⁻] = 0.25 mol kg⁻¹ H₂O, and [CO₃²⁻] = 0.25 mol kg⁻¹ H₂O (Bouzat and Philipponneau, 1991). Dashed lines model predictions with IPs between Al(OH)₄⁻, CO₃²⁻ and SO₄²⁻ set to 0;

Table 3-10 Pitzer IP coefficients (Eq. 1-1) in the system Al-SO₄-CO₃ at elevated pH. Values in regular font were derived from equivalent IPs of OH⁻ and corresponding anions (see text for details).

IP coefficients Eq. 1-1	A	B	C	D	E
$\theta_a(\text{Al(OH)}_4^-, \text{SO}_4^{2-})$	-0.0116	0	1.4531E-01	-2.2723E-03	1.9538E-06
$\theta_a(\text{Al(OH)}_4^-, \text{CO}_3^{2-})$	0.1	0	0	0	0
$\psi_a(\text{Al(OH)}_4^-, \text{Na}^+, \text{SO}_4^{2-})$	-0.0115	-2.5545E+00	0	1.4774E-04	0
$\psi_a(\text{Al(OH)}_4^-, \text{Na}^+, \text{CO}_3^{2-})$	-0.017	0	0	0	0
$\psi_a(\text{Al(OH)}_4^-, \text{K}^+, \text{SO}_4^{2-})$	-0.0097	-4.2090E+01	0	0	0
$\psi_a(\text{Al(OH)}_4^-, \text{K}^+, \text{CO}_3^{2-})$	-0.01	0	0	0	0

3.4.3 Al – Si and polymeric species

At elevated pH conditions aluminium hydroxides are expected to precipitate and in cementitious systems aluminate phases are expected to form. (Pokrovskii and Helgeson, 1995) suggest that oligomeric anions such as Al₂O(OH)₆³⁻, Al(OH)₆³⁻, only occur at aluminate concentrations above 1.5 mol/kg and at very high sodium hydroxide concentrations (> 5 mol/L) (Hummel and Thoenen, 2023). The evaluated experimental data even at very high concentrations of Al and hydroxide solutions show that the aluminium monomeric species Al(OH)₄⁻ with the corresponding Pitzer IPs were sufficient to model the observations. This was confirmed in the comprehensive model for Bayer Liquors by (Königsberger et al., 2006), these solutions are important in the refinement of alumina from bauxite ore. When modelling the solubility of calcium silicate hydrates, which control the pore solution composition in most cementitious systems, measured data could be described by monomeric species alone (Miron et al., 2021) (Al concentration is below millimolar values).

Other species reported in the literature are complexes with the alkali ions Na^+ and K^+ , $\text{NaAl(OH)}_4\text{(aq)}$ and $\text{KAl(OH)}_4\text{(aq)}$, respectively, which were used to describe the solubility of gibbsite and boehmite in alkaline hydroxide solutions (Miron et al., 2016; Pokrovskii and Helgeson, 1997, 1995). These species were used in conjunction with Debye–Hückel–type activity models, and were not required in interaction–based activity models such as SIT or Pitzer. Including them would create an inconsistency with the IPs of Al(OH)_4^- and the alkali ions.

Several studies have suggested possible Al–Si complexation at elevated pH conditions (Gout et al., 1999, 2000; Salvi et al., 1998; Xiong, 2013, 2016). Neither $\text{Al(OH)}_3\text{SiO(OH)}_3^-$ nor $\text{AlSiO}_3(\text{OH})_4^{3-}$ complexes were found to be important for explaining the measured potentiometric and NMR measurements (Gout et al., 2000, 1999) at pH ~12.5 and the $\text{Al(OH)}_3\text{SiO(OH)}_3^-$ complex was later retracted (Hummel and Thoenen, 2023). (Gout et al., 2000) suggest the existence of different polynuclear Al – Si complexes at $m(\text{Al},\text{Si}) > 0.006 \text{ m}$, but there were no data to distinguish them or to determine the properties of these complexes. (Salvi et al., 1998) suggest that Si–Al complexation may be relevant in strongly acidic solutions ($\text{pH} < 2$, AlSiO(OH)_3^{2+} as selected in section 3.2), and above pH 4.5 forming $\text{Al(OH)}_3\text{SiO(OH)}_3^-$. At pH 14 (Gout et al., 2000) the importance of $\text{AlSiO}_3(\text{OH})_4^{3-}$ was suggested. If such complexes were formed in significant amounts under alkaline conditions, they would be relevant to the modelling of cementitious systems and other alkali–rich systems, e.g. zeolites. (Xiong, 2013) developed a Pitzer model for Si and Al in alkaline conditions and found that the use of Al–Si complexes was not necessary to model the solubility experiments in concentrated NaOH solutions up to 90 °C. The important species at experimental conditions were predicted to be the monomeric Si and Al(OH)_4^- . When the CASH+ model (Miron et al., 2021) was developed using the cemdata18 database, which includes the $\text{AlSiO}_3(\text{OH})_4^{3-}$ species, Al(OH)_4^- was the only contributor to the dissolved Al and was sufficient to describe the measured solubility data. Due to the limited information on the importance of Al–Si complexation at 0–100 °C in cementitious systems and the lack of measured data over wide range of conditions to be able to derive Pitzer IPs for these species, they were not selected for inclusion in the THEREDA database.

3.5 Benchmark against experimental data on the solubility of cement hydrates

The newly derived model was compared with independent published solubility data of relevant hydrated cement phases, C–S–H, M–S–H, and various cement phase assemblages at invariant points. The thermodynamic data for the solid phases were taken as such from THEREDA (v2022) and originated from cemdata18 (Lothenbach et al., 2019). For comparisons with solubility measurements for aluminium containing C–S–H, the new CASH+ model and parameterization was used (Kulik et al., 2022; Miron et al., 2022a, 2022b, 2021). It is important to note that the standard thermodynamic properties of these solids were derived from solution data using a different activity model (Lothenbach et al., 2019). In general, the concentrations of these solutions were below 0.5 molal, where the predictions of different activity models converge. Therefore, good agreement with the updated Pitzer dataset is important, but some differences were acceptable and can only be reconciled if the standard thermodynamic data for these cement hydrate phases were retrieved from their solubility measurements modelled using the updated Pitzer dataset and the THEREDA database. Such an endeavour was beyond the scope of the present work.

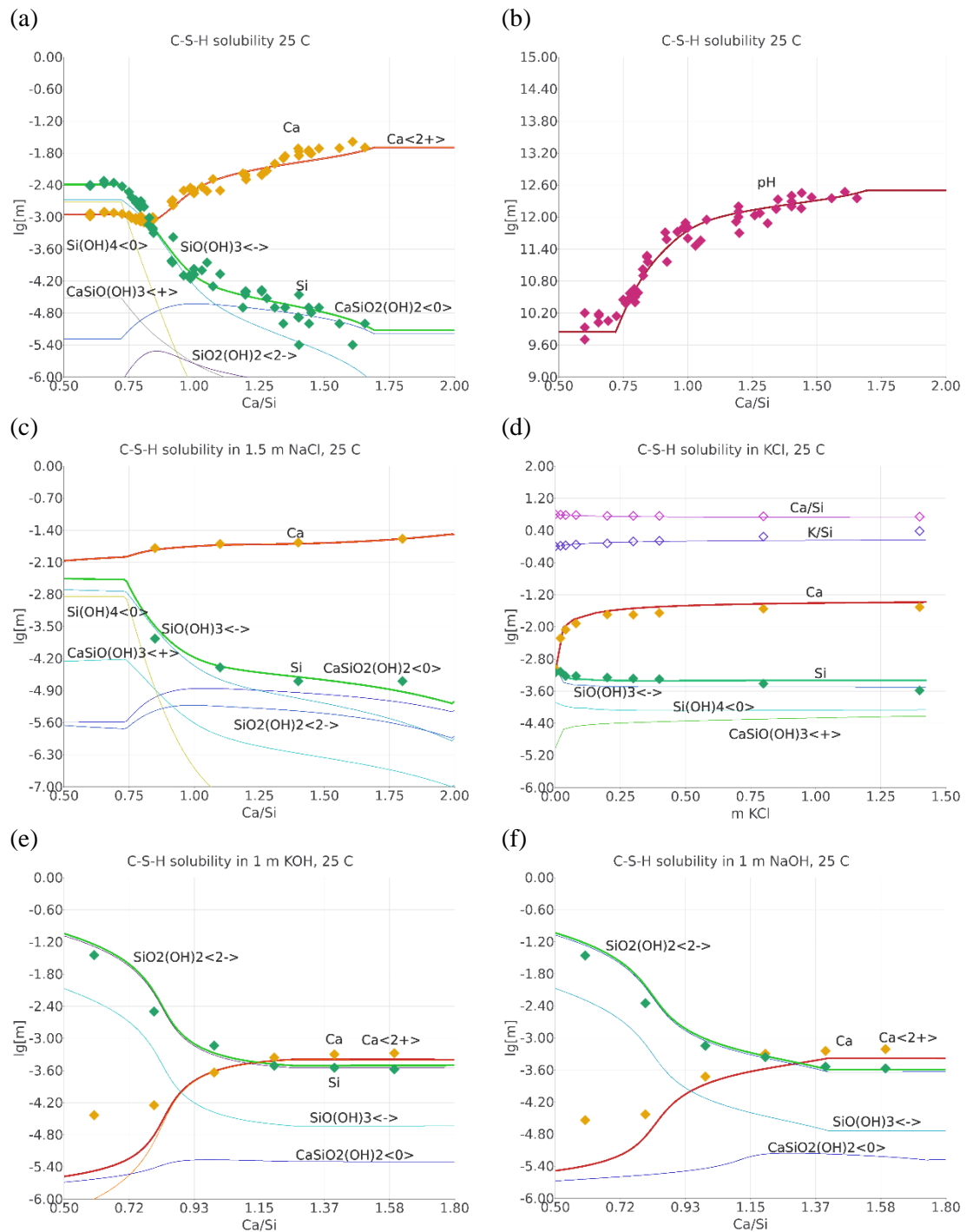


Fig. 3–13 Measured (symbols) and model calculated C–S–H solubility using THEREDA, the updated Pitzer dataset and CASH+ model at 25 °C. Si and Ca concentrations in mol $\text{kg}^{-1} \text{H}_2\text{O}$ vs target ratio (a) in water (Kulik et al., 2022); (b) pH; (c) in NaCl (Glasser et al., 1999) (d) KCl (Plusquellec, 2014), (e) NaOH (Yan et al., 2021), and (f) KOH (Yan et al., 2021) solutions.

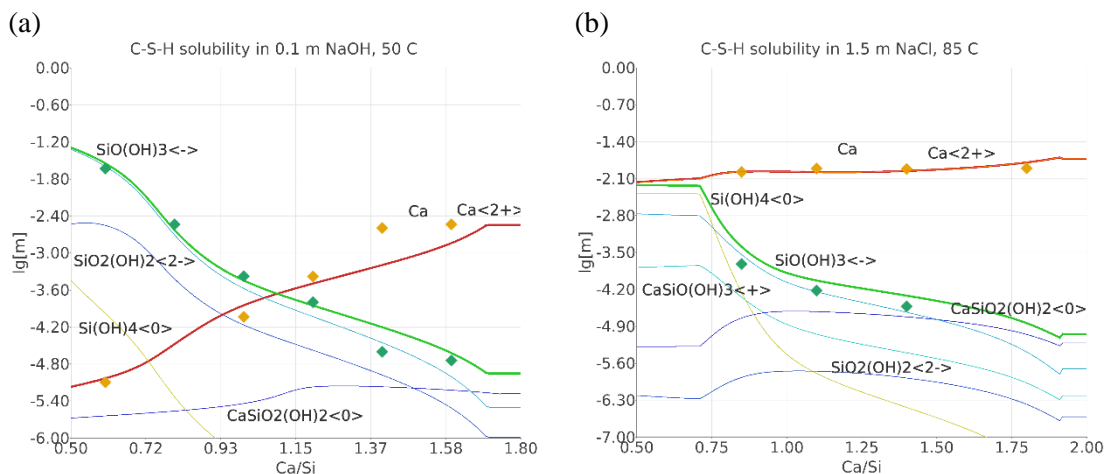


Fig. 3-14 Measured (symbols) and model calculated C–S–H solubility using THEREDA, the updated Pitzer dataset and CASH+ model at elevated temperatures. Si and Ca concentrations in mol kg⁻¹ H₂O vs target ratio (a) in NaOH solution at 50 °C (Myers et al., 2015) (b) in NaCl solution at 85 °C (Glasser et al., 1999).

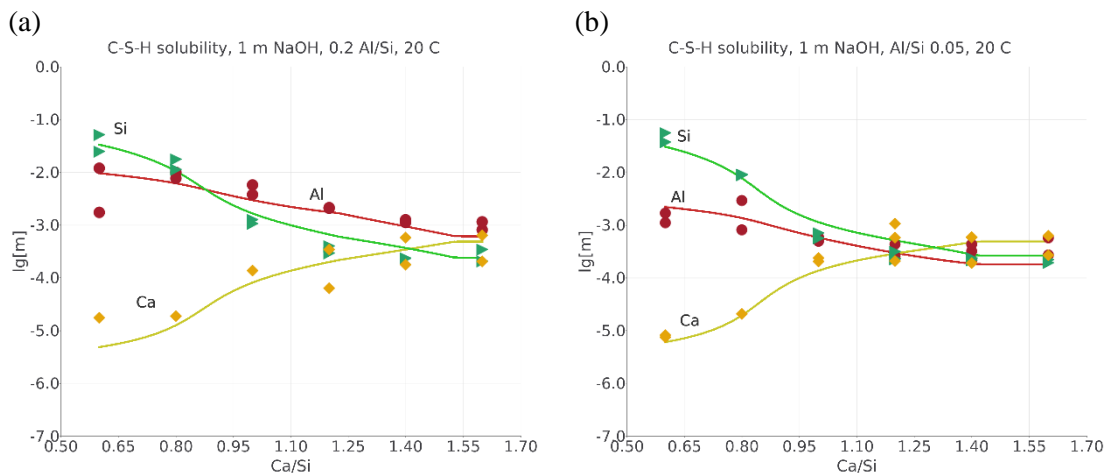


Fig. 3-15 Measured (symbols) (Yan et al., 2022) and model calculated aluminium containing C–S–H solubility using THEREDA, the updated Pitzer dataset and CASH+ model at 20 °C 1 m NaOH and different target Al/Si ratios. Si, Ca, and Al concentrations in mol kg⁻¹ H₂O vs target ratio.

Predictions of solution compositions using the updated Pitzer model were compared with measured C–S–H solubility in different electrolyte solutions and different temperatures (Fig. 3–13–15). The predictions were in good agreement with the measured data. Si speciation is dominated by SiO(OH)_3^- and $\text{Si(OH)}_4^-(\text{aq})$ species at low, SiO(OH)_3^- at intermediate and $\text{CaSiO}_2(\text{OH})_2(\text{aq})$ at high Ca/Si ratios, respectively. The proportions of species change in alkaline solutions where $\text{SiO}_2(\text{OH})_2^{2-}$ becomes dominant and Ca is controlled by $\text{CaSiO}_2(\text{OH})_2(\text{aq})$ instead of Ca^{2+} at low Ca/Si ratios. In general, Ca concentrations in solution were predicted to be around a few millimoles and decreases in alkali hydroxide solutions. Si concentrations were below millimolar at high Ca/Si but they increase in alkali hydroxide solutions at low Ca/Si ratios. Al concentrations decrease with increasing Ca/Si in alkali hydroxide solutions and were exclusively determined by the Al(OH)_4^- species. Some discrepancies with measured Ca concentrations at low

Ca/Si in alkali hydroxide solution can be explained by an inaccurate CASH+ phase model or by measurement problems at very low concentrations and high electrolyte in solution.

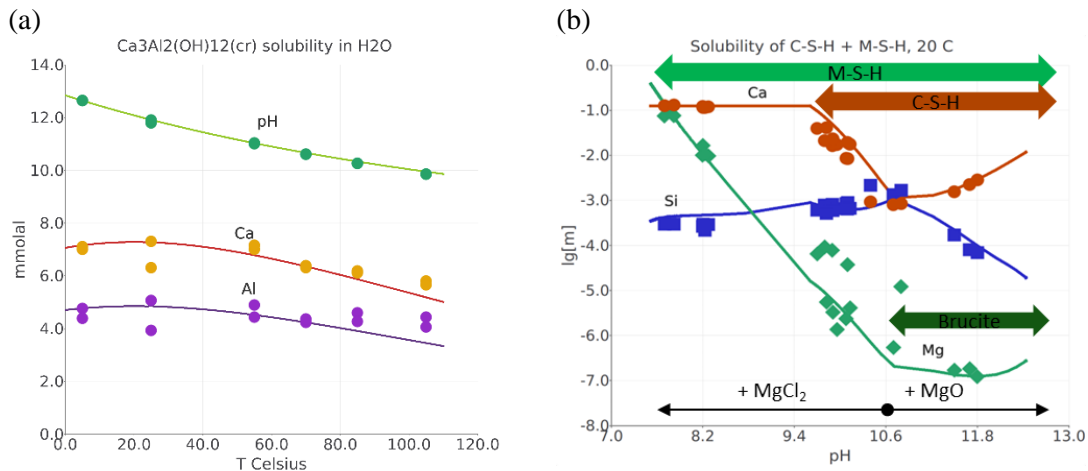


Fig. 3–16 Measured (symbols) and calculated aqueous composition. (a) Ca, Al, pH in equilibrium with CAH at different temperatures (Matschei et al., 2007); (b) Ca, Si, Mg concentrations in $\text{mol kg}^{-1} \text{H}_2\text{O}$ as a function of pH varying by addition of MgCl_2 or MgO (m). Thermodynamic data for M–S–H and measured values from (Bernard et al., 2018).

The updated model predictions agree well with measured CAH (calcium aluminate hydrate, $\text{Ca}_3\text{Al}_2(\text{OH})_{12}(\text{cr})$) solubility in water up to 110 °C (Fig. 3–16). The aqueous composition of a solution in the system $\text{Ca}-\text{Mg}-\text{Si}-\text{Cl}-\text{OH}$ with C–S–H, M–S–H, and brucite phase assemblage is well reproduced by the model (Fig. 3–16).

For a better overview of the model predictions for different relevant cement phases calculations were done for several invariant points and compared with measured values based on data collected by (Prentice, 2018) (Table 3-12, Table 3-12). Good agreement was obtained between the measured and calculated data with few disagreements (Table 3-12) unlikely to be due to the present aqueous model.

Table 3-11 Mineral phases in equilibrium for invariant points calculations. NaOH and KOH solution concentration in mol kg⁻¹ H₂O.

#	Ch		Gp	Ms	Mc	Hc	Cc	Ett	CAH	Gbs	NaOH	KOH
1									+	+		
2	+								+			
3	+								+		0.25	
4	+								+			0.178
5	+		+									
6	+			+					+			
7	+			+					+			
8	+		+						+			
9	+		+									
10	+		+						+			0.178
11	+		+									0.178
12	+		+						+		0.25	
13	+		+								0.25	
14	+					+				+		
15	+				+	+						
16	+				+		+					
17	+							+				

Ch-portalndite; Gp-gypsum; Ms-monosulphate; Mc-monocarbonate; Hc-hemicarbonate; Cc-calcite; Ett-ettringite; CAH-Ca₃Al₂(OH)₁₂(cr); Gbs-gibbsite.

Table 3-12 Measured and calculated elemental concentrations of solutions in equilibrium at invariant points of different cement hydrate phases (Table 3-12) in mmol kg⁻¹.

#	Ca		S		C		Al		pH	
1	8.03	8.77					1.09	1.04	12.10	12.14
2	19.37	20.33					0.09	0.11	12.52	12.50
3	1.56	1.62					0.15	0.76	13.23	13.26
4	2.61	2.11					0.1	0.52		13.15
5	30.69	32.18	12.47	12.70					12.43	12.46
6	19.35	20.33	0.001	0.001			0.09	0.11	12.48	12.50
7	19.35	20.31	0.01	0.01			0.038	0.042	12.48	12.50
8	30.69	32.77	12.47	13.04			5.70E-07	4.58E-07	12.43	12.46
9	30.69	32.77	12.47	13.04					12.43	12.46
10	16.5	16.84	66	65.1						12.75
11	16.65	16.84	66.9	64.8						12.75
12	15.39	16.06	93.9	90.9						12.80
13	15.39	16.07	93.9	90.5						12.80
14	19.37	20.33			8.30E-06	1.46E-06	0.090	0.115	12.48	12.50
15	19.36	20.30			3.00E-04	2.97E-04	0.040	0.030	12.48	12.50
16	19.35	20.29			6.50E-03	7.05E-03	0.007	0.006	12.48	12.50
17	19.34	20.29			6.50E-03	7.05E-03			12.48	12.50

Bold values were model calculated.

4 Status of data, implications and data gaps

The thermodynamic data in the Al–Si–Ca–Mg–Na–K–Cl–SO₄–CO₂–H₂O system have been reviewed, in particular the interactions between aqueous Si and Al species and the oceanic salt ions. The standard thermodynamic properties of Si and Al aqueous species, oxide and hydroxide solids have also been re-evaluated. A summary of the status of the available data and parameters is given in Table 4-1. Based on the available experimental measurements, a polythermal set of IPs was retrieved. In cases where experimental data were not available, to avoid gross errors in calculations, interactions have been estimated based on analogy or correlation with the SIT parameters. Such approximations should provide a qualitative representation of systems with a major binary background electrolyte up to moderate concentrations. The data set updated in THEREDA is consistent with the cemdat18 extension and is valid up to moderate temperatures of 100–150 °C. The available experimental data do not cover the investigated system homogeneously for different compositions and temperatures. There were several shortcomings in the data and additional investigations and experimental measurements are required to evaluate the thermodynamic data of the species and the IPs.

For the Si system, there were limited measured data at high pH conditions relevant to cement systems, especially for the SiO₂(OH)₂²⁻. Further investigations are recommended:

- Solubility data for quartz and SiO₂(am) at high pH and elevated T to constrain the temperature dependence and in KOH-KCl solutions to retrieve the corresponding IPs, currently estimated. Potentiometric measurements of silicic acid hydrolysis in KCl-KOH solutions 0–100 °C. Complementary data to test potential ternary interactions with sulphate and carbonate solutions at high pH. Measurements in ACl₃ solutions for the Si and Al interactions/complexation at low pH.
- Measurements in solutions of CaCl₂, MgCl₂ relevant to high salinity systems to evaluate data Si complexation with alkaline earth metals and investigate if interactions with Si species are needed. These may include solubility measurements of CaSiO₃/MgSiO₃ and thaumasite in CaCl₂ and MgCl₂ solutions.
- Solubility, potentiometric and NMR studies of polymeric Si species that may play a role in Si rich solutions of late stages of degradation of cementitious materials – zeolites and zeolite precursors or highly altered cement interacting with MgCl₂ solutions.. To evaluate their stability constants, IPs and temperature dependencies.

For the Al, there were no data on possible interactions and complex formation with Ca and Mg ions due to their low concentrations in classical cementitious systems. Concentrations may be high for alkali activated systems and for interactions with CaCl₂/MgCl₂ salt solutions. Further investigations are recommended:

- Gibbsite solubility measurements in MgCl₂ and CaCl₂ rich solutions, 0–100 °C, in association with portlandite and brucite.
- Effect of Si on the gibbsite solubility at high pH to understand if Al-Si interactions may be relevant, especially in high concentration solutions at late stages of degradation.

Although outside the scope of this study, solid phases and their properties determine the composition of the pore solution with which they are in equilibrium. Therefore, a good knowledge of these phases is necessary, especially of the various secondary phases and alteration products that may form during cement interactions with salt solutions. The stable phases are influenced by the relative proportions of Si, Al, sulphate and carbonate to the saline electrolyte.

- Measurements of the stability of Kuzel's and Friedel's salts to constrain their stability as a function of temperature.

- Solubility of cement phases in NaCl, NaOH, KCl, KOH (AFm monosulphate, hemicarbonate, Kuzel's and Friedel's salts) and the effect of temperature.

Particularly in the late stages of cement degradation and in alkali activated systems, zeolites and zeolite precursor phases are expected to play a role. Recent studies on these phases (Ma and Lothenbach, 2021, 2020a, 2020b) can be used to provide necessary thermodynamic data for these phases in THEREDA.

The newly derived set of thermodynamic properties and Pitzer IPs can be compared and further improved with new experimental solubility measurements up to the saturation of salts e.g., NaCl, KCl, Na₂SO₄, K₂SO₄, CaCl₂, MgCl₂ in systems containing C-S-H, M-S-H as well as other cement relevant phase assemblages.

Table 4-1 Status of polythermal parameters in the system Al–Si–Ca–Mg–Na–K–Cl–SO₄–CO₂–H₂O. Interactions between ions of the same charge are expected to only be relevant for highly concentrated multicomponent solutions.

from experiments	estimated		no data			<i>limited</i>	
25 °C only	25 °C only		no/low interaction				
	Na ⁺	K ⁺	Ca ²⁺	Mg ²⁺	Cl ⁻	SO ₄ ²⁻	CO ₃ ²⁻
Si(OH)₄(aq)							
SiO(OH)₃⁻							
SiO₂(OH)₂²⁻*							
Si₄O₈(OH)₄⁴⁻*							
Ca/MgSiO(OH)₃⁺*							
Ca/MgSiO₂(OH)₂(aq)*							
Al³⁺							
Al(OH) ²⁺							
Al(OH) ₂ ⁺							
Al(OH) ₃ (aq)							
Al(OH) ₄ ⁻							
AlSiO(OH) ₃ ²⁺							

* uncertain temperature dependence

5 List of References

- Accornero, M. & Marini, L. (2009): Empirical prediction of the Pitzer's interaction parameters for cationic Al species with both $\text{SiO}_2(\text{aq})$ and $\text{CO}_2(\text{aq})$: Implications for the geochemical modelling of very saline solutions. *Applied Geochemistry* 24, 747–759. <https://doi.org/10.1016/J.APGEOCHEM.2009.01.002>
- André, L., Christov, C., Lassin, A. & Azaroual, M. (2018): Thermodynamic model for solution behavior and solid-liquid equilibrium in Na-Al(III)-Fe(III)-Cr(III)-Cl-H₂O system at 25°C. *Acta Scientifica Naturalis* 5, 6–16. <https://doi.org/10.2478/ASN-2018-0002>
- Azaroual, M., Fouillac, C. & Matray, J.M. (1997): Solubility of silica polymorphs in electrolyte solutions, I. Activity coefficient of aqueous silica from 25° to 250°C, Pitzer's parameterisation. *Chemical Geology* 140, 155–165. [https://doi.org/10.1016/S0009-2541\(97\)00046-6](https://doi.org/10.1016/S0009-2541(97)00046-6)
- Bassett, H. & Watt, W. (1950): Pickeringite and the system $\text{MgSO}_4\text{-Al}_2(\text{SO}_4)_3\text{-H}_2\text{O}$. *Journal of the Chemical Society (Resumed)* 1408–1414. <https://doi.org/10.1039/JR9500001408>
- Bénézeth, P., Palmer, D.A. & Wesolowski, D.J. (2001): Aqueous high-temperature solubility studies. II. The solubility of boehmite at 0.03 m ionic strength as a function of temperature and pH as determined by in situ measurements. *Geochimica et Cosmochimica Acta* 65, 2097–2111. [https://doi.org/10.1016/S0016-7037\(01\)00585-3](https://doi.org/10.1016/S0016-7037(01)00585-3)
- Bernard, E., Lothenbach, B., Cau-Dit-Coumes, C., Chlique, C., Dauzères, A. & Pochard, I. (2018): Magnesium and calcium silicate hydrates, Part I: Investigation of the possible magnesium incorporation in calcium silicate hydrate (C-S-H) and of the calcium in magnesium silicate hydrate (M-S-H). *Applied Geochemistry* 89, 229–242. <https://doi.org/10.1016/j.apgeochem.2017.12.005>
- Bouzat, G. & Philipponneau, G. (1991): Physical chemistry models of oxalate and gibbsite solubilities in Bayer solutions. *Light Metals 1991* 97–102.
- Britton, H.T.S. (1922): The system potassium sulphate–aluminium sulphate–water at 25°. *Journal of the Chemical Society, Transactions* 121, 982–986. <https://doi.org/10.1039/CT9222100982>
- Brown, P.L. & Ekberg, C. (2016): Hydrolysis of metal ions at 25°C. Wiley-VCH Verlag GmbH & Co., Weinheim, Germany.
- Brown, R.R., Daut, G.E., Mrazek, R. V. & Gokcen, N.A. (1979): Solubility and Activity of Aluminum Chloride in Aqueous Hydrochloric Acid Solutions. | National Technical Reports Library - NTIS.
- Burge, D.E. (1963): Osmotic Coefficients in Aqueous Solutions: Studies with the Vapour Pressure Osmometer. *J. Phys. Chem.* 67, 2590–2593.
- Busey, R.H. & Mesmer, R.E. (1978): Thermodynamic quantities for the ionization of water in sodium chloride media to 300 °C. *J. Chem. Eng. Data* 23, 175–176. <https://doi.org/10.1021/je60077a025>
- Busey, R.H. & Mesmer, R.E. (1977): Ionization equilibria of silicic acid and polysilicate formation in aqueous sodium chloride solutions to 300.degree.C. *Inorganic Chemistry* 16, 2444–2450. <https://doi.org/10.1021/ic50176a004>
- Chen, C.T.A. & Marshall, W.L. (1982): Amorphous silica solubilities IV. Behavior in pure water and aqueous sodium chloride, sodium sulfate, magnesium chloride, and magnesium sulfate

- solutions up to 350°C. *Geochimica et Cosmochimica Acta* 46, 279–287. [https://doi.org/10.1016/0016-7037\(82\)90255-1](https://doi.org/10.1016/0016-7037(82)90255-1)
- Cheng, W., Li, J., Xu, L., Cheng, F. & Liu, G. (2023): Experiment and prediction for the solubility of $\text{AlCl}_3 \cdot 6\text{H}_2\text{O}$ in FeCl_3 , CaCl_2 , KCl and KCl-FeCl_3 solutions. *Huagong Xuebao/CIESC Journal* 74, 642–652. <https://doi.org/10.11949/0438-1157.20221368>
- Christov, C. (2001): Thermodynamic study of the $\text{K} \square \text{Mg} \square \text{Al} \square \text{Cl} \square \text{SO}_4 \square \text{H}_2\text{O}$ system at the temperature 298.15 K. *Calphad* 25, 445–454. [https://doi.org/10.1016/S0364-5916\(01\)00063-3](https://doi.org/10.1016/S0364-5916(01)00063-3)
- Christov, C., Dickson, A.G. & Moller, N. (2007): Thermodynamic modeling of aqueous aluminum chemistry and solid-liquid equilibria to high solution concentration and temperature. I. the acidic H-Al-Na-K-Cl-H₂O system from 0 to 100°C. *Journal of Solution Chemistry* 36, 1495–1523. <https://doi.org/10.1007/s10953-007-9191-9>
- Clegg, S.L. & Brimblecombe, P. (1990): The solubility and activity coefficient of oxygen in salt solutions and brines. *Geochimica et Cosmochimica Acta* 54, 3315–3328. [https://doi.org/10.1016/0016-7037\(90\)90287-U](https://doi.org/10.1016/0016-7037(90)90287-U)
- Clegg, S.L., Waters, J.F., Turner, D.R. & Dickson, A.G. (2022): Chemical speciation models based upon the Pitzer activity coefficient equations, including the propagation of uncertainties. III. Seawater from the freezing point to 45 °C, including acid-base equilibria. *Marine Chemistry* 104196. <https://doi.org/10.1016/J.MARCHEM.2022.104196>
- Cox, J.D., Wagman, D.D. & Medvedev, V.A. (Vadim A. (1989): CODATA key values for thermodynamics. Hemisphere Pub. Corp, New York.
- Dobbins, J.T. & Addleston, J.A. (1931): A Study of the Soda-Alum System. *The Journal of Physical Chemistry* 39, 637–642. <https://doi.org/10.1021/J150365A007>
- DRUZHININ, I.G., IMANAKUNOV, B. & KUZNETSOV, V.G. (1961): SOLUBILITY IN THE AQUEOUS ALUMINUM, SODIUM, NICKEL, SULPHATE QUATERNARY SYSTEM. *Z. NEORG. CHIM.* 6, 1304–1308.
- Elmer, T.H. & Nordberg, M.E. (1958): Solubility of Silica in Nitric Acid Solutions. *Journal of the American Ceramic Society* 41, 517–520. <https://doi.org/10.1111/j.1151-2916.1958.tb12907.x>
- Farelo, F., Fernandes, C. & Avelino, A. (2005): Solubilities for six ternary systems: $\text{NaCl} + \text{NH}_4\text{Cl} + \text{H}_2\text{O}$, $\text{KCl} + \text{NH}_4\text{Cl} + \text{H}_2\text{O}$, $\text{NaCl} + \text{LiCl} + \text{H}_2\text{O}$, $\text{KCl} + \text{LiCl} + \text{H}_2\text{O}$, $\text{NaCl} + \text{AlCl}_3 + \text{H}_2\text{O}$, and $\text{KCl} + \text{AlCl}_3 + \text{H}_2\text{O}$ at $T = (298$ to $333)$ K. *Journal of Chemical and Engineering Data* 50, 1470–1477. <https://doi.org/10.1021/JE050111J/ASSET/IMAGES/LARGE/JE050111JF00010.jpeg>
- Felmy, A.R., Cho, H., Rustad, J.R. & Mason, M.J. (2001): An aqueous thermodynamic model for polymerized silica species to high ionic strength. *Journal of Solution Chemistry* 30, 509–525. <https://doi.org/10.1023/A:1010382701742>
- Felmy, A.R., Schroeder, C.C. & Mason, M.J. (1994): A solubility model for amorphous silica in concentrated electrolytes , in: Symposium of Scientific Issues Related to Safety and Treatment of Hanford Waste Tanks.
- Gallup, D.L. (1989): Solubility of amorphous silica in geothermal brines. *Transactions - Geothermal Resources Council* 13, 241–245.
- Gao, W., Li, Z. & Asselin, E. (2013): Solubility of $\text{AlCl}_3 \cdot 6\text{H}_2\text{O}$ in the $\text{Fe}(\text{II}) + \text{Mg} + \text{Ca} + \text{K} + \text{Cl} + \text{H}_2\text{O}$ system and its salting-out crystallization with FeCl_2 . *Industrial and Engineering Chemistry Research* 52, 14282–14290.

- https://doi.org/10.1021/IE401850A/ASSET/IMAGES/LARGE/IE-2013-01850A_0014.JPG
- Glasser, F.P., Tyrer, M., Quillin, K. & Environment Agency. (1999): The chemistry of blended cements and backfills intended for use in radioactive waste disposal. Environment Agency, Bristol.
- Gout, R., Pokrovski, G.S., Schott, J. & Zwick, A. (2000): Raman Spectroscopic Study of Aluminum Silicate Complexes at 20°C in Basic Solutions. *Journal of Solution Chemistry* 2000 29:12 29, 1173–1186. <https://doi.org/10.1023/A:1026428027101>
- Gout, R., Pokrovski, G.S., Schott, J. & Zwick, A. (1999): Raman Spectroscopic Study of Aluminum Silicate Complexion in Acidic Solutions from 25 to 150°C. *Journal of Solution Chemistry* 1999 28:1 28, 73–82. <https://doi.org/10.1023/A:1021703408311>
- Grenthe, I., Fuger, J., Konings, R.J.M., Lemire, R.J., Muller, A.B., Nguyen-Trung, C. & Hans, W. (1992): Chemical thermodynamics 1. Chemical Thermodynamics of Uranium.
- Gu, Y., Gammons, C.H. & Bloom, M.S. (1994): A one-term extrapolation method for estimating equilibrium constants of aqueous reactions at elevated temperatures. *Geochimica et Cosmochimica Acta* 58, 3545–3560. [https://doi.org/10.1016/0016-7037\(94\)90149-X](https://doi.org/10.1016/0016-7037(94)90149-X)
- Guillaumont, R., Fanghänel, T., Neck, V., Fuger, J., Palmer, D.A., Grenthe, I. & Rand, M.H. (2003): Update on the chemical thermodynamics of uranium, neptunium, plutonium, americium and technetium. *Chemical Thermodynamics* 5, 919.
- Gunnarsson, I. & Arnórsson, S. (2000): Amorphous silica solubility and the thermodynamic properties of H₄SiO⁴ in the range of 0° to 350°C at Psat. *Geochimica et Cosmochimica Acta* 64, 2295–2307. [https://doi.org/10.1016/S0016-7037\(99\)00426-3](https://doi.org/10.1016/S0016-7037(99)00426-3)
- Harvie, C.E., Møller, N. & Weare, J.H. (1984): The prediction of mineral solubilities in natural waters: The Na-K-Mg-Ca-H-Cl-SO₄-OH-HCO₃-CO₃-CO₂-H₂O system to high ionic strengths at 25°C. *Geochimica et Cosmochimica Acta* 48, 723–751. [https://doi.org/10.1016/0016-7037\(84\)90098-X](https://doi.org/10.1016/0016-7037(84)90098-X)
- Hemingway, B.S. & Robie, R.A. (1977): Enthalpies of formation of low albite (NaAlSi₃O₈), gibbsite (Al(OH)₃), and NaAlO₂; revised values for ΔH_{f,298} and ΔG_{f,298} of some aluminosilicate minerals. *Journal of Research of the U.S. Geological Survey* 5, 413–429.
- Hemingway, B.S., Robie, R.A. & Apps, J.A. (1991): Revised values for the thermodynamic properties of boehmite, AlO(OH), and related species and phases in the system Al-H-O. *American Mineralogist* 76, 445–457.
- Hemingway, B.S., Robie, R.A., Fisher, J.R. & Wilson, W.H. (1977): Heat capacities of gibbsite, Al(OH)₃, between 13 and 480 K and magnesite, MgCO₃, between 13 and 380 K and their standard entropies at 289.15 K, and the heat capacities of calorimetry conference benzoic acid between 12 and 316 K. *J. Res. U.S. Geol. Surv.; (United States)* 5-6.
- Hummel, W., Berner, U., Curti, E., Pearson, F.J. & Thoenen, T. (2002): Nagra/PSI Chemical Thermodynamic Data Base 01/01. *Radiochimica Acta* 90, 805–813. https://doi.org/10.1524/ract.2002.90.9-11_2002.805
- Hummel, W. & Thoenen, T. (2023): The PSI Chemical Thermodynamic Database 2020. Nagra Technical Report, NTB 21-03. Villigen, Switzerland.
- Ingri, N. (1959): Equilibrium Studies of Polyanions. IV. Silicate Ions in NaCl Medium. *Acta Chemica Scandinavica* 13, 758–775. <https://doi.org/10.3891/ACTA.CHEM.SCAND.13-0758>

- Königsberger, E., May, P.M. & Hefter, G. (2006): Comprehensive Model of Synthetic Bayer Liquors. Part 3. Sodium Aluminate Solutions and the Solubility of Gibbsite and Boehmite. *Monatshefte für Chemie / Chemical Monthly* 2006 137:9 137, 1139–1149. <https://doi.org/10.1007/S00706-006-0526-9>
- Kulik, D.A., Miron, G.D. & Lothenbach, B. (2022): A structurally-consistent CASH+ sublattice solid solution model for fully hydrated C-S-H phases: Thermodynamic basis, methods, and Ca-Si-H₂O core sub-model. *Cement and Concrete Research* 151, 106585. <https://doi.org/10.1016/j.cemconres.2021.106585>
- Kulik, D.A., Wagner, T., Dmytryeva, S. V., Kosakowski, G., Hingerl, F.F., Chudnenko, K. V. & Berner, U.R. (2013): GEM-Selektor geochemical modeling package: Revised algorithm and GEMS3K numerical kernel for coupled simulation codes. *Computational Geosciences* 17, 1–24. <https://doi.org/10.1007/s10596-012-9310-6>
- Lagerström, G. (1959): Equilibrium Studies of Polyanions. III. Silicate Ions in NaClO₄ Medium. *Acta Chemica Scandinavica* 13, 722–736. <https://doi.org/10.3891/ACTA.CHEM.SCAND.13-0722>
- Li, Z. & Demopoulos, G.P. (2006): Effect of NaCl, MgCl₂, FeCl₂, FeCl₃, and AlCl₃ on solubility of CaSO₄ phases in aqueous HCl or HCl + CaCl₂ solutions at 298 to 353 K. *Journal of Chemical and Engineering Data* 51, 569–576. <https://doi.org/10.1021/JE0504055/ASSET/IMAGES/LARGE/JE0504055F00017.JPG>
- Linke, W.F. (1965): *Solubilities: inorganic and metal-organic compounds: a compilation of solubility data from the periodical literature.* Amer. Chem. Soc., Washington.
- Liu, S., Asselin, E. & Li, Z. (2022): Preparation of α -High-Strength Hemihydrate from Flue Gas Desulfurization Gypsum in AlCl₃-MgCl₂Solution at Atmospheric Pressure. *Industrial and Engineering Chemistry Research* 61, 14110–14120. https://doi.org/10.1021/ACS.IECR.2C02280/ASSET/IMAGES/MEDIUM/IE2C02280_M028.GIF
- Lothenbach, B., Kulik, D.A., Matschei, T., Balonis, M., Baquerizo, L., Dilnesa, B., Miron, G.D. & Myers, R.J. (2019): Cemdata18: A chemical thermodynamic database for hydrated Portland cements and alkali-activated materials. *Cement and Concrete Research* 115, 472–506. <https://doi.org/10.1016/j.cemconres.2018.04.018>
- Luo, M., Ye, J., Xue, J., Liu, C., Song, X. & Yu, J. (2020): Phase Equilibrium in the Ternary System K₂O-Al₂O₃-H₂O at 323.15, 333.15, 343.15, and 353.15 K. *Journal of Chemical and Engineering Data* 65, 3463–3471. https://doi.org/10.1021/ACS.JCED.0C00017/SUPPL_FILE/JE0C00017_SI_001.PDF
- Ma, B. & Lothenbach, B. (2021): Synthesis, characterization, and thermodynamic study of selected K-based zeolites. *Cement and Concrete Research* 148, 106537. <https://doi.org/10.1016/J.CEMCONRES.2021.106537>
- Ma, B. & Lothenbach, B. (2020a): Synthesis, characterization, and thermodynamic study of selected Na-based zeolites. *Cement and Concrete Research* 135, 106111. <https://doi.org/10.1016/j.cemconres.2020.106111>
- Ma, B. & Lothenbach, B. (2020b): Thermodynamic study of cement/rock interactions using experimentally generated solubility data of zeolites. *Cement and Concrete Research* 135, 106149. <https://doi.org/10.1016/j.cemconres.2020.106149>
- Marshall, W.L. (1980): Amorphous silica solubilities-I. Behavior in aqueous sodium nitrate solutions; 25–300°C, 0–6 molal. *Geochimica et Cosmochimica Acta* 44, 907–913. [https://doi.org/10.1016/0016-7037\(80\)90280-X](https://doi.org/10.1016/0016-7037(80)90280-X)

- Marshall, W.L. & Warakomski, J.M. (1980): Amorphous silica solubilities-II. Effect of aqueous salt solutions at 25°C. *Geochimica et Cosmochimica Acta* 44, 915–924. [https://doi.org/10.1016/0016-7037\(80\)90281-1](https://doi.org/10.1016/0016-7037(80)90281-1)
- Matschei, T., Lothenbach, B. & Glasser, F.P. (2007): Thermodynamic properties of Portland cement hydrates in the system CaO–Al₂O₃–SiO₂–CaSO₄–CaCO₃–H₂O. *Cement and Concrete Research* 37, 1379–1410. <https://doi.org/10.1016/j.cemconres.2007.06.002>
- Meyer, T. (2006): Geochemische Modellierung des Langzeitverhaltens von silikatischen und aluminosilikatischen Materialien. GRS – A – 3350.
- Meyer, T. & Willms, T. (2008): Geochemische Modellierung des Langzeitverhaltens von silikatischen und lumosilikatischen Materialien im Temperaturbereich bis 90 °C. GRS – A – 3493.
- Miron, G.D., Kulik, D.A., Dmytrieva, S. V. & Wagner, T. (2015): GEMSFITS: Code package for optimization of geochemical model parameters and inverse modeling. *Applied Geochemistry* 55, 28–45. <https://doi.org/10.1016/j.apgeochem.2014.10.013>
- Miron, G.D., Kulik, D.A. & Lothenbach, B. (2022a): Porewater compositions of Portland cement with and without silica fume calculated using the fine-tuned CASH+NK solid solution model. *Materials and Structures* 2022 55:8 55, 1–13. <https://doi.org/10.1617/S11527-022-02045-0>
- Miron, G.D., Kulik, D.A. & Lothenbach, B. (2021): Incremental parameterisation of cash+ sublattice solid solution model against recent data for Na, K, and Al uptake in C-S-H. *ERICA CASH II final conference*.
- Miron, G.D., Kulik, D.A. & Thoenen, T. (2020): Generating isocoulombic reactions as a tool for systematic evaluation of temperature trends of thermodynamic properties: Application to aquocomplexes of lanthanides and actinides. *Geochimica et Cosmochimica Acta* 286, 119–142. <https://doi.org/10.1016/j.gca.2020.07.020>
- Miron, G.D., Kulik, D.A., Yan, Y., Tits, J. & Lothenbach, B. (2022b): Extensions of CASH+ thermodynamic solid solution model for the uptake of alkali metals and alkaline earth metals in C-S-H. *Cement and Concrete Research* 152, 106667. <https://doi.org/10.1016/j.CEMCONRES.2021.106667>
- Miron, G.D., Wagner, T., Kulik, D.A. & Heinrich, C.A. (2016): Internally consistent thermodynamic data for aqueous species in the system Na-K-Al-Si-O-H-Cl. *Geochimica et Cosmochimica Acta* 187. <https://doi.org/10.1016/j.gca.2016.04.026>
- Mosgovykh, G.Y., Nurkeev, S.S., Romanov, L.G., Zaripova, A.G. & Eremin, N.I. (1984): . *Zh. Prikl. Khim.* 57, 2104–2107.
- Myers, R.J., L'Hôpital, E., Provis, J.L. & Lothenbach, B. (2015): Effect of temperature and aluminium on calcium (alumino)silicate hydrate chemistry under equilibrium conditions. *Cement and Concrete Research* 68, 83–93. <https://doi.org/10.1016/j.cemconres.2014.10.015>
- Nicoleau, L. & Schreiner, E. (2017): Determination of Ca²⁺ complexation constants by monomeric silicate species at 25 °C with a Ca²⁺ ion selective electrode. *Cement and Concrete Research* 98, 36–43. <https://doi.org/10.1016/j.cemconres.2016.12.007>
- Palmer, D.A., Bénézeth, P. & Wesolowski, D.J. (2001): Aqueous high-temperature solubility studies. I. The solubility of boehmite as functions of ionic strength (to 5 molal, NaCl), temperature (100–290°C), and pH as determined by in situ measurements. *Geochimica et Cosmochimica Acta* 65, 2081–2095. [https://doi.org/10.1016/S0016-7037\(01\)00584-1](https://doi.org/10.1016/S0016-7037(01)00584-1)

- Palmer, D.A. & Wesolowski, D.J. (1993): Aluminum speciation and equilibria in aqueous solution: III. Potentiometric determination of the first hydrolysis constant of aluminum(III) in sodium chloride solutions to 125 °C. *Geochim. Cosmochim. Acta* 57, 2929–2938. [https://doi.org/10.1016/0016-7037\(93\)90284-4](https://doi.org/10.1016/0016-7037(93)90284-4)
- Palmer, D.A. & Wesolowski, D.J. (1992): Aluminum speciation and equilibria in aqueous solution. II. The solubility of gibbsite in acidic sodium chloride solutions from 30 °C to 70 °C. *Geochim. Cosmochim. Acta* 56, 1093–1111. [https://doi.org/10.1016/0016-7037\(92\)90048-n](https://doi.org/10.1016/0016-7037(92)90048-n)
- Park, H. & Englezos, P. (1999a): Osmotic coefficient data for NaOH-NaCl-NaAl(OH)₄-H₂O system measured by an isopiestic method and modeled using Pitzer's model at 298.15 K. *Fluid Phase Equilibria* 155, 251–259. [https://doi.org/10.1016/S0378-3812\(98\)00460-9](https://doi.org/10.1016/S0378-3812(98)00460-9)
- Park, H. & Englezos, P. (1999b): Osmotic coefficient data for NaOH-NaCl-NaAl(OH)₄-H₂O system measured by an isopiestic method and modeled using Pitzer's model at 298.15 K. *Fluid Phase Equilibria* 155, 251–259. [https://doi.org/10.1016/S0378-3812\(98\)00460-9](https://doi.org/10.1016/S0378-3812(98)00460-9)
- Park, H. & Englezos, P. (1998): Osmotic coefficient data for Na₂SiO₃ and Na₂SiO₃–NaOH by an isopiestic method and modeling using Pitzer's model. *Fluid Phase Equilibria* 153, 87–104. [https://doi.org/10.1016/S0378-3812\(98\)00400-2](https://doi.org/10.1016/S0378-3812(98)00400-2)
- Parkhurst, D.L. & Appelo, C. a. J. (2013): *Description of Input and Examples for PHREEQC Version 3 — A Computer Program for Speciation, Batch-Reaction, One-Dimensional Transport, and Inverse Geochemical Calculations. U.S. Geological Survey Techniques and Methods, book 6, chapter A43, 497 p.*, Techniques and Methods, book 6, chapter A43. U.S. Geological Survey.
- Patel K. & Seshardi S. (1966): Phase rule study of quaternary system KCl-AlCl₃-MgCl₂-H₂O at 25 °C. *Ind. J. Chem.* 6, 379–381.
- Phair, J.W., Van Deventer, J.S.J. & Smith, J.D. (2001): Interaction of sodium silicate with zirconia and its consequences for polysialation. *Colloids and Surfaces A: Physicochemical and Engineering Aspects* 182, 143–159. [https://doi.org/10.1016/S0927-7757\(00\)00737-8](https://doi.org/10.1016/S0927-7757(00)00737-8)
- Pitzer, K.S. (1991): *Activity coefficients in electrolyte solutions (2nd ed.)*.
- Pitzer, K.S. & Mayorga, G. (1973): Thermodynamics of electrolytes. II. Activity and osmotic coefficients for strong electrolytes with one or both ions univalent. *Journal of Physical Chemistry* 77, 2300–2308. https://doi.org/10.1021/J100638A009/SUPPL_FILE/J100638A009_SI_001.PDF
- Pitzer, K.S. & Silvester, L.F. (1978): Thermodynamics of electrolytes. 11. Properties of 3:2, 4:2, and other high-valence types. *Journal of Physical Chemistry* 82, 1239–1242. https://doi.org/10.1021/J100500A009/ASSET/J100500A009.FP.PNG_V03
- Plusquellec, G. (2014): Analyse in situ de suspensions de silicate de calcium hydraté: application aux interactions ioniques à la surface des particules. Ph.D. Thesis. Ph.D. thesis, Université de Bourgogne, Bourgogne, France, 203p [in French].
- Plyasunov, A., Fanghänel, T. & Grenthe, I. (1998): Estimation of the Pitzer equation parameters for aqueous complexes. A case study for uranium at 298.15 K and 1 atm. *Acta Chemica Scandinavica* 52, 250–260. <https://doi.org/10.3891/acta.chem.scand.52-0250>
- Pokrovski, G.S., Schott, J., Harrichoury, J.C. & Sergeyev, A.S. (1996): The stability of aluminum silicate complexes in acidic solutions from 25 to 150°C. *Geochimica et Cosmochimica Acta* 60, 2495–2501. [https://doi.org/10.1016/0016-7037\(96\)00123-8](https://doi.org/10.1016/0016-7037(96)00123-8)

- Pokrovskii, V.A. & Helgeson, H.C. (1997): Thermodynamic properties of aqueous species and the solubilities of minerals at high pressures and temperatures: The system Al₂O₃-H₂O-KOH. *Chemical Geology*. [https://doi.org/10.1016/S0009-2541\(96\)00167-2](https://doi.org/10.1016/S0009-2541(96)00167-2)
- Pokrovskii, V.A. & Helgeson, H.C. (1995): Thermodynamic properties of aqueous species and the solubilities of minerals at high pressures and temperatures: the system Al₂O₃- H₂O-NaCl. *American Journal of Science* 295, 1255–1342. <https://doi.org/10.2475/AJS.295.10.1255>
- Prentice, D. (2018): Thermodynamic modelling of ultra-long-term durability of cementitious binders for waste immobilisation. The University of Sheffield.
- Provis, J.L., Duxson, P., Lukey, G.C., Separovic, F., Kriven, W.M. & Van Deventer, J.S.J. (2005): Modeling speciation in highly concentrated alkaline silicate solutions. *Industrial and Engineering Chemistry Research* 44, 8899–8908. https://doi.org/10.1021/IE050700I/SUPPL_FILE/IE050700ISI20050825_035233.PDF
- Reardon, E.J. (1990): An ion interaction model for the determination of chemical equilibria in cement/water systems. *Cement and Concrete Research* 20, 175–192. [https://doi.org/10.1016/0008-8846\(90\)90070-E](https://doi.org/10.1016/0008-8846(90)90070-E)
- Reardon, E.J. (1988): Ion interaction parameters for AlSO₄ and application to the prediction of metal sulfate solubility in binary salt systems. *Journal of Physical Chemistry* 92, 6426–6431. https://doi.org/10.1021/J100333A046/ASSET/J100333A046.FP.PNG_V03
- Reardon, E.J. & Stevens, R. (1991): Aluminum Potassium Sulfate Dodecahydrate Solubility in Mixed K₂SO₄ + Al₂(SO₄)₃ Solutions. *Journal of Chemical and Engineering Data* 36, 422–424. https://doi.org/10.1021/JE00004A022/ASSET/JE00004A022.FP.PNG_V03
- Richter, U., Brand, P., Bohmhammel, K. & Könnecke, T. (2000): Thermodynamic investigations of aqueous solutions of aluminium chloride. *The Journal of Chemical Thermodynamics* 32, 145–154. <https://doi.org/10.1006/JCHT.1999.0557>
- Robie, R. & Hemingway, B.S. (1995): Thermodynamic Properties of Minerals and Related Substances at 298.15K and 1 Bar, U.S. Geological Survey Bulletin.
- Robinson, R.A. (1937): The Osmotic and Activity Coefficient Data of Some Aqueous Salt Solutions from Vapor Pressure Measurements. *Journal of the American Chemical Society* 59, 84–90. https://doi.org/10.1021/JA01280A019/ASSET/JA01280A019.FP.PNG_V03
- Robinson, R.A. & Stokes, R.H. (1965): *Electrolyte Solutions: Second Revised Edition*, 2nd ed, Courier Corporation. Dover Publications.
- Rowland, D., Königsberger, E., Heftner, G. & May, P.M. (2015): Aqueous electrolyte solution modelling: Some limitations of the Pitzer equations. *Applied Geochemistry* 55, 170–183. <https://doi.org/10.1016/j.apgeochem.2014.09.021>
- Ruff, T.J., Toghiani, R.K., Smith, L.T. & Lindner, J.S. (2008): Studies on the Gibbsite to Boehmite Transition. <http://dx.doi.org/10.1080/01496390802121784> 43, 2887–2899. <https://doi.org/10.1080/01496390802121784>
- Russell, A.S., Edwards, J.D. & Taylor, C.S. (1955): Solubility and Density of Hydrated Aluminas in NaOH Solutions. *JOM* 7, 1123–1128. <https://doi.org/10.1007/bf03377627>
- Salvi, S., Pokrovski, G.S. & Schott, J. (1998): Experimental investigation of aluminum-silica aqueous complexing at 300°C. *Chemical Geology* 151, 51–67. [https://doi.org/10.1016/S0009-2541\(98\)00070-9](https://doi.org/10.1016/S0009-2541(98)00070-9)
- Santschi, P.H. & Schindler, P.W. (1974): Complex formation in the ternary systems CaII-H₄SiO₄⁻H₂O and MgII-H₄SiO₄⁻H₂O. *J. Chem. Soc., Dalton Trans.* 181–184. <https://doi.org/10.1039/DT9740000181>

- Sefcik, J. & McCormick, A. V. (1997): Thermochemistry of aqueous silicate solution precursors to ceramics. *AIChE Journal* 43, 2773–2784. <https://doi.org/10.1002/AIC.690431324>
- Seward, T.M. (1974): Determination of the first ionization constant of silicic acid from quartz solubility in borate buffer solutions to 350°C. *Geochimica et Cosmochimica Acta* 38, 1651–1664. [https://doi.org/10.1016/0016-7037\(74\)90183-5](https://doi.org/10.1016/0016-7037(74)90183-5)
- Simoes, M.C., Hughes, K.J., Ingham, D.B., Ma, L. & Pourkashanian, M. (2016): Estimation of the pitzer parameters for 1-1, 2-1, 3-1, 4-1, and 2-2 single electrolytes at 25 °C. *Journal of Chemical and Engineering Data* 61, 2536–2554. <https://doi.org/10.1021/ACS.JCED.6B00236>
- Sipos, P., Huang, F.J., Turonek, M., Radnai, T., Buchner, R., Samani, F., Schibeci, M., May, P. & Hefter, G. (1998): Fundamentals of Alumina Precipitation. AMIRA Project P380B, Confidential Annual Report, 186 pp.
- Sjöberg, S. (1996): Silica in aqueous environments. *Journal of Non-Crystalline Solids* 196, 51–57. [https://doi.org/10.1016/0022-3093\(95\)00562-5](https://doi.org/10.1016/0022-3093(95)00562-5)
- Sjöberg, S., Hägglund, Y., Nordin, A. & Ingri, N. (1983): Equilibrium and structural studies of silicon(IV) and aluminum(III) in aqueous solution. 5. Acidity constants of silicic acid and the ionic product of water in the medium range 0.05–2.0 M Na(Cl) at 25 °C. *Mar. Chem.* 13, 35. [https://doi.org/10.1016/0304-4203\(83\)90047-6](https://doi.org/10.1016/0304-4203(83)90047-6)
- Sjöberg, S., Nordin, A. & Ingri, N. (1981): Equilibrium and structural studies of silicon(IV) and aluminium(III) in aqueous solution. II. Formation constants for the monosilicate ions $\text{SiO}(\text{OH})_3^-$ and $\text{SiO}_2(\text{OH})_2^{2-}$. A precision study at 25°C in a simplified seawater medium. *Marine Chemistry* 10, 521–532. [https://doi.org/10.1016/0304-4203\(81\)90005-0](https://doi.org/10.1016/0304-4203(81)90005-0)
- Sjöberg, S. & Öhman, L.O. (1985): Equilibrium and structural studies of silicon(IV) and aluminum(III) in aqueous solution. 13. A potentiometric and Al-27 nuclear magnetic resonance study of speciation and equilibria in the aluminum(III) oxalic acid hydroxide system. *J. Chem. Soc. Dalton Trans.* 12, 2665–2669. <https://doi.org/10.1039/dt9850002665>
- Sjöberg, S., Öhman, L.-O., Ingri, N., Andersen, L., Lindqvist, O. & Zemlicka, M. (1985): Equilibrium and Structural Studies of Silicon(IV) and Aluminium(III) in Aqueous Solution. 11. Polysilicate Formation in Alkaline Aqueous Solution. A Combined Potentiometric and ^{29}Si NMR Study. *Acta Chemica Scandinavica* 39a, 93–107. <https://doi.org/10.3891/ACTA.CHEM.SCAND.39A-0093>
- Verdes, G., Gout, R. & Castet, S. (1992): Thermodynamic properties of the aluminate ion and of bayerite, boehmite, diaspore and gibbsite. *European Journal of Mineralogy* 4, 767–792. <https://doi.org/10.1127/EJM/4/4/0767>
- Voigt, W. (2011): Chemistry of salts in aqueous solutions: Applications, experiments, and theory. *Pure and Applied Chemistry* 83, 1015–1030. <https://doi.org/10.1351/PAC-CON-11-01-07>
- Walker, C.S., Sutou, S., Oda, C., Mihara, M. & Honda, A. (2016): Calcium silicate hydrate (C-S-H) gel solubility data and a discrete solid phase model at 25 °C based on two binary non-ideal solid solutions. *Cement and Concrete Research* 79, 1–30. <https://doi.org/10.1016/j.cemconres.2015.07.006>
- Wang, J., Petit, C., Zhang, X. & Cui, S. (2016): Phase Equilibrium Study of the $\text{AlCl}_3\text{-CaCl}_2\text{-H}_2\text{O}$ System for the Production of Aluminum Chloride Hexahydrate from Ca-Rich Flue Ash. *Journal of Chemical and Engineering Data* 61, 359–369. https://doi.org/10.1021/ACS.JCED.5B00603/ASSET/IMAGES/LARGE/JE-2015-006038_0007.JPG

- Wesolowski, D.J. (1992): Aluminum speciation and equilibria in aqueous solution: I. The solubility of gibbsite in the system Na-K-Cl-OH-Al(OH)₄ from 0 to 100°C. *Geochimica et Cosmochimica Acta* 56, 1065–1091. [https://doi.org/10.1016/0016-7037\(92\)90047-M](https://doi.org/10.1016/0016-7037(92)90047-M)
- Wilhelm, S. (2013): Polythermal thermodynamic data set for cement minerals and their reaction products THEREDA II - Final Report, AF-Consult Report, No. 1936/02, THEREDA.
- Xiong, Y. (2016): Solubility constants of hydroxyl sodalite at elevated temperatures evaluated from hydrothermal experiments: Applications to nuclear waste isolation. *Applied Geochemistry* 74, 138–143. <https://doi.org/10.1016/j.apgeochem.2016.09.009>
- Xiong, Y. (2013): A thermodynamic model for silica and aluminum in alkaline solutions with high ionic strength at elevated temperatures up to 100 °C: Applications to zeolites. *American Mineralogist* 98, 141–153. <https://doi.org/10.2138/am.2013.4089>
- Yan, Y., Ma, B., Miron, G.D., Kulik, D.A., Scrivener, K. & Lothenbach, B. (2022): Al uptake in calcium silicate hydrate and the effect of alkali hydroxide. *Cement and Concrete Research* 162, 106957. <https://doi.org/10.1016/J.CEMCONRES.2022.106957>
- Yan, Y., Yang, S.-Y., Miron, G.D., Collings, I., Skibsted, J., Winnefeld, F., Scrivener, K. & Lothenbach, B. (2021): Effect of alkali hydroxide on calcium silicate hydrate (C-S-H). *Cement and Concrete Research* in review.
- Yasunishi, A. & Yoshida, F. (1979): Solubility of Carbon Dioxide in Aqueous Electrolyte Solutions. *Journal of Chemical and Engineering Data* 24, 11–14. https://doi.org/10.1021/JE60080A007/ASSET/JE60080A007.FP.PNG_V03
- Zarubin, D.P. & Nemkina, N. V. (1990): The solubility of amorphous silica in an alkaline aqueous medium at constant ionic strength. *Russ. J. Inorg. Chem.* 35, 16–21.
- Zeng, X., Zeng, Y. & Li, Z. (2019): Measurements and Modeling of the Phase Equilibria in AlCl₃ + NaCl + CaCl₂ + H₂O and AlCl₃ + CaCl₂ + NH₄Cl + H₂O Systems. *Journal of Chemical and Engineering Data* 64, 2791–2800. https://doi.org/10.1021/ACS.JCED.9B00175/ASSET/IMAGES/LARGE/JE-2019-00175U_0011.jpeg
- Zhang, H., Zhang, X., Graham, T.R., Pearce, C.I., Hlushko, H., Laverne, J.A., Liu, L., Wang, S., Zheng, S., Zhang, Y., Clark, S.B., Li, P., Wang, Z. & Rosso, K.M. (2021): Crystallization and Phase Transformations of Aluminum (Oxy)hydroxide Polymorphs in Caustic Aqueous Solution. *Inorganic Chemistry* 60, 9820–9832. https://doi.org/10.1021/ACS.INORGCHEM.1C01111/ASSET/IMAGES/LARGE/IC1C0111_0016.jpeg
- Zhang, X., Cui, W., Hu, J.Z., Wang, H.W., Prange, M.P., Wan, C., Jaegers, N.R., Zong, M., Zhang, H., Pearce, C.I., Li, P., Wang, Z., Clark, S.B. & Rosso, K.M. (2019): Transformation of Gibbsite to Boehmite in Caustic Aqueous Solution at Hydrothermal Conditions. *Crystal Growth and Design* 19, 5557–5567. https://doi.org/10.1021/ACS.CGD.9B00468/ASSET/IMAGES/LARGE/CG9B00468_0010.jpeg
- Zhou, J., Chen, Q.Y., Li, J., Yin, Z.L., Zhou, X. & Zhang, P.M. (2003): Isopiestic measurement of the osmotic and activity coefficients for the NaOH-NaAl(OH)₄-H₂O system at 313.2 K. *Geochimica et Cosmochimica Acta* 67, 3459–3472. [https://doi.org/10.1016/S0016-7037\(03\)00133-9](https://doi.org/10.1016/S0016-7037(03)00133-9)